

## 4. SITE 1208<sup>1</sup>

Shipboard Scientific Party<sup>2</sup>

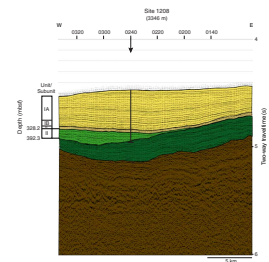
### PRINCIPAL RESULTS

#### Background

Site 1208 is located at lower bathyal (3346 m) water depth, close to center of the Central High of Shatsky Rise. The site lies on seismic line TN037-8 (Fig. F1). Sediments of the Central High have not been cored before; thus, the stratigraphy was unknown prior to drilling at Site 1208. Moreover, correlation of reflectors and the major seismic units with the Southern and Northern Highs, where units and reflectors are calibrated with drill holes, is speculative. Site 1208 coring was designed to provide knowledge of the stratigraphy of the Central High, as well as correlation of units and reflectors with the Southern and Northern Highs. The site was located at the point where the stratigraphic sequence appears to be most complete.

The objective at Site 1208 was to recover a Paleogene through Upper Cretaceous section for paleoceanographic investigation. Highly tentative predrilling correlation with the Southern High seismic units of Sliter and Brown (1993) suggested relatively thick seismic Units 1 (Neogene) and 2 (Paleogene) characterized by predominantly weak, largely horizontal reflectors and a relatively thin Unit 3 (Upper Cretaceous). The Upper Cretaceous to Holocene sequence was expected to contain a number of minor disconformities as indicated by prominent, but horizontal reflectors. At depth, a major angular unconformity suggests erosion of a significant part of the mid-Cretaceous sequence (Fig. F1). The total thickness of the sedimentary section at Site 1208 was estimated at ~785 m. Basement underlying the site was formed during Magneto-chron CM15 in the Berriasian (Nakanishi et al., 1989). The drilling strategy was to double core down to the uppermost chert horizon in the Upper Cretaceous using the advanced piston corer/extended core barrel (APC/XCB).

F1. Interpretation of seismic reflection profile, Site 1208, p. 35.



<sup>1</sup>Examples of how to reference the whole or part of this volume.  
<sup>2</sup>Shipboard Scientific Party addresses.

Coring at Site 1208 revealed a dramatically different sequence than predicted. The upper ~260 m is an expanded upper Miocene to Holocene section below which lies almost 60 m of less expanded lower and middle Miocene section. Reflectors that were thought to represent transitions between different units are probably individual horizons with substantially different bulk density values, probably diatom-rich levels. The Paleogene is almost entirely missing at this site and only a short segment of the Upper Cretaceous was encountered beneath a prominent, deep reflector at 328.2 meters below seafloor (mbsf) (Fig. F1; see line 8 in oversized Figure F7, p. 13, in Klaus and Sager, this volume). We drilled a total of 392.3 m through a major angular unconformity where Campanian ooze and chalk rest unconformably on middle Albian chalk and chert. This chert prevented further drilling with the XCB. Because only a small portion of the section will contribute to the major goals of the leg, we decided not to core a second hole.

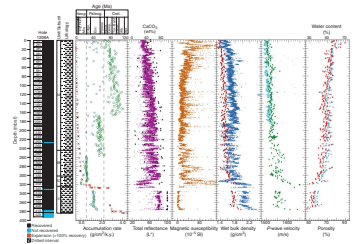
### Summary of Results

A thick, apparently complete upper Miocene to Holocene section was recovered between 0 and 251.6 mbsf (Fig. F2; lithologic Subunit IA). This section is composed of nannofossil ooze and nannofossil clay. Most intervals have significant (5%–20%) amounts of diatoms and minor amounts of foraminifers, radiolarians, and silicoflagellates, and numerous discrete ash horizons. The entire Neogene section is composed of prominent lithologic cycles on a decimeter to meter scale. These cycles were also detected in multisensor track (MST) and color reflectance data throughout the section; preliminary biochronology suggests that they have dominant frequencies of ~40 and 100 k.y. and thus represent obliquity and eccentricity rhythms. The section shows highly promising magnetostratigraphy as well as properties suitable for paleointensity records. The average sedimentation rate of the upper Miocene to Holocene section is ~42 m/m.y.; thus, it will be an excellent candidate for high-resolution biochronologic and paleoceanographic investigations.

The recovered section contains an interval (lithologic Subunit IC; 311.65 to 328.15 mbsf) with at least four unconformities separated by sediments (claystone to nannofossil ooze and chalk) deposited at extremely slow rates (0.08 to 4.2 m/m.y.). These highly condensed claystones contain some zeolite minerals (phillipsite), manganese micro-nodules, and rare foraminifers. Nannofossil biostratigraphy allows us to piece together the history of this highly disjointed section. The section shows some striking similarities to the major unconformity at Site 1207, as well as some minor differences. Combining results from both sites will enable us to reconstruct the regional depositional history for the Central and Northern Highs of Shatsky Rise.

The zeolitic claystone at the base of lithologic Subunit IC at Site 1208 suggests that the site was close to or below the calcite compensation depth (CCD) for much of the late Paleocene, Eocene, and Oligocene. Directly above the unconformity between the Campanian and Paleogene, distinct nannofossils allow us to identify a narrow time slice across the Paleocene/Eocene boundary in Section 198-1208A-36X-CC. This section may contain a highly condensed interval of the Paleocene–Eocene Thermal Maximum (PETM) and thus may provide important information on the response of the deep ocean to this abrupt global warming event. An overlying interval of nannofossil ooze indicated an abrupt deepening in the CCD in the earliest Oligocene coincident with the earliest Oligocene (Oi-1) cooling step (Zachos et al., 1993, 1996).

**F2.** Coring results, Hole 1208A, p. 36.



## Highlights

### Expanded Neogene Section for Paleoceanography and Chronology

Sedimentation rates at Site 1208 averaged 42.4 m/m.y. from the Holocene to late early Pliocene (0 to 3.82 Ma), 22.3 m/m.y. from the late early Pliocene to the early late Miocene (3.82 Ma to 8.28 Ma), then decrease to 5.9 m/m.y. in the early late Miocene to late early Miocene (8.28 to 18.2 Ma). The rates in the late Miocene to Holocene are far higher than typical pelagic sedimentation. The detrital clay and silt component of the sediment may have been derived by eolian transport. However, we suspect that a large component of the sediment must have been delivered by bottom currents. A number of recent Ocean Drilling Program (ODP) legs have targeted sediment drifts for high-resolution paleoceanographic investigation. These include Leg 162 in the Iceland Basin and Norwegian-Greenland Sea and Leg 172 on the Blake-Bahama Outer Ridge and Bermuda Rise. The Site 1208 sedimentation rates, although significant, are not as high as the rates at the majority of these sites.

Sedimentation rates in the lower Pliocene to Holocene interval were more or less constant. Sedimentation rates in contemporaneous intervals at sites drilled during Leg 145 in the North Pacific peaked in the Pliocene and decreased above this interval (Barron et al., 1995). The Pliocene peak, which is considerably higher than rates at Site 1208, is associated with a massive flux of diatoms, the so-called "diatom dump."

The Neogene section at Site 1208 has a number of additional advantages for high-resolution biochronology. These include a combination of siliceous and calcareous microfossils, a high-resolution magnetostratigraphy, a marked orbital cyclicity, numerous ash layers with potential for radiometric dating and intrasite correlation, and a potential magnetic paleointensity record.

Foraminiferal preservation is generally poor, but sufficient for stable isotope stratigraphy in selected intervals. Nannofossil and planktonic foraminiferal assemblages show considerable variation that appears to record climatic change. Diatoms, radiolarians, and silicoflagellates also show sharp changes in abundance that are likely related to changing water-mass properties. Thus, the section has significant potential for high-resolution paleoceanographic investigations.

### Orbital Rhythms: A Strong Climate Signal

Marked cyclic variations are observed in MST data throughout the upper Miocene to Holocene section at Site 1208. These variations are expressed as strong lithologic cycles that have frequencies at the decimeter to meter scale. Preliminary shipboard biochronology suggests that the dominant periodicities correspond to eccentricity (~100 k.y.) cycles for the last 0.8 m.y. and to a combination of eccentricity and obliquity (~40 k.y.) cycles in the interval from 0.6 to 2.7 Ma. These cycles are marked by relatively subtle to sharp changes in color that are associated with variations in the amount of clay, pyrite, and different biogenic particles. For most of the upper Miocene to Holocene section the cycles are predominantly between nannofossil clay with diatoms and nannofossil ooze with clay and diatoms. The darker gray to green interbeds tend to have more abundant diatoms and clay, more dissolved nannofossil assemblages, and more abundant reduced iron minerals

(i.e., pyrite). The lighter, gray, tan, and white interbeds contain fewer diatoms, less clay, and a better preserved nannofossil assemblage.

Upper Miocene to Holocene sediments (lithologic Subunit IA) recovered at Site 1208 contain few to common diatoms (up to 20%)—lower percentages than in sediments recovered at Site 1207, but higher percentages than contemporaneous units from sites on the Southern High of Shatsky Rise, where diatoms are usually <5%. Site 1208 is ~1° south of Site 1207 and ~4° north of the Southern High sites. As at Site 1207 (see “**Principal Results,**” p. 1, in the “Site 1207” chapter), diatom-rich layers are thought to represent intervals during which colder, more productive, transitional, and subarctic water masses shifted southward over the site. Lighter-colored layers that are poorer in diatoms represent warmer intervals during which Site 1208 was located in a subtropical water mass, similar to its location today and similar to sites on the Southern High through most of the Neogene. As the site is considerably higher than the surrounding deep-ocean floor, there may also be a topographic effect to the productivity and productivity variation.

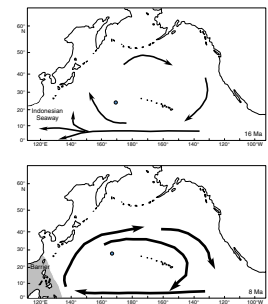
Diatoms increase markedly in abundance across the transition from lithologic Subunit IA to IB at 251.6 mbsf (~8 Ma). This interval lies just after a change in Pacific Ocean circulation associated with the closure of the Indonesian seaway that caused intensification of North Pacific gyral circulation (Fig. F3) (Kennett et al., 1985); a strengthened west wind drift likely increased upwelling along this boundary and created a more well-established North Pacific transitional water mass separated from the northern subpolar region.

Changes in the geographic distribution of water masses through time also affected other fossil groups at Site 1208. In particular, Neogene planktonic foraminifers show distinct stratigraphic changes between assemblages dominated by subtropical and tropical taxa and those dominated by taxa with cool, temperate affinities. Moreover, faunas at Site 1208 are considerably richer in warmer, tropical taxa than at Site 1207, which is located only ~1° to the north. This suggests that for much of the Neogene, Sites 1207 and 1208 were located in a region with sharp temperature gradients.

### Origin of Regional Unconformities

The interval between the lower Miocene and the upper Campanian (lithologic Subunit IC; Cores 198-1208A-35X and 36X; 311.65–328.15 mbsf) is marked by at least three distinct unconformities (see “**Biostratigraphy,**” p. 16). These unconformities separate the upper Oligocene and lower Oligocene, the upper Eocene and lower Eocene, and the Paleocene/Eocene boundary interval and the upper Campanian. Additionally, most of these intervals are characterized by extremely slow sedimentation that locally resulted in the postdepositional precipitation of zeolites and manganese micronodules. Carbonate layers occur sporadically and are generally composed of dissolved nannofossils and sparse benthic and planktonic foraminifers. The only coring gap that affects interpretation lies between Sections 198-1208A-36X-2 and 36X-CC in the lower Eocene between nannofossil Subzone CP9b and combined Zones CP10 and CP11. The estimated sedimentation rates for the key intervals containing unconformities are 0.09 m/m.y. for the late Paleocene to early Eocene transition and 4.2 m/m.y. for the earliest Oligocene.

F3. Change in circulation in North Pacific associated with closure of Indonesian Seaway, p. 37.



The lower Miocene to Campanian interval at Site 1208 shows stratigraphic and lithologic similarities to the contemporaneous interval at Site 1207 on the Northern High. This suggests that events that caused the unconformity were regional in scale. However, the unconformity record at Site 1208 is more complex than that at Site 1207. The near continuous record at Site 1208 allows us to distinguish highly condensed intervals from major breaks in sedimentation. The presence of carbonate provides a record of CCD variations through time.

Several of the unconformities at Site 1208 appear to result from shoaling of the CCD. The history of the CCD in the North Pacific shows a slow rise from 70 to 50 Ma (early Maastrichtian to early Eocene), a rapid rise from 50 to 30 Ma (early Eocene to early Oligocene), and a long-term deepening from 30 to 14 Ma (early Oligocene to middle Miocene) (Rea et al., 1995). The CCD remained above the current depth of Site 1208 from 39 to 15 Ma (middle Eocene to middle Miocene). One of the clearest lithologic changes lies close to the Eocene/Oligocene boundary in interval 198-1208A-36X-2, 0–20 cm where a distinct color change reflects a sharp upsection increase in carbonate content that likely corresponds to an abrupt drop in the CCD. This interval, within nannofossil Subzone CP16a and the lower part of Subzone CP16b, corresponds to a global deepening of the CCD (Zachos et al., 1996) that is thought to correspond to the Oi-1 cooling event.

The uppermost Paleocene to lowermost Eocene interval appears highly condensed. Preliminary biostratigraphy suggests that this interval is complete to the limits of resolution. The presence of highly dissolved nannofossil assemblages and depauperate foraminifers in some samples and other samples that are devoid of carbonate suggests that the site rested close to the CCD through this interval.

The absence of zonal markers in the lower Miocene to lower Oligocene transition complicates age interpretation (see “**Biostratigraphy**,” p. 16). This transition lies in an interval of nannofossil ooze, chalk, and claystone that is dark orange to brown in color, indicative of slow sedimentation. However, given poor biostratigraphic resolution, it is also possible that one or more unconformities lie within this transition. The similarity in the age of the sediment overlying this interval (early Miocene foraminiferal Zone N9; 14.7–15.1 Ma) at Sites 1207 and 1208 also suggests that the unconformity represents a regional event. Seismic reflection profiles at Site 1207 indicate that a major Oligocene–early Miocene interval of erosion and slumping removed much of the section underlying this unconformity. The stratigraphy at Site 1208 suggests that this erosive event may have been regional, perhaps driven by the intensification of deepwater circulation during long-term early Neogene cooling (e.g., Kennett et al., 1985).

The record of hiatuses at Site 1208 and other sites in the North Pacific also shows a number of similarities. The section at Site 883 on Emperor Seamount has unconformities in the upper to middle Miocene, the lower Miocene to lower Oligocene and the lower Eocene (Barron et al., 1995). Keller and Barron (1987) show four widespread hiatuses in the latest Oligocene to earliest middle Miocene interval. Thus, the early Miocene to early Oligocene erosive event is not limited to Shatsky Rise but is a regional phenomenon.

A major angular unconformity occurs between the Campanian and the middle Albian (Fig. F1). This unconformity contact was not recovered at Site 1208, but its nature can be inferred from regional seismic interpretations. Seismic stratigraphy indicates that the age of the units

overlying the Campanian becomes younger to the east of Site 1208. In this direction, the truncation of the inferred mid-Cretaceous section beneath the unconformity suggests a lengthy phase of nondeposition and erosion at some stage during the Late Cretaceous or Paleogene (Fig. F4). Campanian horizons appear to depositonally onlap the unconformity surface at Site 1208. The mid-Cretaceous horizons appear to have draped the rough basement topography across the Central Rise, and the Campanian horizons appear to have smoothed out this topography. The horizons on either side of the unconformity between the upper Campanian and the upper Paleocene are parallel. This suggests most likely that the unconformity resulted from an interval when the site was below the CCD, an interval that was not recovered in Core 198-1208A-36X. We cannot rule out the possibility that a minor amount of erosion complemented this dissolutional episode. The similarity in age of the Campanian horizons underlying the unconformity at Sites 1207 and 1208 (nannofossil Zone CC22; 75–76 Ma) suggests that the Late Cretaceous and early Paleogene interval of dissolution was regional in scope.

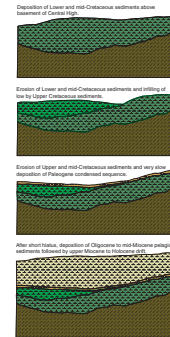
### Deepwater Record of the Paleocene–Eocene Boundary Transition

The interval of time surrounding the Paleocene/Eocene boundary was characterized by rapid changes in climate and ocean circulation that led to profound changes in marine and terrestrial biotas (i.e., papers in Aubry et al., 1998). Superimposed on this interval of long-term transition was an abrupt global warming event at the Paleocene/Eocene boundary, known as the PETM. The deep sea and high latitude oceans warmed by 4° and 8°C, respectively, during the PETM. The warming, in turn, led to profound changes in precipitation and continental weathering patterns (Gibson et al., 1993; Robert and Kennett, 1994). The climatic changes also affected biota on a global scale triggering rapid turnover of benthic and planktonic organisms in the ocean (i.e., Thomas, 1990; Kelly et al., 1996).

The carbon isotopic composition of the ocean decreased by 3‰–4‰ coeval with the warming event, suggesting a massive perturbation to the global carbon cycle (Kennett and Stott, 1991; Bains et al., 1999). The large magnitude and rate (~–3‰–4‰/5 k.y.) of the carbon isotope excursion is consistent with a sudden injection of a large volume of isotopically depleted carbon into the ocean/atmosphere system. Dickens et al. (1995, 1997) suggested that the largest source of depleted carbon was the vast reservoir of methane clathrates stored in continental slope sediments. Much of this methane would have quickly converted to CO<sub>2</sub>, stripping O<sub>2</sub> from deepwaters and lowering alkalinity. The expected response of this massive input of CO<sub>2</sub> into the ocean-atmosphere system is a sharp rise in the level of the CCD. The response of the CCD in the Pacific can be determined by comparison of carbonate preservation in Shatsky Rise sediments at various water depths.

At Site 1208, the upper Paleocene–lower Eocene transition rests unconformably above the Campanian in Section 198-1208A-36X-CC. Preliminary nannofossil biostratigraphy suggests that this section lies close to the Paleocene/Eocene boundary and the PETM. Three events that lie close to the boundary—the last occurrence (LO) of the genus *Fasciculithus* and the first occurrences of *Tribraehiatus bramlettei* and *Discoaster diastypus*—occur within 6 cm of each other (see “Biostratigraphy,”

F4. Interpretation of evolution of the stratigraphic section, Site 1208, p. 38.



p. 16). These events lie just within or just above the PETM and are separated by ~330 k.y. (Aubry et al., 1996; Bralower et al., 1995).

Poorly preserved nannofossil assemblages and intervals barren of carbonate suggest that the CCD was close to the depth of the site during the Paleocene/Eocene boundary transition interval. Combined with results from other Leg 198 drill sites, the recovered section may hold important clues about the Paleocene–Eocene transition in the North Pacific. High-resolution bulk carbon isotope analyses and carbonate variations will be used to identify the event. In addition, the clay-rich lithology will provide an excellent opportunity to derive detailed clay mineralogical records that could be used to monitor changes in atmospheric circulation.

## **BACKGROUND AND OBJECTIVES**

Site 1208 is located in lower bathyal (3346 m) water depth close to center of the Central High of Shatsky Rise. According to the reconstruction of Nakanishi et al. (1989), basement underlying the site was formed in Magnetochron CM15 in the Berriasian (~136 Ma). The paleo-depth of this site was ~1400 m in the early Maastrichtian based on the estimate of Barrera et al. (1997) for Site 305. However, the site probably subsided at a faster initial rate than typical crust (e.g., McNutt et al., 1990). Since this site lies ~4° north of sites on the Southern High, it likely crossed the equatorial high productivity zone several million years earlier (R. Larson, pers. comm., 2001), and thus the uppermost chert horizon is predicted to lie in an older part of the stratigraphic section (Fig. F1).

The Central High has not been drilled before; thus, the stratigraphy was unknown prior to our drilling of Site 1208. The site is located on seismic line TN037-8 (Fig. F1). The ages of reflectors and the major seismic units cannot be correlated with the Southern or the Northern Highs with any degree of certainty. Site 1208 drilling was designed to provide knowledge of the stratigraphy of the Central High as well as correlation of units and reflectors with the Southern and Northern Highs. Tentative predrilling correlation with the Southern High seismic units of Sliter and Brown (1993) suggested relatively thick seismic Units 1 and 2 (Neogene and Paleogene) characterized by predominantly weak, largely horizontal reflectors, and relatively thin Unit 3 (Upper Cretaceous). The Upper Cretaceous to Holocene sequence was expected to contain a number of disconformities as suggested by parallel but prominent reflectors. An angular unconformity indicates erosion of part or most of the mid-Cretaceous sequence (Fig. F1). The total thickness of the sedimentary record at Site 1208 was estimated at ~785 m using velocity data for the different units from Site 305.

Site 1208 lies in the middle of the Shatsky Rise depth and latitudinal transects. The site will be included in broad leg-based objectives that include

1. Reconstructing changes in the properties of surface and deepwaters through the Cretaceous and Paleogene. This will help to constrain the character and stability of intermediate- and deep-water circulation, vertical thermal gradients, and basin fractionation during ancient intervals of extreme warmth as well as during transitions from and to cooler intervals.

2. Shedding light on the origin of transient climatic events such as the Eocene/Oligocene boundary and the PETM. The depth transect will also help address questions concerning the nature of chemical (i.e., CCD, nutrients, and oxygenation) and physical oceanographic changes (temperature gradients) during these events.
3. Determining the significance of unconformities in the stratigraphic section. Are they related to local changes in currents or to regional/basinal changes in the CCD?
4. Charting changes in biotic assemblages and relating them to environmental changes over long time periods as well as during transient climatic events.
5. Understanding the origin of orbital cycles in the sedimentary record. Using petrography, geochemistry, and fossil assemblages to determine whether these cycles reflect changes in productivity or dissolution.
6. Using the Neogene section, which is expected to be clay-rich, to reconstruct eolian dispersal patterns and sources of wind-blown material (e.g., Chinese Loess Province).

## **OPERATIONS**

### **Transit from Site 1207 to 1208**

The 242-nmi transit to Site 1208 was made in 22.5 hr at an average speed of 10.8 kt. Upon arrival at the site coordinates, the ship's crew commenced lowering thrusters and hydrophones, and the ship was switched over to dynamic positioning mode, initiating operations at Site 1208 at 2315 hr on 14 September.

### **Hole 1208A**

After deploying an operational beacon, an APC/XCB was assembled and lowered close to the seafloor. After one unsuccessful attempt at obtaining a mudline core, a 4.75-m core was retrieved at 0920 hr on 15 September, initiating Hole 1208A. The recovery of the mudline core indicates a seafloor depth of 3356.8 meters below rig floor (mbrf), or 3345.7 meters below sea level (mbsl).

Piston coring advanced to 185.2 mbsf, with recovery averaging 105.3% (Table T1). Cores 3H through 20H were oriented. Attempted retrieval of Core 20H resulted in overpull of ~75 kilopounds (kips), which required drilling over with the primary bit to free the core. We continued coring with the XCB, taking 22 cores (Cores 21X through 42X), extending the hole to 392.3 mbsf. Average recovery for the XCB interval was 73.5%. At Core 42X, only 0.25 m of chert was recovered, and the hole was terminated. The drill string was retrieved, clearing the rotary table at 1330 hr on 17 on September, ending drilling at Site 1208. After recovery of the beacon and retraction of the thrusters and hydrophones, the ship began the transit to Site 1209.

---

T1. Coring summary, p. 78.

---

## LITHOSTRATIGRAPHY

### Description of Lithologic Units

The lithostratigraphy at Site 1208 is based on the recovered portion of the 392.3 m of pelagic sediment and sedimentary rocks cored in Hole 1208A. First APC and then XCB coring techniques were used, with excellent to good recovery rates, respectively.

The section at Hole 1208A has been subdivided into two major lithologic units (Table T2; Fig. F5). Unit I extends from 0.0 to 328.15 mbsf. Overall recovery of this unit was excellent (95%). This unit is of Cenozoic age and is characterized by rhythmically alternating intervals of nannofossil ooze/chalk (light) and nannofossil clay/claystone (dark) with diatoms and radiolarians that are punctuated by occasional volcanic ash layers. The average carbonate content is 53 wt% (Fig. F5) (see “Carbonate,” p. 24, in “Organic Geochemistry”). The base of the unit is defined by an unconformity where Paleocene to Miocene claystone (base of Unit I) overlies Campanian nannofossil ooze (top of Unit II). Unit II extends from 328.15 to 392.3 mbsf and consists primarily of Campanian nannofossil ooze with interbedded chert (Fig. F5). In contrast to Unit I, the average carbonate content of Unit II is 96 wt% (Fig. F5). XCB coring of this largely unconsolidated unit resulted in much poorer recovery rates (54%). Drilling was terminated at this site when a significant cherty horizon effectively reduced the recovery rate to 0.25%. Scrapings made from the chalk/porcellanite rims on the chert fragments in Section 198-1208A-42X-CC are of middle Albian age, which suggests that the drilled interval for this terminal core spans a major Cretaceous unconformity (see “Biostratigraphy,” p. 16).

### Lithologic Unit I

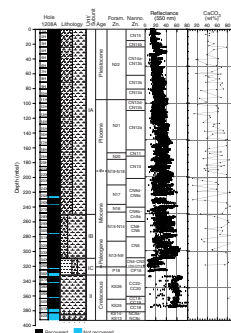
Interval: 198-1208A-1H-1, 0 cm, through 36X-CC, 25 cm  
Depth: 0.0 to 327.66 mbsf  
Age: Holocene to Paleocene

Unit I at Site 1208 is composed of alternating intervals of nannofossil clay and nannofossil ooze with diatoms and radiolarians that become more lithified downsection, passing into nannofossil claystone and nannofossil chalk. This transition from ooze to chalk can be seen in Core 198-1208A-24X (209.8–219.4 mbsf), where interbeds are alternately lithified and unlithified. However, intervals of ooze are present below this interval, indicating that lithification at this site is variable and not simply a function of burial depth.

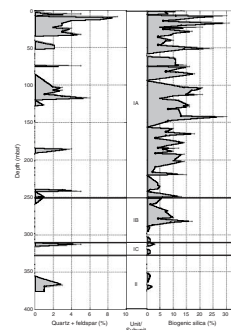
The rhythmic beds that characterize Unit I change in nature and composition down through this interval. This is illustrated in Figure F5, in which carbonate values and reflectance both increase downhole through Unit I. The abundance of siliceous microfossils (Fig. F6) and terrigenous silt also decreases downsection (Fig. F6). These changes, although somewhat gradational, allow for the subdivision of Unit I into three subunits (Fig. F5). Specifically, Subunit IA is predominantly greenish gray (5GY 6/1) in color and characterized by higher clay content, moderate content of siliceous microfossils, color banding, pyrite, and ash layers, whereas Subunit IB, although similar in composition, is distinctly more yellowish orange in color with common *Zoophycos*, *Chondrites*, and *Planolites* burrows. The Subunit IA/IB contact is placed at the top of the first pale yellowish brown (10YR 6/2) nannofossil claystone

T2. Summary of color and sedimentary features, Subunit IA, p. 79.

F5. Core recovery, lithology, lithologic units, age with corresponding biostratigraphic zonation, color reflectance, and percent carbonate, Hole 1208A, p. 39.



F6. Downhole plots of smear slide estimates, p. 40.



in Section 198-1208A-28X-3 at 50 cm. The Subunit IA/IB color change also marks the downhole disappearance of ash beds and a decrease in pyrite in the sediments. *Zoophycos* burrows, although present near the base of Subunit IA (Table T2), are more common (or perhaps just more visible) below Core 198-1208A-28X in Subunit IB. The proportion of darker nannofossil claystone is highest in Subunit IC, progressing to claystone at the base of the subunit (Unit I/II boundary). Siliceous microfossils are only trace components of this subunit. The Subunit IB/IC contact is placed at the top of the first of a series of meter-thick nannofossil claystone units at 5 cm in Section 198-1208A-34X-4. The nature and the origin of the subunit lithologic changes are discussed further in the interpretation section.

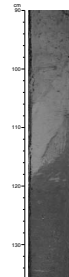
### Subunit IA

Subunit IA extends from 0.0 to 251.6 mbsf. The higher than expected (average 100.1%) recovery rate in this interval can be attributed to slight core expansion. Where this interval was recovered by APC (0.0–185.2 mbsf; Cores 198-1208A-1H through 20H), there is no indication of drilling deformation, but below this interval (185.2–190.4 mbsf; Cores 198-1208A-21X through 28X), recovery decreases, and the core is progressively more disturbed, exhibiting biscuits and fractures.

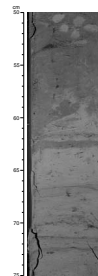
Subunit IA extends from the mudline at the top of Core 198-1208A-1H down to Section 28X-3 at 50 cm. Below a 35-cm surface layer of dark yellowish brown clay (10YR 4/2) with nannofossils is an interval of mainly olive gray (5Y 4/1) nannofossil clay to clayey nannofossil ooze (Section 198-1208-1H to Section 3H-3) with a few abrupt, high-angle bedding contacts (Fig. F7; Table T2). The remainder of the subunit (Cores 198-1208A-4H to 28X) is characterized by alternating light and dark layers of nannofossil ooze and nannofossil clay, locally with diatoms, radiolarians, and foraminifers. These lithologies exhibit gradational to thoroughly bioturbated upper and lower contacts (Fig. F8). Lithologies often grade incrementally from extreme light/dark endmembers within a core interval, making the “gradation” the dominant lithology (e.g., clayey nannofossil ooze). At certain intervals, the rhythms are outlined by starkly contrasting lithologic changes (e.g., Core 198-1208A-8H), whereas elsewhere the cycle variations are more subtly manifested (e.g., Core 198-1208A-19H). The lighter lithologies are generally light gray in color, whereas the darker lithologies are dominantly shades of greenish to olive gray (Table T2). Downsection trends in sediment color are outlined in Table T2. Cycle thickness (light/dark interval) varies on a decimeter to meter scale so that rhythm character is best seen in the whole-core photographs. Core-scale cyclicity is displayed in Figure F9 using a combination of digital images, color reflectance, and bulk density data.

Darker and lighter intervals generally are defined by differing proportions of biocalcareous, detrital clay, and biosiliceous material, in decreasing order of importance. Smear slide estimates of composition (see “Site 1208 Smear Slides,” p. 43) show that the biocalcareous components are dominated by nannofossils (averaging 54% and ranging up to 88%) with a minor percentage of foraminifers (averaging 4% and ranging up to 12%). In addition to clay minerals (averaging 25% and ranging up to 56%), the siliceous mud fraction includes detrital quartz and feldspar silt (see Fig. F6) as well as trace amounts of volcanic glass and associated accessory minerals. Biosiliceous components (see Fig. F6 for distribution) are dominantly diatoms (averaging 6% and ranging up to 20%) and radiolarians (averaging 5% and ranging up to 15%), with

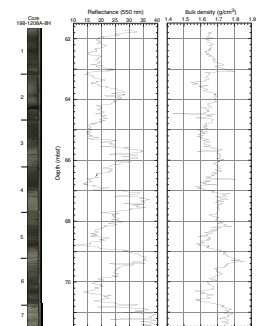
F7. Subparallel discontinuities that could be the product of repeated erosion, faulting, or slumping, p. 41.



F8. Subhorizontal, diffuse color bands just below a burrowed contact between two types of nannofossil ooze, p. 42.



F9. Composite digital photograph, color reflectance, and bulk density, Core 198-1208A-8H, p. 43.



lesser (averaging 1%–2%) silicoflagellates and sponge spicules. Other minor components include inorganic carbonate, opaque minerals (pyrite), and zeolites.

Vitric ash layers and laminae are found throughout but are most abundant in the middle of Subunit IA (Table T2; Cores 198-1208A-5H and 13H). They range in thickness from a few millimeters to 10 cm and in color from lighter to darker shades of gray. Where thick, they are graded and locally exhibit parallel lamination. Most exhibit abrupt to scoured bases (Fig. F10). Some have been disrupted and redistributed by burrowing organisms. Isolated, well-rounded pumice clasts  $\leq 1$  cm in diameter are limited to the middle of the subunit (Table T2). Additionally, volcanic glass is a common trace component throughout Subunit IA.

The cores in Subunit IA are mostly moderately bioturbated, with intervals showing rare to common bioturbation, including burrow mottling. Specific ichnofauna could be identified only in a few intervals. These trace fossils show a crude downhole progression (Table T2) from *Chondrites* (Cores 198-1208A-2H to 4H), to vertical burrows (Fig. F11; *Trichichnus?*; Cores 2H, 13H, and 18H), to *Zoophycos* (Cores 27X and 28X) to composite burrows (Core 28X).

The sediment in Subunit IA is characterized by diagenetic features, including diffuse color banding and pyrite. Color bands are generally subhorizontal, but locally are circular to oblate where centered on discrete burrows. The color bands are present in both light and dark lithologies but are particularly visible where they contrast with lighter nanofossil ooze (Fig. F8). The bands range in color from greenish gray to grayish green (5GY 4/1, 5GY 6/1, and 10G 4/2) to dark gray (N3) and grayish purple (5P 4/2). They become less prominent near the base of the subunit (Table T2). Distinct, green millimeter- to centimeter-thick clay-rich laminae are locally associated with the color bands.

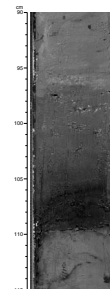
Another unique feature of Subunit IA is the presence of pyrite in various forms. Pyrite most commonly occurs within millimeter- to centimeter-scale burrow fills (blebs/pods and bands) and forms hard concretions where better developed/crystallized (Fig. F8).

### Subunit IB

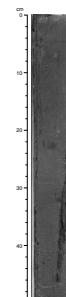
Subunit IB extends from 251.6 to 311.65 mbsf. Recovery decreases to 78% in this subunit, in part because of variable induration (e.g., intervals of ooze and chalk) and XCB coring. The core is moderately disturbed with common biscuiting and fracturing.

Subunit IB consists of alternating lighter and darker lithologies that exhibit gradational to bioturbated contacts. These lithologies are variably indurated, exhibiting alternations of ooze/chalk and clay/claystone within the core. The overall average carbonate content calculated for Subunit IB is 63 wt% (Fig. F5), reflecting a mixture of nanofossil ooze/chalk and nanofossil clay/claystone. Again, as in Subunit IA, the gradational and bioturbatively mixed lithologies (clayey nanofossil ooze/chalk and nanofossil ooze/chalk with clay) are often the dominant lithology. The colors of the end member lithologies are more strongly distinct than those of Subunit IA, reflecting contrasting differences in carbonate and clay content. The lighter-colored lithologies range from very light gray (N8) to moderate yellowish brown (10YR 5/4) and very pale orange (10YR 8/2). Measured carbonate values for these lighter units range up to 89 wt%, whereas the darker units range as low as 28 wt%. Darker intervals range in hue from dusky yellow (5Y 6/4) to moderate yellowish brown (10YR 5/4). Figure F8 shows that the darker

F10. Dark, greenish black (5G 2/1) ash overlying abrupt contact, p. 44.



F11. Near-vertical burrow structure partly filled by dark pyrite that crosscuts core diagonally, p. 45.



beds (carbonate minima) in Subunit IB are somewhat more calcareous (>20 wt%) than those at the base (<20 wt%) of Subunit IA.

Bioturbation ranges from rare to abundant (Figs. F12, F13, F14). The color contrast between light and dark layers serves to highlight burrow structures. The trace fossil assemblage includes common *Zoophycos* (Fig. F12), *Chondrites* (Fig. F12), *Planolites* (Fig. F13), and composite burrows (Fig. F14). Pyrite is present in some burrows in Core 198-1208A-28X and in Sections 29X-1 and 29X-2 but was not noted in the remainder of the subunit.

Smear slide analyses indicate that nannofossils are the dominant component of the lighter intervals, with generally lesser quantities of clay minerals (7%–25%), foraminifers (3%–5%), carbonate (3%–6%), biosiliceous material (1%–8%; diatoms, radiolarians, sponge spicules, and silicoflagellates), volcanic glass (trace), and quartz (trace). In comparison, the darker intervals generally contain higher percentages of biosiliceous material (5%–17%) and clay minerals (20%–45%).

### Subunit IC

Subunit IC extends from 311.65 to 327.66 mbsf. As in Subunit IB, the core exhibits moderate drilling disturbance (biscuiting), but core recovery rates were slightly higher (86%) in Subunit IC.

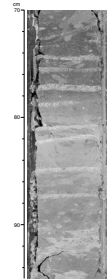
This subunit consists of alternating meter- to decimeter-thick intervals of (1) dark yellowish brown to grayish brown nannofossil clay/claystone, and/or claystone with nannofossils, and/or claystone (at the base of the subunit), and (2) lighter grayish orange to yellowish brown nannofossil ooze/chalk. A limited number of carbonate analyses from this unit indicate a range of values (36–83 wt%) similar to those of overlying Subunit IB. However, in Subunit IC there is a greater proportion (~66%) of thicker, darker, carbonate-poor beds. Smear slide estimates of composition (see “Site 1208 Smear Slides,” p. 43) indicate that the darker beds are relatively clay rich (50%–93%) and carbonate poor (0%–50%), with traces of volcanic glass and up to a few percent radiolarians. Lighter beds contain less clay (5%–30%) and more nannofossils (60%–90%). Both light and dark layers contain trace to minor amounts of zeolites (phillipsite?), foraminifers (trace–10%), and opaque minerals, including iron oxides.

Subunit IC is characterized by variable bioturbation, from abundant to rare. Discrete trace fossils include *Zoophycos*, *Planolites*, and composite burrows. Downsection, contacts between lighter and darker intervals become less bioturbated and sharper. In addition, the darker lithologies become increasingly depleted in carbonate, culminating in barren claystone at the base of Section 198-1208A-36X-CC (see Fig. F17), just above the unconformity that also serves as the Unit I/II boundary (Section 198-1208A-36X-CC, 25 cm). Biostratigraphic data indicate that this is a condensed section (see “Biostratigraphy,” p. 16). A digital image across the unconformity and into the base of a condensed section is shown in Figure F15, along with the magnetic susceptibility and reflectance records.

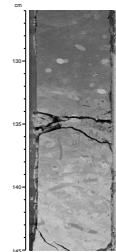
### Lithologic Unit II

Interval: 198-1208A-36X-CC, 25 cm, to 42X-CC, 25 cm  
Depth: 327.66–392.3 mbsf  
Age: Campanian to Albian

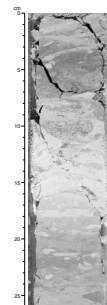
F12. *Zoophycos*, *Chondrites*, and *Planolites* burrows, p. 46.



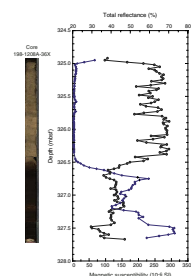
F13. Distinct *Planolites* burrows and example of “abundant” level of bioturbation where 100% of surface is burrowed, p. 47.



F14. Composite burrow and less distinct *Zoophycos* and *Planolites* burrows, 0–26 cm, p. 48.



F15. Composite digital photograph, color reflectance, and magnetic susceptibility, Core 198-1208A-36X, p. 49.



Unit II consists of relatively pure nannofossil ooze with minor (<1%) chert. The overall recovery rate is 54%, with better core recovery in chert-free intervals. The chert hampered drilling rates and reduced the downhole recovery rate to 0.03%. Generally the core in Unit II appeared undisturbed except in areas where chert had been fragmented (drilling breccia).

The ooze has an average carbonate content of 96 wt%, making this a relatively pure pelagic unit. In addition to the dominant nannofossil component, smear slide estimates of sediment composition (see “[Site 1208 Smear Slides](#),” p. 43) list minor (trace–5%) percentages of foraminifers, micrite, radiolarians, chert, and clay. The nannofossil ooze is dominantly very pale orange (10YR 8/2) but varies to pinkish gray (5YR 8/1) at the base. The chert fragments in the core range from yellowish to reddish brown in the Campanian section but are dominantly moderate reddish brown (5YR 5/4) in the Albian section (Core 198-1208A-42X). The only chalk in the working half of the core encrusted the surface of chert fragments, but in addition to chert fragments, the micropaleontology sample from the core catcher included 5 cm of whitish chalk.

The unit is generally moderately bioturbated, with burrow mottling but no identifiable trace fossils. Larger white blebs of nannofossil ooze may be burrow fills or diagenetic features. Two intervals in Core 198-1208A-41X contain fragments of *Inoceramus*: one interval is unconsolidated (fragmented during drilling?), and the other is cemented.

Unit II is relatively unconsolidated ooze that has undergone little cementation. However, authigenic carbonate (silt-sized, rod-shaped crystals) identified in smear slides may be incipient cement.

## Interpretation

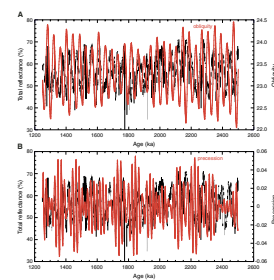
### Sedimentation

The homogeneous to moderately bioturbated nature of the Subunit IA sediment implies that it was deposited under oxic conditions. The prominent color and compositional cycles in Subunit IA are similar to those observed in Subunit IA at Site 1207. As at Site 1207, the prominent cyclicity within this unit is likely tied to variations in productivity and/or carbonate dissolution. However, at Site 1208 the cycles appear to be somewhat less dependent on variations in biosiliceous material and more dependent on the interplay between clay and calcareous nannofossil fluxes. The darker-colored intervals generally do contain somewhat greater amounts of reasonably well-preserved biosiliceous material than the light-colored intervals; thus, the former may represent periods of higher surface water productivity and higher clay input from zonal winds.

The cycle frequency in Unit I appears to be similar to that of glacial–interglacial cycles, with the dark beds representing glacial periods and the light beds representing interglacials. A preliminary analysis of the frequency of the dark–light cycles using color reflectance data (Fig. F16) suggests that the dominant period of the cycles corresponds to eccentricity (100 k.y.) from 0 to 0.8 Ma and obliquity (41 k.y.) for the period from 0.8 to 2.7 Ma, but a trend that represents the long period of eccentricity is superimposed on the latter cycles.

Regional studies (e.g., Natland, 1993) of ash distribution across the Shatsky Rise suggest that ash beds present in Subunit IA are wind-borne sediments that likely were carried to the site from volcanic eruptions

**F16.** Color reflectance plotted with obliquity, and precession, Hole 1208A, p. 50.



along the Japan and/or Kurile magmatic arc systems. The maxima and subsequent waning of ash input expressed in the frequency of ash beds in Table T2 could be linked to changes in volcanic activity along the arc systems or to changes in wind patterns over time. Isolated pumice clasts were most likely rafted to the site by surface currents (Kuroshio) that pass across the submerged, pumice-producing calderas of the Izu-Bonin magmatic arc to the west (described in Taylor et al., 1990) and flow directly over Shatsky Rise.

As in Subunit IB at Site 1207, the sediment of Subunit IB at Site 1208 is more oxidized, as indicated by the yellow to orange hues and an increase in the red/blue reflectance ratios. Cyclic dark and light intervals are present throughout the subunit, but the average thickness of the cycles (decimeter scale) is less than those in Subunit IA (meter scale). The low average sedimentation rate of 5.9 m/m.y. (Fig. F23) in combination with sediment color and composition suggests that, as at Site 1207, these oxidized sediments are products of lower surface water productivity, slower sediment accumulation, and/or carbonate dissolution. Note that the estimated sedimentation rate does not take into account the effects of sediment compaction, and thus these rates may have been slightly higher.

The condensed zone within Subunit IC (Fig. F17) probably reflects the influence of strong currents sweeping the top of the Central High and the effects of carbonate dissolution. These conditions probably prevailed during much of the Paleogene, preventing the accumulation of significant amounts of sediment. The CCD is estimated to have been at 3–3.3 km in the Pacific through much of the Paleogene and early Miocene, with the exception of the Oligocene when it deepened by 1 km (van Andel, 1977; Rea and Leinen, 1985; Rea et al., 1995). The condensed interval is slightly thicker at Site 1208 than at Site 1207, suggesting either less erosion or dissolution at Site 1208. Higher sedimentation rates at Site 1208 deterred the growth of authigenic phases such as manganese oxides (no macroscopic concretions), phillipsite (only minor amounts in smear slide estimates of composition), and chert (none observed in Unit I). The alternating carbonate- and clay-rich lithologies suggest that the process(es) responsible for slow sedimentation was somewhat cyclic, perhaps related to fluctuating CCD levels (discussed above) and/or intensity of erosional currents. Furthermore, the transitional nature of Subunits IC and IB suggests that the intensity of this process(es) gradually waned over time.

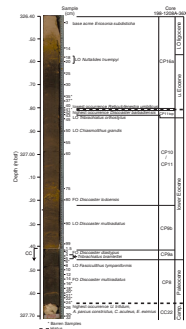
Unit II is a pelagic unit, deposited in open ocean conditions above the CCD.

## Diagenesis

The similarity of the lithologic units/subunits at Sites 1207 and 1208 is paralleled by their similar diagenetic features and histories: (1) in Subunit IA, the green-gray color, presence of pyrite, and “diagenetic laminae” and (2) formation of chert and lack of cementation in Cretaceous oozes (see “Diagenesis,” p. 17, in “Lithostratigraphy” in the “Site 1207” chapter for discussion of the origin of these features).

Additionally, ooze/chalk transitions at Site 1208 occurred sporadically throughout the Neogene sequence. This suggests that in a setting like the Shatsky Rise, the degree of ooze lithification (cementation) may be more tied to sediment composition (e.g., clay content and mineralogy, siliceous microfossils, organic content) and texture (degree of bioturbation, abundance of foraminifers) rather than to burial history (see

F17. Positions of nannofossil toothpick samples and age-diagnostic nannofossil datums, p. 51.



“Physical Properties,” p. 26, in the “Site 1210” chapter for further discussion).

### General Lithostratigraphy and Comparison to Site 1207

The lithologic units and subunit boundaries at Site 1208 roughly correlate with changes in sedimentation rate (see “Sedimentation and Accumulation Rates,” p. 22). The Campanian to Holocene section recovered at Site 1208 is in many ways similar to the section encountered at Site 1207 on the Northern High of Shatsky Rise; lithologic units are based on roughly parallel changes in sediment character, which correspond to similar breaks in rates of sedimentation. Two notable exceptions are the thicker condensed section above the Paleocene/Campanian unconformity (discussed previously) and the expanded Pliocene–Pleistocene section at Site 1208. Prior to ~3 Ma, sediment accumulation rates at Site 1208 (22.3 m/m.y.) were approximately the same as those at Site 1207 (18.4 m/m.y.), but after 3 Ma, the rates at Site 1208 increased to 42.4 m/m.y. (Fig. F23). This rate of sedimentation is surprisingly high and warrants further discussion.

Site 1208 is situated on the Central High of the Shatsky Rise. A seismic reflection profile across this site shows a stratified lens of sediment that extends from a canyon, which is interpreted as an erosional trough to the west and laps onto a sediment-covered basement high to the east. The seismic character of the sedimentary section, along with the very high sedimentation rates that prevailed during the Neogene–Quaternary, strongly suggest that the stratified lens of sediment is a drift deposit formed by current redistribution of sediment that settled on the Central High.

Whereas currents likely played a part in the formation of the Campanian/Paleocene unconformity and overlying Paleogene to Miocene condensed section (Subunit IC), there is no distinct sedimentological evidence (e.g., winnowed lags and contourites) to support drift deposition in the overlying section (Subunits IB and IA) at Site 1208. One exception may be the high-angle contacts in this uppermost part of Subunit IA; similar features on the Southern High of the Shatsky Rise have been interpreted as erosional features (e.g., Storms et al., 1991). Alternatively, evidence for winnowing, such as thin foraminiferal lags, could have been subsequently destroyed (dispersed) by burrowing organisms. But significant winnowing seems unlikely because, in the same intervals that are likely to have been affected by such currents (Subunit IA), bioturbation was not of sufficient intensity to completely disperse centimeter-scale ash beds. This analogy may not completely hold because it assumes that the burrowing organisms did not eschew the ash layers.

Perhaps the more classical contour deposits are concentrated within and adjacent to the trough, and Site 1208 received the fallout from current-generated fine-grained suspensions that drifted from the furrow to the east, most likely as a nepheloid layer. Such a mechanism should then have been active throughout the history of the drift, not only in the post–3 Ma portion of Subunit IA. Interestingly, there are post–3 Ma increases in the percentages of biosiliceous (Fig. F6), terrigenous (Fig. F6), and pyroclastic (Table T2) components at Site 1208. The concomitant increase in these components helps explain the high sedimentation rates across the post–3 Ma interval, but this rise in “background” sedimentation may not fully explain the magnitude of that increase. Alternatively, this site may have been situated in a favorable position with respect to atmospheric circulation patterns to receive a higher propor-

tion of eolian and/or ash components, as well as to preserve a higher proportion of siliceous microfossils from 3 Ma to the present.

The sediment drift deposits at Site 1208 are somewhat similar to those drilled along the Meiji Seamount on Leg 145 in that both comprise fine-grained sediment devoid of sedimentary structures except for bioturbation (Rea et al., 1993). Furthermore, the post-3 Ma sections at the Meiji sites are generally more enriched in glacially derived components (e.g., dropstones) and ash beds (Rea et al., 1995). However, these higher latitude sites experienced an earlier pulse in biosiliceous sedimentation in the Miocene to early Pliocene not recorded at Site 1208 (Rea et al., 1993, 1995); at Site 1208, this shift occurred in the late Pliocene and continued into the Pleistocene.

## **BIOSTRATIGRAPHY**

An apparently continuous middle Miocene to Pleistocene section of nannofossil ooze, chalk, and clay was cored in Hole 1208A. Calculated sedimentation rates are high for the Pleistocene to Pliocene (42.4 m/m.y.) but decrease in the lower Pliocene to upper Miocene (22.3 m/m.y.) and are low in the upper to middle Miocene (5.9 m/m.y.) (see [“Sedimentation and Accumulation Rates,”](#) p. 22). The middle Miocene (Sections 198-1208A-31X-CC through 34X-CC) overlies a predominantly condensed lower? Miocene to Paleogene claystone section (interval 198-1208A-35X-4, 50 cm, through 36X-CC, 24 cm), which is thought to contain at least three unconformities, separating lower Miocene to upper Oligocene (interval 198-1208A-35X-4, 50 cm, to 35X-5, 10 cm), lower Oligocene to uppermost Eocene (interval 198-1208A-35X-5, 50 cm, to 36X-2, 40 cm), and lower Eocene to upper Paleocene (interval 198-1208A-36X-2, 42 cm, to 36X-CC, 24 cm) sequences. The upper Paleocene brown claystone lies unconformably on white Campanian nannofossil ooze at the bottom of Section 198-1208A-36X-CC. A relatively complete mid- to lower Campanian section, in turn, lies unconformably on a middle Albian chalk and chert horizon recovered at the base of Hole 1208A.

The Miocene sediments overlying the uppermost condensed section and unconformity, and the Campanian sediments underlying the penultimate unconformity are identical in age to sediments observed on either side of the major unconformity at Site 1207, suggesting a sedimentation and/or erosional history of regional significance.

All core catcher samples were examined, and supplementary samples were used to refine the stratigraphy of the condensed intervals and unconformities. Calcareous nannofossils are generally abundant and moderately to well preserved in Neogene and Cretaceous sediments. The condensed claystone intervals generally yield etched assemblages dominated by robust taxa or occasional barren samples. In general, Neogene planktonic foraminifers are moderately to well preserved, but foraminiferal abundances are relatively low, due to selective dissolution and fragmentation. Cretaceous planktonic foraminifers are well preserved and abundant.

Studies of benthic foraminifers were conducted on selected core catcher samples. Neogene benthic foraminifers are well preserved and rare to common in abundance; Paleogene and Cretaceous forms are moderately well preserved and rare. The 125- to 250- $\mu\text{m}$  size fraction was examined when specimens were too rare in the 250- $\mu\text{m}$  size fraction.

## Calcareous Nannofossils

### Neogene

The Neogene section ranges from upper Pleistocene (Zone CN15) to lower Miocene (Zone CN1) and appears to be relatively complete, at least within the biostratigraphic resolution achieved on board ship (Table T3). Nannofossils are abundant throughout, and preservation is moderate to good. A short hiatus may be present at the base of the Miocene. Most of the zones of Okada and Bukry (1980) were recognized, but division at subzonal level was not always possible. Though they were relatively rare, sphenoliths and discoasters occur in greater abundance relative to the Site 1207 assemblages. This slight increase in abundance may be due to closer proximity to tropical latitudes.

The thick Pliocene–Pleistocene section was subdivided using the standard Okada and Bukry (1980) markers. We were not able to identify the Pleistocene *Gephyrocapsa* subzonal events (first occurrence [FO] *Gephyrocapsa caribbeanica* and *Gephyrocapsa parallela*), due to difficulties in discerning these two taxa from the other species of *Gephyrocapsa* and *Reticulofenestra* that are present in the assemblages. Notably, *Reticulofenestra asanoi* and small reticulofenestrids are particularly abundant in Samples 198-1208A-6H-CC and 7H-CC; the former has a short range across the CN13/CN14 boundary.

The middle to upper Miocene section was divided using datums based on species of *Catinaster*, *Discoaster*, and *Amaurolithus*, but *Discoaster kugleri*, *Discoaster hamatus*, and *Discoaster loeblichii* were not observed.

The oldest Neogene section is difficult to date and subdivide, because of the paucity of the sphenoliths, which are used to define the top and bottom of Zone CN2 and the bottom of CN5. These assemblages are directly comparable with those from the lower Neogene of Holes 1207A and 1207B, being characterized by low diversity, high abundances of *Discoaster deflandrei* and *Cyclicargolithus floridanus*, the presence of *Calcidiscus premacintyreii*, and occasional occurrences of the marker taxon *Sphenolithus heteromorphus*. Samples 198-1208A-32X-CC and 33X-CC contain both *Cyclicargolithus floridanus* and large (<7 µm) *Reticulofenestra pseudoumbilicus*, indicating a Subzone CN5a age; the former taxon may be somewhat unreliable but is not thought to range above Zone CN5 (Young, 1998). Samples 198-1208A-34X-CC and 35X-4, 12 cm, contain *Sphenolithus heteromorphus*, indicating Zones CN3 and CN4. Sample 198-1208A-35X-4, 50 cm, was assigned to Zone CN1 based on the presence of *Triquetrorhabdulus carinatus* and the absence of *Cyclicargolithus abisectus* (Young, 1998); rare specimens of *Reticulofenestra bisectus* and *R. umbilica* in this sample and a number of underlying samples are considered to be reworked.

### Paleogene

The Paleogene is represented by etched assemblages dominated by robust taxa but generally including useful marker species. The nannofossil biostratigraphy indicates a number of condensed intervals including the upper Oligocene, lower Oligocene–uppermost Eocene, and lower Eocene–upper Paleocene, bounded by short unconformities.

Samples 198-1208A-35X-4, 99 cm, to 35X-4, 10 cm, are correlated to Subzone CN1a–Zone CP19 (basal Miocene to upper Oligocene) based on the presence of *Cyclicargolithus abisectus*; however, precise dating of

---

T3. Calcareous nannofossil datums, ages, and depths, p. 80.

---

the interval is hampered by the absence of sphenoliths and the presence of reworked taxa, such as *Reticulofenestra umbilica*. Zones CP17 and CP18 (lower Oligocene) were not identified, and a short unconformity may be present in this interval.

Interval 198-1208A-35X-5, 50–51 cm, to 36X-2, 30 cm, is assigned to Zone CP16 (lowermost Oligocene to uppermost Eocene) with all three subzones identified by the absence of *Discoaster saipanensis* and *Discoaster barbadiensis*, the top acme of *Ericsonia subdisticha* (Sample 198-1208A-36X-1, 70 cm), the LO of *Coccolithus formosus* (Sample 198-1208A-35X-CC), and the continued presence of common *Reticulofenestra umbilica*, respectively. Zones CP12 to CP15 (middle to upper Eocene) were not identified, and an unconformity is likely to correspond to this interval.

The deepest Paleogene interval is restricted to Sections 198-1208A-36X-2 and 36X-CC and rests unconformably on Campanian sediment at the base of Section 36X-CC (Fig. F17). The assemblages are poorly to moderately preserved and pervasively etched and consequently dominated by large and robust taxa. Within this interval, the FO of *Discoaster lodoensis* defines the base of Zone CP10 and the LO of *Tribrachiatus orthostylus* occurs toward the top of Zone CP11.

The assemblages in samples toward the base of the Paleogene show some degree of mixing that may be due to downhole contamination during drilling or core handling and/or a small amount of reworking. The contaminated component can be separated from the in situ component by observing continuity of ranges; contaminated taxa tend to be more abundant upsection and are discontinuously present. Three events that are thought to lie close to the Paleocene/Eocene boundary, the LO of the genus *Fasciculithus* and the FOs of *Tribrachiatus bramlettei* and *Discoaster diastypus*, are present within 6 cm of each other in Section 198-1208A-36-CC (Fig. F17). These events lie just within or just above the PETM and are separated by ~330 k.y. (Bralower et al., 1995; Aubry et al., 1996). The lowermost 10 cm of the Paleocene section is barren.

## Cretaceous

The Cretaceous section ranges from upper Campanian (Zone CC22) to middle Albian (Subzone NC8c). Much of the mid- to lower Campanian was recovered; drilling was terminated below an unconformity in a chert-rich interval of middle Albian age. The nannofossils are generally abundant and moderately well preserved, but the single Albian sample (198-1208A-42X-CC) displayed poor to moderate preservation. Moderate overgrowth is present in all samples of Cretaceous age, and etching is prevalent in the Albian sample.

The relatively common and consistent presence of the *Aspidolithus parvus* coccoliths and *Ceratolithoides* and *Uniplanarius* nannoliths in the upper part of the Upper Cretaceous section allowed confident subdivision of the Campanian (Table T3). Zones CC18 to CC19 could not be completely subdivided, due to the absence of the nannolith *Marthasterites furcatus*.

The single Albian sample (198-1208A-42X-CC) is placed in Subzone NC8c based on the presence of *Tranolithus orionatus*, *Eprolithus floralis*, and *Prediscosphaera columnata* and the absence of *Axopodorhabdus albianus*.

## Planktonic Foraminifers

### Neogene

Planktonic foraminiferal abundance varies from abundant to common through the Pleistocene and upper Pliocene but declines in the Miocene to few to rare relative to siliceous microfossils and clay. Like Site 1207, temperate-water species dominate many of the Neogene planktonic foraminiferal assemblages at Site 1208. The abundance of the upwelling indicator species *Globigerina bulloides*, together with an abundance of diatoms, radiolarians, and a diverse benthic fauna consisting of benthic foraminifers, echinoderms, ostracodes, and sponges, suggest that (seasonal) productivity was high over this site during much of the Pliocene and Pleistocene. Productivity may have also varied cyclically, as suggested by the pronounced decimeter-scale lithologic cycles observed in lithologic Unit I (see “**Lithostratigraphy**,” p. 9).

Many biostratigraphically useful tropical-subtropical taxa are present in low to moderate abundances, including *Globorotalia menardii*, *Globorotalia tumida*, *Globorotalia plesiotumida*, and *Paragloborotalia mayeri* (Table T4). In addition, secondary marker taxa are used to make biostratigraphic assignments and/or confirm zonal assignments. For example, the LOs of *Globigerinoides extremus*, *Dentoglobigerina altispira*, *Sphaeroidinellopsis seminulina*, *Globorotalia margaritae*, and *Globoturborotalita nepenthes*, and the FOs of *Globorotalia crassaformis*, *Globoconella puncticulata*, and *Globoconella conomiozea* are used to delineate positions within Zones N21 and N19–N20. The FOs of *Globorotalia margaritae* and *Globigerinoides conglobatus* are useful within Zone N17.

Common Pliocene–Pleistocene taxa include *Globigerina bulloides*, *Globorotalia inflata*, *G. crassaformis*, *G. puncticulata*, *G. conomiozea*, *Neogloboquadrina dutertrei*, and *Neogloboquadrina pachyderma* (dextral). Persistent late Miocene taxa include *Orbulina universa*, *Neogloboquadrina acostaensis*, *Sphaeroidinellopsis seminulina*, and *Globoturborotalita nepenthes*. A marked decrease in the number of taxa and specimens characterizes the middle Miocene sediments (Sections 198-1208A-32X-CC to 34X-CC), which contain few orbulinids, *Globoquadrina dehiscens*, *Globigerina venezuelana*, *S. seminulina*, *Sphaeroidinellopsis disjuncta*, and rare *Globoconella conoidea*, *Globoconella miozea*, and *Paragloborotalia mayeri*. Based on the absence of *G. nepenthes* and the presence of *O. universa*, this assemblage is interpreted to lie within Zones N13 to N9. The underlying Section 198-1208A-35X-CC yields rare *Tenuitella gemma*, *Globorotaloides suteri*, and *Tenuitellinata angustiumbilicata*, suggesting the lower Oligocene Zone P18.

### Cretaceous

The mid- to lower Campanian nannofossil ooze and chalk recovered at Site 1208 contains generally abundant and well-preserved assemblages of planktonic foraminifers. The composition of the assemblages is similar to those recovered at Site 1207. The upper boundary of the Campanian at both sites is truncated at the same age, ~75.7–76.0 Ma, based on the absence of *Radotruncana calcarata* and presence of *Globotruncanita atlantica*. Common taxa through this Campanian sequence include *Archaeoglobigerina cretacea*, *Contusotruncana fornicata*, *Contusotruncana patelliformis*, *Globigerinelloides messinae*, *G. cf. Globigerinelloides prairiehillensis*, *Globotruncana arca*, *Globotruncana linneiana*, *Globotruncana orientalis*, *Globotruncanita stuartiformis*, *Globotruncanita subspinosa*, *Hedbergella holmdelensis*, *Heterohelix carinata*, *Heterohelix globulosa*, *Laevi-*

---

T4. Planktonic foraminifer datums, ages, and depths, p. 81.

---

*heterohelix pulchra*, *Pseudoguembelina costulata*, *Pseudotextularia nuttalli*, and *Rugoglobigerina rugosa*. The FO of *Globotruncanita atlantica* serves to distinguish the *Globotruncanita ventricosa* Zone (Zone KS26) in Sections 198-1208A-36X-CC to 39X-CC from the *Globotruncanita elevata* Zone (Zone KS25) in Sections 198-1208A-40X-CC to 41X-CC. A major unconformity separates the lower Campanian and middle Albian strata.

Site 1208 terminated in middle Albian chert-bearing chalk of the *Ticinella primula* Zone (Zone KS13). Common taxa include *T. primula*, *Ticinella roberti*, *Ticinella raynaudi*, *Hedbergella planispira*, *Hedbergella delrioensis*, and *Hedbergella rischi* in the absence of *Biticinella breggiensis*. A similar assemblage was recovered at Site 1207. The large size and diversity of the ticinellids indicates that these sediments represent the upper part of the *T. primula* Zone.

## Benthic Foraminifers

### Neogene and Paleogene

In the interval representing the Pleistocene to early Pliocene (Samples 198-1208A-1H-CC through 21X-CC), the main components of benthic foraminifers are calcareous trochospiral and planispiral species (*Oridorsalis tener*, *Pullenia bulloides*, cibicidoidids, *Nonion* spp., and gyroidinoidinids), uvigerinids (*Uvigerina hispidocostata* and *Uvigerina hispida*), miliolids (*Pyrgo lucernula* and *Pyrgo murrhina*), and *Eggerella bradyi* (Table T5).

In Sample 198-1208A-23X-CC, uvigerinids are absent. Trochospiral forms, together with abundant *Globocassidulina subglobosa*, *Pyrgo murrhina*, and *Eggerella bradyi*, characterize the benthic assemblage. The benthic assemblage in Sample 198-1208A-24X-CC is dominated by *Oridorsalis tener*, *Cibicidoides cicatricosus*, *Cibicidoides wuellerstorfi*, *Cibicidoides* spp., *Gyroidinoides girardanus*, *Gyroidina neosoldanii*, *Nonion* spp., *Melonis barleanus*, *Pullenia bulloides*, and abundant *Globocassidulina subglobosa*, *Pyrgo murrhina*, and *Eggerella bradyi*. Uvigerinids are present again and dominate the benthic assemblage in Sample 198-1208A-25X-CC. Other characteristic forms are *Stilostomella abyssorum*, *Stilostomella subspinosa*, *O. tener*, *C. cicatricosus*, *Cibicidoides* spp., *G. girardanus*, *G. neosoldanii*, and *Eggerella bradyi*.

Abundant stilostomellids (*Stilostomella abyssorum*, *Stilostomella* spp., and *S. subspinosa*) replace uvigerinids in Sample 198-1208A-29X-CC. Other components are generally the same as in Sample 198-1208A-25X-CC, although the miliolids decrease in abundance.

In Sample 198-1208A-31X-CC, the stilostomellids (*Stilostomella abyssorum*, *Stilostomella* spp., and *S. subspinosa*) are again common. Other characteristic species are *Oridorsalis tener*, *Anomalinooides globulosus*, *Cibicidoides praemundulus*, *Cibicidoides* spp., *Gyroidinoides neosoldanii*, *G. girardanus*, *Pullenia bulloides*, *Dentalina* spp., *Pyrgo murrhina*, *Martinottiella* sp., and *Eggerella bradyi*. In Sample 198-1208A-34X-CC, the stilostomellids remain dominant, but some changes are observed in the representatives of the calcareous trochospiral and planispiral taxa (*Anomalinooides globulosus*, *Oridorsalis umbonatus*, *O. tener*, *Cibicidoides mundulus*, and *Pullenia bulloides*) and the agglutinated species *Vulvulina spinosa*.

In Sample 198-1208A-36X-2, 18–20 cm, only *Vulvulina spinosa* and *Vulvulina mexicana* are present in the >250- $\mu$ m size fraction. In the 125- to 250- $\mu$ m size fraction, trochospiral species (*Nuttallides truempyi*, *Cibicidoides bradyi*, *C. praemundulus*, *Cibicidoides subspiratus*, *Cibicidoides* spp., *Oridorsalis umbonatus*, and *O. tener*), *Stilostomella subspinosa*, and *Stilos-*

---

T5. Cenozoic and Cretaceous benthic foraminifers, p. 82.

---

*tomella* spp. characterize the benthic assemblage. The LO of *N. truempyi* slightly precedes the Eocene/Oligocene boundary, and therefore its presence in Sample 198-1208A-36X-2, 18–20 cm, indicates that the top of the condensed interval is older than the Oligocene.

Pleistocene to middle Miocene benthic foraminifers indicate upper abyssal paleowater depths (2000–3000 m) (Pflum et al., 1976; Tjalsma and Lohmann, 1983; Woodruff, 1985; van Morkhoven et al., 1986).

### Cretaceous

No benthic foraminifers were found in Sample 198-1208A-36X-CC (Campanian age). In Sample 198-1208A-37X-CC, the benthic assemblage is characterized by *Oridorsalis umbonatus*, osangulariids (*Osangularia plummerae*, *O. mexicana*), *Nuttallides truempyi*, and *Sliterella lobulata*, *Dentalina* spp., *Pleurostomella* spp., *Gaudryina pyramidata*, and *Marssonella trochoides*. Abundant *Pyramidina szajnochae* and trochospiral forms such as *O. umbonatus*, *S. lobulata*, *Gyroidinoides globosus*, *Gyroidinoides infracretaceus*, *Conorbinoides hillebrandti*, and *Serovaina spissiformis* dominate Sample 198-1208A-39X-CC. In Sample 198-1208A-41X-CC, the benthic assemblage is represented by trochospiral forms (*C. hillebrandti*, *O. umbonatus*, *N. truempyi*, *Nuttallinella florealis*, *S. spissiformis*, and *Osangularia plummerae*), *Aragonia velascoensis*, *Aragonia ouezzanensis*, *Bulimina* spp., *Lenticulina* spp., and *Pleurostomella* spp., together with abundant agglutinated taxa, including *G. pyramidata* and *M. trochoides*.

Sample 198-1208A-42X-CC of middle Albian age is characterized by abundant trochospiral benthic forms of *Protosangularia albiana*, *G. infracretaceus*, and *Pseudoclavulina rugolosa*. Other components are *Protosangularia cenomaniensis*, buliminids, nodosariids, and *Remesella* spp.

The Cretaceous benthic assemblages at Site 1208 are similar to those recorded at Site 1207 and suggest the same deepening trend from upper lower bathyal (~1000- to 1500-m paleowater depth) in the Albian to upper abyssal (~2000- to 3000-m paleowater depth) by the Campanian.

## PALEOMAGNETISM

As at Site 1207, all archive halves of core sections from Hole 1208A that did not show a large degree of drilling-related deformation were measured on the shipboard pass-through magnetometer. Many of the measured cores from the Paleogene and Cretaceous part of the section, however, are in poor condition, due to either drilling disturbance or disturbance induced during the splitting of core sections. In addition to the 20 APC cores (198-1208A-1H through 20H), measurements included 18 of 21 XCB cores (only Cores 198-1208A-34X through 36X were not measured). Many of the XCB cores showed “biscuiting” (fragmentation) into segments several centimeters to tens of centimeters in length. This deformation has the potential to render the pass-through magnetometer data useless, owing to the averaging of divergent magnetic vectors when several “biscuits” and/or intervening drilling slurry are in the instrument sensing region. Many XCB cores, however, displayed consistent remanence inclination data that implied the measurements were worthwhile.

The natural remanent magnetization (NRM) of core sections was measured at 5-cm intervals and at two alternating-field (AF) demagnetization steps (10- and 20-mT peak fields). When time was available, ad-

ditional AF demagnetization steps (usually at peak fields of 15 mT) were measured. NRM measurements typically ranged over two orders of magnitude in intensity, from  $10^{-3}$  to  $10^{-1}$  A/m, but several spikes in cores from near the bottom of the hole reached values as high as 5.8 A/m (Fig. F18). NRM inclinations uniformly showed steep downward directions indicative of a drill-string induced overprint. This overprint was progressively removed with AF demagnetization, typically disappearing by the 15- to 20-mT demagnetization step. After 20-mT demagnetization, magnetization intensities mostly ranged from  $10^{-4}$  to  $10^{-2}$  A/m. In the upper 90 mbsf, magnetization intensities declined by about a factor of 10, with short wavelength variations superimposed (Fig. F18).

The AF demagnetized magnetization directions have inclination values clustering around  $\pm 55^\circ$ , the geocentric axial dipole value for the location of Site 1208. Changes between positive and negative inclination were compared with declination values to identify magnetic reversals. In the APC cores (0–185 mbsf), the data give an expanded magnetostratigraphic record, showing all of the polarity chrons in the Cande and Kent (1995) timescale from C3n (Gilbert) to C1n (Brunhes) (Fig. F19). Magnetic chron depths indicate that the sedimentation rate increased through the Miocene and Pliocene–Pleistocene, eventually reaching rates as high as 40 m/m.y. during the last 3 m.y. (Fig. F20). Pliocene–Pleistocene magnetic records of comparable resolution are available for the Atlantic realm; however, this record is unique for the Pacific.

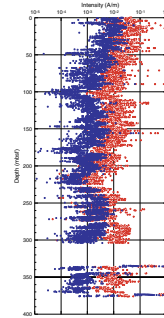
In the XCB-cored section, below 185 mbsf, the polarity record is more difficult to interpret because the cored record is not continuous and the data are noisier as a result of the core deformation. Nevertheless, we interpret a long reversed polarity interval just below 200 mbsf as Chron C3r and a long normal polarity interval at ~275 mbsf as Chron C5n. Other intervals of normal and reversed polarity are interpreted between C2r and C5n and correlated to other Miocene polarity chrons, but with less certainty (Fig. F19).

## SEDIMENTATION AND ACCUMULATION RATES

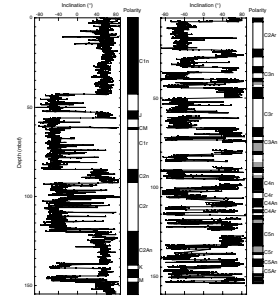
Unconformities and changes in sedimentation rate in Hole 1208A are illustrated in a plot of calcareous microfossil datum ages (first and last occurrences) vs. depth (Fig. F21). These rates rely on major calcareous nannofossil and planktonic foraminiferal datums presented in Tables T3 and T4. The Pleistocene–middle Albian section cored at Site 1208 is punctuated by three condensed intervals and at least four unconformities. Condensed intervals in the lower Miocene to lower Oligocene and uppermost Eocene and in the lower Eocene to uppermost Paleocene accumulated at rates of ~0.08–0.09 m/m.y (Fig. F22)

An expanded view of the Neogene (Fig. F23) shows that the upper lower Miocene–lower upper Miocene part of the section accumulated at an average rate of 5.9 m/m.y., increasing to 22.3 m/m.y. in the upper Miocene–basal Pliocene, and 42.4 m/m.y. in the lower Pliocene–Pleistocene interval. Dark-colored, clay-rich sediments in Section 198-1208A-35X-4 and in the upper part of Section 35X-5 represent a condensed interval spanning the lower Miocene to lower Oligocene (Fig. F24). Calcareous nannofossil data suggest the presence of an unconformity separating the condensed lower Miocene–lower Oligocene interval and basal Oligocene nannofossil ooze (Fig. F24). The basal Oligocene ooze accumulated at an average rate of 4.2 m/m.y.

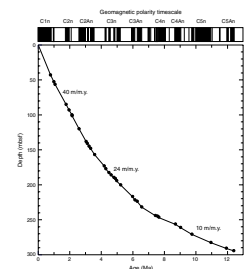
F18. Archive-half magnetization intensities prior to and after AF demagnetization at peak fields of 20 mT, Hole 1208A, p. 52.



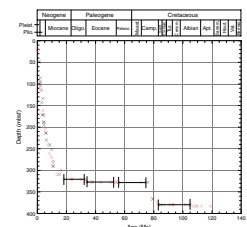
F19. Inclination after AF demagnetization at peak fields of 20 mT, Hole 1208A, p. 53.



F20. Age-depth curve derived from magnetic stratigraphy p. 54.



F21. Age-depth plot of calcareous nannofossil and planktonic foraminiferal datums, Hole 1208A, p. 55.



Dark-colored sediments in interval 198-1208A-36X-2, 10 cm, through 36X-CC, 25 cm, contain a condensed uppermost Eocene sequence, supported by the occurrence of the benthic foraminifer *Nuttallides truempyi* in interval 198-1208A-36X-2, 18–20 cm, unconformably overlying a condensed section of lower Eocene–uppermost Paleocene. A major Eocene unconformity occurs within this condensed section between Samples 198-1208A-36X-2, 42 and 43 cm (see Fig. F17).

A major unconformity at Sample 198-1208A-36X-CC, 25 cm, separates the condensed lower Eocene–uppermost Paleocene interval from mid-Campanian nannofossil ooze. The mid- to lower Campanian part of the section accumulated at a nearly constant rate of ~10.4 m/m.y. (Fig. F25). Another unconformity separates the lower Campanian and middle Albian in Core 198-1208A-42X. The middle Albian chalk recovered in Sample 198-1208A-42X-CC is from the upper *Ticinella primula* Zone, suggesting that Hole 1208A terminated in strata older than 105 Ma and probably not older than 107–108 Ma (see “Biostratigraphy,” p. 16).

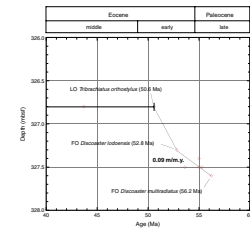
Mass accumulation rates for the bulk sediment, carbonate, and non-carbonate fractions were calculated using dry bulk density (see “Index Properties,” p. 31, in “Physical Properties”) and carbonate concentration (see “Organic Geochemistry,” p. 24) data through three linear sedimentation rate segments in the Neogene (Fig. F23). These segments were chosen to reflect the major changes in sedimentation rate. The three segments are (1) 0–166.66 mbsf (lower Pliocene–Pleistocene), (2) 166.66–256.71 mbsf (upper Miocene–lower Pliocene), and (3) 256.71–314.17 mbsf (middle Miocene–upper Miocene).

Accumulation rates in the lowermost interval examined (256.1–314.17 mbsf; middle Miocene–upper Miocene) are relatively low and show little temporal change (Fig. F26). Bulk sediment accumulation rates average 0.54 g/cm<sup>2</sup>/k.y. Average accumulation rates of the carbonate (0.3 g/cm<sup>2</sup>/k.y.) and noncarbonate (0.2 g/cm<sup>2</sup>/k.y.) fractions suggest that the contribution from each of these fractions was nearly equal throughout this interval.

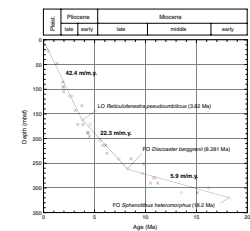
Increased accumulation rates are associated with a higher average sedimentation rate between 3.82 and 8.28 Ma (166.66–256.71 mbsf). The upper Miocene–lower Pliocene bulk sediment accumulation rates average 1.8 g/cm<sup>2</sup>/k.y. The average rates at which the carbonate and noncarbonate fractions accumulated during this interval are 1.2 and 0.6 g/cm<sup>2</sup>/k.y., respectively, indicating an increased contribution to the sediment column from the carbonate fraction.

The bulk sediment accumulation rates of the lower Pliocene–Pleistocene interval average 3.11 g/cm<sup>2</sup>/k.y. (Fig. F26) but decrease overall from ~3.2 g/cm<sup>2</sup>/k.y. (lower Pliocene) to ~2.4 g/cm<sup>2</sup>/k.y. (Pleistocene). Although quite variable, average accumulation rates for the carbonate and noncarbonate fractions (1.5 and 1.4 g/cm<sup>2</sup>/k.y., respectively) suggest that the overall contribution of each of these fractions to the bulk sediment was approximately equal throughout late early Pliocene–Pleistocene time (Fig. F26). Because the accumulation rate for the carbonate fraction shows relatively little change from the underlying interval, the data suggest that the increase in sedimentation rates beginning in late early Pliocene time are related primarily to an increase in the contribution of the noncarbonate fraction. Although there is an increase in the biogenic silica component, possibly indicating an increase in biologic productivity, the major noncarbonate constituent through this interval is detrital clay and silt (see “Lithostratigraphy,” p. 9). These observa-

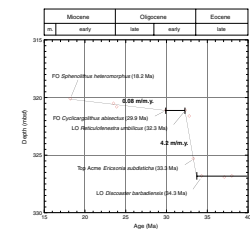
F22. Age-depth plot of middle Eocene–late Paleocene calcareous nannofossil and planktonic foraminiferal datums, Hole 1208A, p. 56.



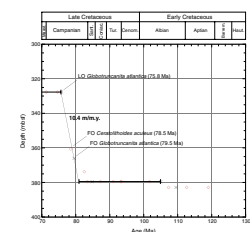
F23. Age-depth plot of Neogene calcareous nannofossil and planktonic foraminiferal datums, Hole 1208A, p. 57.



F24. Age-depth plot of early Miocene–late Eocene calcareous nannofossil and planktonic foraminiferal datums, Hole 1208A, p. 58.



F25. Age-depth plot of Cretaceous calcareous nannofossil and planktonic foraminiferal datums, Hole 1208A, p. 59.



tions are consistent with the character of seismic reflection profiles over the Central High of Shatsky Rise, which suggest that the Neogene sequence penetrated at Site 1208 is a drift deposit.

## ORGANIC GEOCHEMISTRY

### Volatile Hydrocarbons

Headspace gas analysis was conducted as part of the standard protocols required for shipboard safety and pollution prevention monitoring. A total of 38 cores from Hole 1208A were evaluated (Table T6). The concentrations of CH<sub>4</sub> were low ( $\leq 10 \mu\text{L/L}$  [ppmv]), and no hydrocarbon gases higher than C<sub>1</sub> were detected. The downhole profile of CH<sub>4</sub> concentration shows a subsurface maximum in gas concentrations from ~50 to 200 mbsf in Subunit IA that is associated with a minimum in sulfate concentrations. At shallower depths (upper 52 mbsf), CH<sub>4</sub> generation increases exponentially as sulfate is depleted, a trend exemplified by the strong inverse correlation ( $R^2 = 0.959$ ) between CH<sub>4</sub> and sulfate concentrations (Fig. F27). At greater depths (below 239 mbsf), CH<sub>4</sub> concentrations decrease toward background levels, whereas sulfate concentrations remain at 21–23 mM.

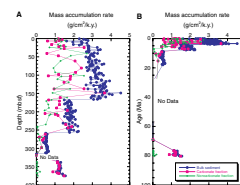
Significant production of CH<sub>4</sub> by methanogenesis generally does not occur until sulfate is depleted by bacterial sulfate reduction (Martens and Berner, 1974; Claypool and Kvenvolden, 1983). Exceptions to this principle have been noted recently in carbonate sediments (Mitterer et al., 2001), providing further convincing evidence that the two microbial processes are not necessarily exclusive (Oremland and Taylor, 1978; Oremland et al., 1982). At Site 1208 the coincidence of the peak in CH<sub>4</sub> concentrations with the minimum in sulfate concentrations is consistent with co-occurring sulfate reduction and methanogenesis, albeit at subsistence levels.

Examination of data from analyses of hydrocarbon gases and interstitial waters at other sites reveals other occurrences of coincident CH<sub>4</sub> generation and sulfate depletion in carbonate sequences. The depth trend relationships at Site 1208 show marked similarities to Sites 846 and 849 in the eastern equatorial Pacific (Shipboard Scientific Party, 1992a, 1992b) (Fig. F28): an initial rise in CH<sub>4</sub> concentrations with increasing depth coupled with a concomitant decline in sulfate concentrations, followed successively by a zone of elevated CH<sub>4</sub> concentrations and a subsequent decrease in CH<sub>4</sub> accompanying an increase in sulfate concentrations (Fig. F28). The trend is also similar to that observed at shallow depths at Site 1009 (Shipboard Scientific Party, 1997). All four sites show similar inverse exponential correlations between CH<sub>4</sub> and sulfate concentrations in the upper 50–80 m.

### Carbonate

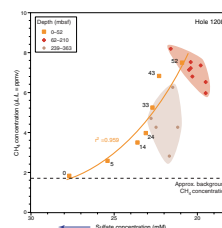
Carbonate determinations by coulometry were made for a total of 108 samples from Hole 1208A (Table T7). Samples were selected to provide a measure of the carbonate content within different units and to assess the influence of content on color reflectance. The values for carbonate range from 10 to 89 wt% (Table T7) in Unit I, reflecting variations in the relative proportions of clay, biogenic silica, and carbonate. The carbonate content profile shows alternating values downcore (Fig.

F26. Mass accumulation rates vs. depth and age for the Neogene, Hole 1208A, p. 60.

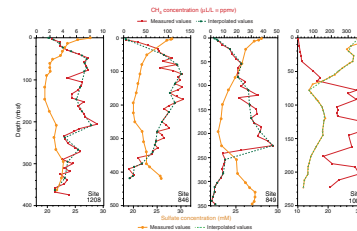


T6. Headspace CH<sub>4</sub> concentrations, p. 84.

F27. Decreasing sulfate vs. CH<sub>4</sub> concentrations, p. 61.



F28. CH<sub>4</sub> vs. sulfate concentrations at Sites 1208, 846, 849, and 1009, p. 62.



T7. Carbonate content, p. 85.

F29). The variations observed are primarily an artifact of the dominant criterion for sample selection: namely the choice of intervals that are representative of extremes in color and lithology. Carbonate contents are high (~97 wt%) and show little variability in the calcareous oozes of the Campanian (Unit II), comparable to Site 1207.

### Assessment of Extractable Hydrocarbons

Analysis of extractable organics in Sample 198-1208A-1H-1, 68–69 cm, revealed trace amounts of *n*-alkanes in the C<sub>25+</sub> range, extending to C<sub>33</sub> with pronounced odd/even predominance. This profile is characteristic of vascular plant waxes and suggests contributions from eolian dust (Simoneit, 1978; Zafiriou et al., 1985; Gagosian and Peltzer, 1986; Gagosian et al., 1987). No other components could be detected from the small sample size (~1 g), and the low yield of extractable organics precluded effective investigations of lipid components in other samples.

## INORGANIC GEOCHEMISTRY

### Interstitial Water Chemistry

At Site 1208, 20 interstitial water samples were collected; 11 samples between 0 and 90.2 mbsf (one sample per core) and 9 between 118.7 and 363.4 mbsf (approximately one sample every three cores). Details of analytical methods are provided in “**Inorganic Geochemistry**,” p. 21, in the “Explanatory Notes” chapter. Filtered (0.45 μm) samples were analyzed for pH, salinity, chlorinity (Cl<sup>-</sup>), alkalinity, sulfate (SO<sub>4</sub><sup>2-</sup>), phosphate (HPO<sub>4</sub><sup>2-</sup>), ammonium (NH<sub>4</sub><sup>+</sup>), silica (Si(OH)<sub>4</sub>), boron (H<sub>3</sub>BO<sub>3</sub>), iron (Fe<sup>2+</sup>), manganese (Mn<sup>2+</sup>), and major cations (Na<sup>+</sup>, K<sup>+</sup>, Mg<sup>2+</sup>, Ca<sup>2+</sup>, Li<sup>+</sup>, Sr<sup>2+</sup>, and Ba<sup>2+</sup>). A compilation of data is provided in Table T8. Cited values for average seawater composition are from Millero and Sohn (1992) and Broecker and Peng (1982); values for North Pacific Deep Water composition are from Rea et al. (1993).

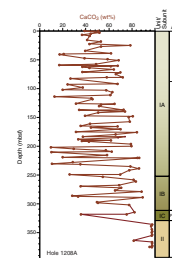
The interstitial water samples span the range of sediments in lithologic Units I (0.0–328.15 mbsf) and II (328.15–392.3 mbsf). The major lithologic trends that affect pore water chemistry include a transition from nannofossil clay and ooze to nannofossil chalk (Subunit IA/IB boundary) and the subsequent appearance of clayey sediments (Subunit IC [311.65–328.15 mbsf]). Throughout Units I and II there are intermittent occurrences of pyrite and volcanic ash. In Unit II, nannofossil ooze is the dominant lithology and chert is common.

### pH, Salinity, Chlorinity, and Sodium

The pH decreases downcore from a value of 7.51 in the shallowest sample to 7.19 at 147.2 mbsf (Table T8). Subsequently, the pH abruptly increases to 7.47 at 175.7 mbsf. Salinity was nearly constant throughout Hole 1208A, with an average value of 34.7 ± 0.2 g/kg (1 σ).

Chloride (Cl<sup>-</sup>) concentrations show little variation downcore (560 ± 4 mM). Sodium (Na<sup>+</sup>) concentrations, calculated by charge balance (see Broecker and Peng, 1982), exhibit little variability, averaging 479 ± 5 mM (1 σ). This is only slightly higher than the average seawater concentration of 470 mM.

F29. Carbonate profile, p. 63.



T8. Geochemical analyses, Hole 1208A, p. 86.

## Alkalinity, Sulfate, Ammonium, Phosphate, Iron, and Manganese

The distinct downcore alkalinity curve (Fig. F30) reflects a change in the redox conditions affecting the generation of  $\text{HCO}_3^-$ , likely a result of organic matter degradation. Alkalinity increases from a surface value of 2.89 mM to a maximum of 8.17 mM at 61.7 mbsf. At this depth, a reversal occurs, and alkalinity decreases to 4.79 mM at the bottom of the hole (363.4 mbsf). The subsurface maximum implies an enhanced reducing environment extending downcore from ~60 mbsf. This is supported by the sulfate ( $\text{SO}_4^{2-}$ ) and  $\text{NH}_4^+$  downcore trends (Fig. F30). At Site 1208, the uppermost interstitial waters have  $\text{SO}_4^{2-}$  concentrations of 27.7 mM—only slightly lower than average seawater (28 mM). Below 4.7 mbsf, pore water  $\text{SO}_4^{2-}$  decreases gradually, reaching a minimum concentration of 19.5 mM at 118.7 mbsf. Here, the pore water  $\text{SO}_4^{2-}$  content slowly increases to a subsurface maximum of 22.8 mM at 295.9 mbsf, before declining to 21.7 mM at 363.4 mbsf.

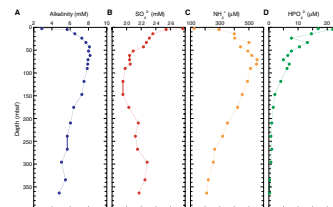
Figure F31 compares ammonium and phosphate ( $\text{NH}_4^+$  and  $\text{HPO}_4^{2-}$ ) concentrations with alkalinity data. The correlation among the data ( $R^2 = 0.91$  and  $0.89$ , respectively) implies that the enhanced carbonate ion production (alkalinity) is linked to the decomposition of organic matter.  $\text{SO}_4^{2-}$  reduction is also reflected in the sediments by the presence of pyrite ( $\text{FeS}_2$ ), observed intermittently throughout the core (see “Lithostratigraphy,” p. 9).

In core from Hole 1208A, the  $\text{NH}_4^+$  and  $\text{HPO}_4^{2-}$  concentrations range from 125 to 556  $\mu\text{M}$ , and 0 to 22  $\mu\text{M}$ , respectively (Fig. F30). The  $\text{NH}_4^+$  concentrations are lowest at the sediment/water interface (125  $\mu\text{M}$ ) and steadily increase to 556  $\mu\text{M}$  at 71.2 mbsf. Below this interval,  $\text{NH}_4^+$  decreases steadily to the bottom of the hole. Based on the relationship between alkalinity and  $\text{NH}_4^+$  (Fig. F31), it follows that  $\text{NH}_4^+$  is being generated by decomposition of organic matter. Because both  $\text{NH}_4^+$  and  $\text{HPO}_4^{2-}$  are produced largely in pore waters by the decomposition of organic matter (Gieskes, 1983), the observed trends in both species should be similar. However, the  $\text{HPO}_4^{2-}$  profile exhibits a trend opposite of  $\text{NH}_4^+$  in the upper section of the hole. The  $\text{HPO}_4^{2-}$  profile shows a maximum concentration of 22  $\mu\text{M}$  at 4.7 mbsf, declining steadily downcore (Fig. F30). Only below ~100 mbsf are the  $\text{NH}_4^+$  and  $\text{HPO}_4^{2-}$  trends coincident. Consequently, the  $\text{HPO}_4^{2-}$  and alkalinity relationship is significant only for  $\text{HPO}_4^{2-}$  data below 147.2 mbsf. In the upper section of the hole,  $\text{HPO}_4^{2-}$  maybe being consumed during the adsorption or precipitation reactions (e.g., a calcium phosphate phase).

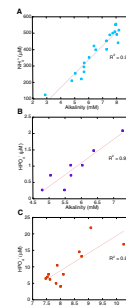
Large downcore fluctuations in pore water iron ( $\text{Fe}^{2+}$ ) concentrations ( $83 \pm 56.7 \mu\text{M}$  [1  $\sigma$ ]) occur in Hole 1208A (Fig. F32). Variations in the  $\text{Fe}^{2+}$  profile are attributed to the close proximity of iron sources, such as volcanic ash, to areas of sulfate reduction and pyrite ( $\text{FeS}_2$ ) formation. Below 209.8 mbsf, ash content declines and  $\text{Fe}^{2+}$  concentrations decrease to a minimum of 19  $\mu\text{M}$  at 295.5 mbsf. The decreasing  $\text{Fe}^{2+}$  may also reflect diffusion between sites of high and low  $\text{Fe}^{2+}$  concentrations.

The manganese ( $\text{Mn}^{2+}$ ) concentration profile in these pore waters is characterized by a subsurface maximum (28  $\mu\text{M}$ ) at 23.7 mbsf and subsequent decrease to 5  $\mu\text{M}$  at 90.2 mbsf (Fig. F32). The elevated  $\text{Mn}^{2+}$  concentrations in the shallowest samples suggest that the degradation of organic matter is sufficient to deplete oxygen in the upper part of the

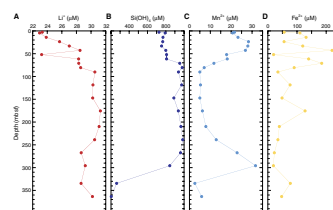
F30. Alkalinity, sulfate, ammonium, and phosphate profiles, p. 64.



F31. Crossplots implying related processes in Hole 1208A, p. 65.



F32. Lithium, silicate, manganese, and iron profiles, p. 66.



sediment column, above the depth at which the sulfate and alkalinity profiles imply that  $\text{SO}_4^{2-}$  reduction is occurring (~50 mbsf). The sharp decrease to low and uniform concentrations suggests that a manganese-rich phase may be forming within this interval. The requisite reducing conditions in the sediment column are consistent with the alkalinity and  $\text{SO}_4^{2-}$  data discussed previously and may also be implied by low red/blue (680/420 nm) ratios in color reflectance (see “[Lithostratigraphy](#),” p. 9).

The  $\text{Mn}^{2+}$  concentration curve (5–8  $\mu\text{M}$ ) between 90.2 and 209.8 mbsf is likely the result of upward diffusion of  $\text{Mn}^{2+}$  between high concentrations associated with  $\text{Mn}^{2+}$  minerals and lower concentrations in overlying sediments. This is supported by a dramatic decrease from 32  $\mu\text{M}$  (295.9 mbsf) to 3  $\mu\text{M}$  (334.5 mbsf). The excursion to a maximum  $\text{Mn}^{2+}$  concentration is coincident with the upper boundary of Subunit IC (311.7–328.2 mbsf), at which an unconformity, with inferred Mn-rich phases, is present. For this reason, the  $\text{Mn}^{2+}$  profile is interpreted to reflect both upward and downward diffusion of  $\text{Mn}^{2+}$  cations from this Mn-rich horizon.

### Potassium, Silica, and Lithium

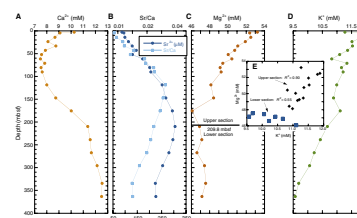
Potassium ( $\text{K}^+$ ) concentrations decrease gradually downcore from a maximum of 11.8 mM at 14.2 mbsf to values close to that of average seawater (10.2 mM) in the deepest sample at 363.4 mbsf (Fig. F33). Elevated pore water concentrations of  $\text{K}^+$  (relative to seawater) correspond to the distribution of volcanic ash in the upper section of the hole (see “[Lithostratigraphy](#),” p. 9), suggesting that the major source for  $\text{K}^+$  in the pore water is glass-rich silicic volcanic material.  $\text{K}^+$  is liberated from the solid phase via leaching and weathering reactions that produce clays (i.e., smectite). The downcore decrease in  $\text{K}^+$  to concentrations below that of average seawater likely reflects a diminishing source of volcanic ash, diffusion toward greater depths, and possible exchange with basement.

The dissolved silica ( $\text{Si}(\text{OH})_4$ ) concentrations of the interstitial waters from Hole 1208A (above ~300 mbsf) ( $871 \pm 95 \mu\text{M}$  [ $1 \sigma$ ]) are greater than in the overlying water (North Pacific Deep Water value = 160  $\mu\text{M}$ ). At ~300 mbsf, the pore water  $\text{Si}(\text{OH})_4$  concentrations (Fig. F32) start decreasing to a minimum of 204  $\mu\text{M}$  at 363.4 mbsf. This dramatic decrease coincides with the appearance of chert (Subunit IC/Unit II boundary). It is likely that this significant removal of  $\text{Si}(\text{OH})_4$  from pore waters may be induced by the recrystallization of opal-A to opal-CT or quartz (e.g., Baker, 1986; Gieskes, 1981).

### Calcium, Strontium, Magnesium, Boron, and Barium

In Hole 1208A, there are several processes influencing the downcore calcium ( $\text{Ca}^{2+}$ ) concentrations. The pore water  $\text{Ca}^{2+}$  content of the uppermost sample is 10.25 mM, which is approximately the  $\text{Ca}^{2+}$  concentration of average seawater (10.30 mM).  $\text{Ca}^{2+}$  concentrations decrease between 0 and 80.7 mbsf, then increase to 12.5 mM by the base of the hole (Fig. F33). The interval of low Ca concentrations centered around 75 mbsf suggests precipitation of a Ca-rich diagenetic phase. However, no obvious Ca-rich diagenetic phases were apparent from core descriptions nor the few XRD analyses performed. The correlation between  $\text{Ca}^{2+}$  and  $\text{HPO}_4^{2-}$  may indicate precipitation of a calcium phosphate

F33. Cation profiles, p. 67.



mineral. The  $\text{Ca}^{2+}$  increase below ~100 mbsf is a result of diffusion from the base or below the cored interval. Dissolution of carbonate is a reasonable possibility for the increase in  $\text{Ca}^{2+}$  at depth. However, note that the maximum  $\text{Ca}^{2+}$  content is ~200 m lower than the maximum Sr concentration, which is a sensitive indicator of carbonate alteration (Baker et al., 1982).

Strontium concentrations show a gradual downcore increase from seawater-like values (87  $\mu\text{M}$ ; 0 mbsf) to a maximum of 305  $\mu\text{M}$  at 209.8 mbsf. Below this depth, the profile reverses and the  $\text{Sr}^{2+}$  interstitial water concentration decreases to 226  $\mu\text{M}$ . The  $\text{Sr}^{2+}$  and Sr/Ca ratio data are interpreted to reflect the dissolution and/or recrystallization of carbonates at ~200 mbsf, release of  $\text{Sr}^{2+}$  cations into solution, and subsequent diffusion. The decreasing Sr/Ca ratios below ~150 mbsf may also be indicative of dissolution of carbonate but only if  $\text{Ca}^{2+}$  is not being sourced from a different reaction(s) below.

The downcore magnesium ( $\text{Mg}^{2+}$ ) profile ranges between a low of 46.1 mM (175.7 mbsf) and seawater-like concentrations of 53.2 mM in the uppermost pore water sample. The linear decrease in  $\text{Mg}^{2+}$  between the surface and 175.7 mbsf implies that  $\text{Mg}^{2+}$  is being consumed and a diffusion gradient exists between high and low concentrations. However, this trend does not extend below ~175 mbsf. The change in the behavior of  $\text{Mg}^{2+}$  is evident in Figure F33E, where  $\text{K}^+$  and  $\text{Mg}^{2+}$  are compared. The linearity of these data for pore water samples from the upper section (between 0.0 and 209.8 mbsf;  $R^2 = 0.90$ ) implies that  $\text{Mg}^{2+}$  is being consumed and  $\text{K}^+$  is being generated via volcanic weathering reactions and subsequent diffusion (see above). In addition, formation of Mg-rich phases (e.g., saponitic green laminae) could be responsible for the decrease in pore water  $\text{Mg}^{2+}$  (see “Diagenesis,” p. 12, in “Lithostratigraphy” in the “Site 1210” chapter). Below 209.8 mbsf,  $\text{Mg}^{2+}$  concentrations are essentially uniform ( $29.5 \pm 0.4$  mM [1  $\sigma$ ]), yet  $\text{K}^+$  concentrations continue to decline. This change in the slope of the profile implies that  $\text{Mg}^{2+}$  cations are being mobilized into the pore waters below 209.8 mbsf. However, the process responsible for such a reaction cannot be determined with available data.

The interstitial barium ( $\text{Ba}^{2+}$ ) concentrations are consistently higher than that of average seawater (0.10  $\mu\text{M}$ ), averaging  $0.72 \pm 0.49$   $\mu\text{M}$  (1  $\sigma$ ) (Table T8). These elevated  $\text{Ba}^{2+}$  concentrations relative to seawater are likely a consequence of the presence of skeletal debris and ash ( $\text{Ba}^{2+}$  sources), as well as local dissolution of biogenic  $\text{BaSO}_4$  in reducing environments. Boron ( $\text{H}_3\text{BO}_3$ ) concentrations do not change appreciably, with the exception of a large excursion in the  $\text{H}_3\text{BO}_3$  profile at 52.2 mbsf ( $449 \pm 14$   $\mu\text{M}$  [1  $\sigma$ ], excluding excursion datum). The significance of this change is not understood, although there are deviations at this depth in the  $\text{Ba}^{2+}$ ,  $\text{Sr}^{2+}$ ,  $\text{Ca}^{2+}$ ,  $\text{Mg}^{2+}$ , and  $\text{Cl}^-$  data. Similarly, alkalinity,  $\text{Ca}^{2+}$ ,  $\text{Si}(\text{OH})_4$ ,  $\text{HPO}_4^{2-}$ , and  $\text{NH}_4^+$  profiles show reversals in trends or are significantly altered at approximately this depth. Based on the available data, it cannot be determined whether these fluctuations are related, much less whether a specific process is simultaneously affecting the interstitial water chemistry of these species.

## PHYSICAL PROPERTIES

Physical properties at Site 1208 were measured on both whole-round sections and discrete samples from split-core sections. Whole-round

measurements included the continuous determination of magnetic susceptibility, gamma ray attenuation (GRA) bulk density, and *P*-wave velocity and some measurements of natural gamma radiation using the MST, as well as discrete measurements of thermal conductivity. Additionally, discrete *P*-wave velocities and index properties were measured at a frequency of at least one measurement per split-core section in Hole 1208A.

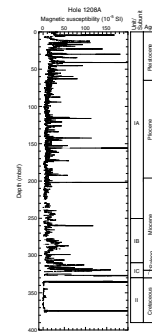
### MST Measurements

All core sections from Hole 1208A were routinely measured on the MST for magnetic susceptibility and GRA density at 2.5-cm intervals in Cores 198-1208A-1H through 17H, at 3-cm intervals in Cores 198-1208A-18H through 23X, and at 5-cm intervals in Cores 198-1208A-24X through 42X (Figs. F34, F35). MST *P*-wave velocity was routinely measured at 2.5 cm in all Hole 1208A APC cores (Fig. F36) but was not measured in the XCB cores because of the poor contact between the sediment and core liner. Natural gamma radiation was measured at 10-cm intervals in Cores 198-1208A-34X through 36X (Fig. F37). All collected MST data are archived in the ODP Janus database.

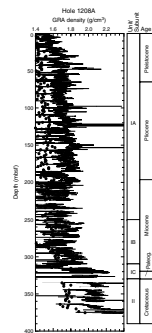
Magnetic susceptibility data (Fig. F34) are generally higher in magnitude in the uppermost 80 m of the Site 1208 sedimentary column, compared to the relatively lower values evident from 80 to 240 mbsf (these depth intervals are located in lithologic Subunits IA and IB) (see “**Lithostratigraphy**,” p. 9). Peaks in magnetic susceptibility in lithologic Subunit IA may correlate with distinctive ash layers. As already observed in sediment cores drilled at Site 1207, the Pleistocene–Pliocene section of Site 1208 reveals an excellent correlation between magnetic susceptibility data and color reflectance measurements, the latter represented by the total reflectance value ( $L^*$ ) and the 550-nm wavelength. Both magnetic susceptibility and color reflectance data in this interval reveal a pronounced cyclicity, which may be useful to identify astronomically controlled climatic and depositional processes (see “**Lithostratigraphy**,” p. 9). Magnetic susceptibility values are higher in lithologic Subunits IB and IC, relative to values between 60 and ~252 mbsf in Subunit IA. Magnetic susceptibility values are generally close to background values in lithologic Unit II (Campanian–Aptian) and do not exhibit any consistent downhole variation.

MST GRA bulk density data exhibit a general downhole increase in magnitude (Fig. F35), resulting from sediment compaction and dewatering processes with increased overburden pressure. In addition to the overall downhole trend, GRA bulk density data also show distinct variations that relate to lithologic changes at several distinct horizons. GRA bulk density values exhibit a decrease at ~160 mbsf, correlating to the depth at which coring changed from APC to XCB. An increase in GRA bulk density values at ~252 mbsf correlates to the boundary between lithologic Subunits IA and IB. Cyclical variation in GRA bulk density values, similar to that evident in magnetic susceptibility (see above) and color reflectance data, is also found within Pleistocene–Miocene lithologic Subunits IA and IB. However, GRA bulk density values are consistently higher than discrete wet bulk density measurements (Table T9) throughout Hole 1208A. These overestimated GRA bulk density values can be explained by the relatively high carbonate content, porosity, and moisture content of sediments; the calibration procedure for the MST GRA sensor is optimized for mixed-lithology sediments. Consequently, the GRA method overestimates the density in carbonate-rich

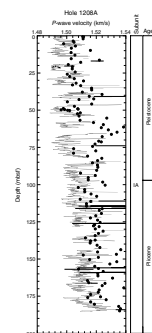
F34. Whole-core magnetic susceptibility vs. depth, p. 68.



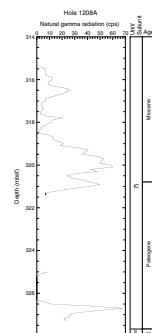
F35. Whole-core GRA bulk density vs. depth, p. 69.



F36. Whole-core *P*-wave velocity vs. depth, p. 70.



F37. MST natural gamma radiation data vs. depth, p. 71.



sediments of all lithologic units, and this effect is most pronounced in Unit II because this unit has the highest carbonate content (see “**Organic Geochemistry**,” p. 24).

MST *P*-wave velocities were recorded at 10-cm intervals in Hole 1208A sections to a depth of ~185 mbsf (Fig. F36). A general trend to higher velocities with increased depth in the sediment column can be discerned from values lying between 1490 and 1530 m/s. However, the magnitude of the discrete measurements of *P*-wave velocity (Table T10) are generally offset to higher values from the MST *P*-wave logger values, a trend similar to that found in the physical properties data at Site 1207.

Natural gamma radiation data were collected at 10-cm intervals, using the MST, for Hole 1208A between 315.4 and 327.3 mbsf in order to investigate the Cretaceous–Paleogene unconformity (see “**Biostratigraphy**,” p. 16) recovered in this interval (Fig. F37). These data show a peak in magnitude that relates to the presence of clay-rich sediments.

### P-Wave Velocity

Discrete measurements of compressional *P*-wave velocity were obtained on Site 1208 split-core sections using the modified Hamilton frame (PWS3) velocimeter. These data are listed in Table T9 and illustrated in Figure F38. Data were collected at a routine sampling frequency of one measurement per section. Velocities vary between ~1500 and ~1650 m/s, with most values occurring below 1600 m/s. Discrete *P*-wave measurements show an overall increase in velocity with depth, which is similar to that evident in the reliable data obtained with the MST. Although the general downhole trend is one of increasing *P*-wave velocity, small-scale variations within the data set can also be seen. At ~230 mbsf, an increase in the range of *P*-wave velocities may be due to the onset of the ooze–chalk transition (see “**Lithostratigraphy**,” p. 9) and increasingly variable sediment lithologies. This lithologic variability is most pronounced in Subunit IB. A rise in *P*-wave velocity is observed at ~310 mbsf that correlates well with the top of Subunit IC and increasing clay content in the sediments recovered. *P*-wave velocities reach a maximum of ~1660 m/s immediately above the Campanian–Paleogene unconformity. *P*-wave velocities below this unconformity are considerably slower (~1550 m/s) and characterize most of Unit II. Increasing *P*-wave velocities at the base of Unit II (~375 mbsf) may be concurrent with an increase in lithification. *P*-wave velocities are positively correlated with discrete bulk density measurements (Fig. F39) ( $R^2 = 0.68$ ).

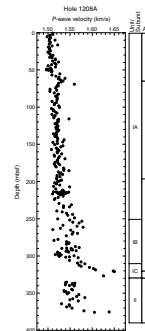
### Thermal Conductivity

Thermal conductivity data from Site 1208, obtained using the TK04 system, are listed in Table T11 and shown in Figure F40. Measurements were made on Sections 1 and 3 of each core from Hole 1208A. Average thermal conductivity for the 80 data points is 0.93 W/(m·K), with a standard deviation of 0.31. Site 1208 thermal conductivity values also exhibit a general increase in magnitude with depth below seafloor, increasing from ~0.80 W/(m·K) near the seafloor, to ~1.25 W/(m·K) at ~374 mbsf. The downhole increase in thermal conductivity values broadly correlates ( $R^2 = 0.77$ ) with a decrease in porosity (Table T9) as shown in Figure F41 and as would be expected from increased sediment consolidation at greater depths.

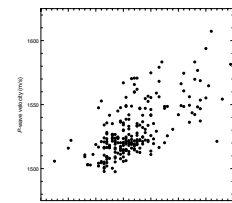
T9. Discrete index properties measurements, p. 87.

T10. Discrete measurements of *P*-wave velocity, p. 91.

F38. Discrete *P*-wave velocities vs. depth, p. 72.

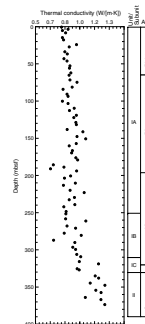


F39. Discrete *P*-wave velocities vs. discrete wet bulk density, p. 73.



T11. Discrete measurements of thermal conductivity, p. 93.

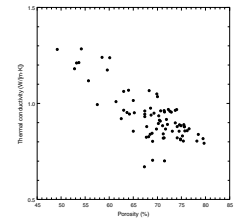
F40. Whole-core thermal conductivity vs. depth, p. 74.



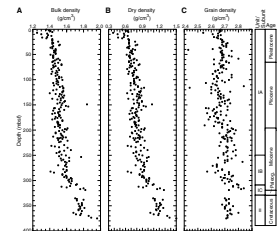
## Index Properties

Index properties were determined for discrete samples from Hole 1208A. These data are listed in Table T9 and shown in Figures F42 and F43. Index properties primarily reflect progressive sediment compaction and fluid expulsion with depth in the sediment column but also indicate changes in sediment composition as defined by lithologic units and subunits. Bulk and dry densities increase slightly in magnitude between the seafloor and ~20 mbsf in lithologic Subunit IA. The greatest increase in bulk and dry densities at Site 1208 occurs in lithologic Subunit IB, between ~290 and ~310 mbsf. Values further increase in lithologic Subunit IC, then remain approximately constant to ~375 mbsf through lithologic Unit II. By comparison, grain density exhibits a small downhole increase in magnitude between the seafloor and ~30 mbsf. Below ~30 mbsf, grain density values remain largely constant, with no discernible changes at lithologic boundaries. Water content, porosity, and void ratio (Fig. F43) all exhibit a general downhole decrease in magnitude in Subunits IA and IB. The largest downhole decrease in each of these properties occurs within Subunit IC and Unit II.

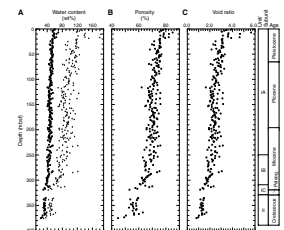
F41. Whole-core thermal conductivity vs. discrete porosity measurements, p. 75.



F42. Discrete wet, dry, and grain density vs. depth, p. 76.



F43. Calculated water content, porosity, and void ratio vs. depth, p. 77.



## REFERENCES

- Aubry, M.-P., Berggren, W.A., Stott, L., and Sinha, A., 1996. The upper Paleocene–lower Eocene stratigraphic record and the Paleocene/Eocene boundary carbon isotope excursion: implications for geochronology. *In* Knox, R.W.O'B., Corfield, R.M., and Dunay, R.E. (Eds.), *Correlation of the Early Paleogene in Northwestern Europe*. Spec. Publ.—Geol. Soc. Am., 101:353–380.
- Aubry, M.-P., Lucas, S., and Berggren, W.A. (Eds.), 1998. *Late Paleocene and Early Eocene Climatic and Biotic Evolution*: New York (Columbia Univ. Press).
- Bains, S., Corfield, R.M., and Norris, R.D., 1999. Mechanisms of climate warming at the end of the Paleocene. *Science*, 285:724–727.
- Baker, P.A., 1986. Pore-water chemistry of carbonate-rich sediments, Lord Howe Rise, Southwest Pacific Ocean. *In* Kennett, J.P., von der Borch, C.C., et al., *Init. Repts. DSDP, 90* (Pt. 2): Washington (U.S. Govt. Printing Office), 1249–1256.
- Baker, P.A., Gieskes, J.M., and Elderfield, H., 1982. Diagenesis of carbonates in deep-sea sediments—evidence from Sr<sup>2+</sup>/Ca<sup>2+</sup> ratios and interstitial dissolved Sr<sup>2+</sup> data. *J. Sediment. Petrol.*, 52:71–82.
- Barrera, E., Savin, S.M., Thomas, E., and Jones, C.E., 1997. Evidence for thermohaline-circulation reversals controlled by sea level change in the latest Cretaceous. *Geology*, 25:715–718.
- Barron, J.A., Basov, I.A., Beaufort, L., Dubuisson, G., Gladenkov, A.Y., Morley, J.J., Okada, M., Ólafsson, D.K., Pak, D.K., Roberts, A.P., Shilov, V.V., and Weeks, R.J., 1995. Biostratigraphic and magnetostratigraphic summary. *In* Rea, D.K., Basov, I.A., Scholl, D.W., and Allan, J.F. (Eds.), *Proc. ODP, Sci. Results*, 145: College Station, TX (Ocean Drilling Program), 559–575.
- Bralower, T.J., Parrow, M., Thomas, E., and Zachos, J.C., 1995. Data report: Stable isotopic stratigraphy of the Paleogene pelagic cap at Site 865, Allison Guyot. *In* Winterer, E.L., Sager, W.W., Firth, J.V., and Sinton, J.M. (Eds.), *Proc. ODP, Sci. Results*, 143: College Station, TX (Ocean Drilling Program), 581–586.
- Broecker, W.S., and Peng, T.-H., 1982. *Tracers in the Sea*: Palisades, NY (Lamont-Doherty Geol. Observ.).
- Cande, S.C., and Kent, D.V., 1995. Revised calibration of the geomagnetic polarity timescale for the Late Cretaceous and Cenozoic. *J. Geophys. Res.*, 100:6093–6095.
- Claypool, G.E., and Kvenvolden, K.A., 1983. Methane and other hydrocarbon gases in marine sediment. *Ann. Rev. Earth Planet. Sci.*, 11:299–317.
- Dickens, G.R., Castillo, M.M., and Walker, J.G.C., 1997. A blast of gas in the latest Paleocene: simulating first-order effects of massive dissociation of oceanic methane hydrate. *Geology*, 25:259–262.
- Dickens, G.R., O'Neil, J.R., Rea, D.K., and Owen, R.M., 1995. Dissociation of oceanic methane hydrate as a cause of the carbon isotope excursion at the end of the Paleocene. *Paleoceanography*, 10:965–971.
- Gagosian, R.B., and Peltzer, E.T., 1986. The importance of atmospheric input of terrestrial organic material to deep sea sediments. *In* Leythaeuser, D., and Rullkötter, J. (Eds.), *Advances in Organic Geochemistry 1985*: Oxford (Pergamon Press), *Org. Geochem.*, 10:897–903.
- Gagosian, R.B., Peltzer, E.T., and Merrill, J.T., 1987. Long range transport of terrestrially derived lipids in aerosols from the south Pacific. *Nature*, 325:800–803.
- Gibson, T.G., Bybell, L.M., and Owens, J.P., 1993. Latest Paleocene lithologic and biotic events in neritic deposits of southwestern New Jersey. *Paleoceanography*, 8:495–514.
- Gieskes, J.M., 1981. Deep-sea drilling interstitial water studies: implications for chemical alteration of the oceanic crust, layers I and II. *In* Warme, J.E., Douglas, R.G., and Winterer, E.L. (Eds.), *The Deep Sea Drilling Project: A Decade of Progress*. Spec. Publ.—Soc. Econ. Paleontol. Mineral., 32:149–167.

- , 1983. The chemistry of interstitial waters of deep-sea sediments: interpretation of deep-sea drilling data. *In* Riley, J.P., and Chester, R. (Eds.), *Chemical Oceanography* (Vol. 8): London (Academic), 221–269.
- Keller, G., and Barron, J.A., 1987. Paleodepth distribution of Neogene deep-sea hiatuses. *Paleoceanography*, 2:697–713.
- Kelly, D.C., Bralower, T.J., Zachos, J.C., Premoli Silva, I., and Thomas, E., 1996. Rapid diversification of planktonic foraminifera in the tropical Pacific (ODP Site 865) during the late Paleocene thermal maximum. *Geology*, 24:423–426.
- Kennett, J.P., Keller, G., and Srinivasan, M.S., 1985. Miocene planktonic foraminiferal biogeography and paleoceanographic development of the Indo-Pacific region. *In* Kennett, J.P. (Ed.), *The Miocene Ocean: Paleoceanography and Biogeography*. Mem.—Geol. Soc. Am., 163:197–236.
- Kennett, J.P., and Stott, L.D., 1991. Abrupt deep-sea warming, paleoceanographic changes and benthic extinctions at the end of the Palaeocene. *Nature*, 353:225–229.
- Laskar, J., 1990. Chaotic motion of the solar system: numerical estimate of chaotic zones. *Icarus*, 88:266–291.
- Martens, C.S., and Berner, R.A., 1974. Methane production in the interstitial waters of sulfate-depleted marine sediments. *Science*, 185:1167–1169.
- McNutt, M.K., Winterer, E.L., Sager, W.W., Natland, J.H., and Ito, G., 1990. The Darwin Rise: a Cretaceous superswell? *Geophys. Res. Lett.*, 17:1101–1104.
- Millero, F.J., and Sohn, M.L., 1992. *Chemical Oceanography*: Boca Raton (CRC Press).
- Mitterer, R.M., Malone, M.J., Swart, P.K., Wortmann, U.G., Logan, G.A., Feary, D.A., and Hine, A.C., 2001. Co-generation of hydrogen sulfide and methane in marine carbonate sediments. *Geophys. Res. Lett.*, 28:3931–3934.
- Nakanishi, M., Tamaki, K., and Kobayashi, K., 1989. Mesozoic magnetic anomaly lineations and seafloor spreading history of the Northwestern Pacific. *J. Geophys. Res.*, 94:15437–15462.
- Natland, J.H., 1993. Volcanic ash and pumice at Shatsky Rise: sources, mechanisms of transport, and bearing on atmospheric circulation. *In* Natland, J.H., Storms, M.A., et al., *Proc. ODP, Sci. Results*, 132: College Station, TX (Ocean Drilling Program), 57–66.
- Okada, H., and Bukry, D., 1980. Supplementary modification and introduction of code numbers to the low-latitude coccolith biostratigraphic zonation (Bukry, 1973; 1975). *Mar. Micropaleontol.*, 5:321–325.
- Oremland, R.S., Marsh, L.M., and Polcin, S., 1982. Methane production and simultaneous sulphate reduction in anoxic, salt marsh sediments. *Nature*, 296:143–145.
- Oremland, R.S., and Taylor, B.F., 1978. Sulfate reduction and methanogenesis in marine sediments. *Geochim. Cosmochim. Acta*, 42:209–214.
- Pflum, C.E., and Frerichs, W.E., 1976. *Gulf of Mexico Deep-water Foraminifers*. Spec. Publ.—Cushman Found. Foraminiferal Res., 14.
- Rea, D.K., Basov, I.A., Janecek, T.R., Palmer-Julson, A., et al., 1993. *Proc. ODP, Init. Repts.*, 145: College Station, TX (Ocean Drilling Program).
- Rea, D.K., Basov, I.A., Kriisek, L.A., and the Leg 145 Scientific Party, 1995. Scientific results of drilling the North Pacific transect. *In* Rea, D.K., Basov, I.A., Scholl, D.W., and Allan, J.F. (Eds.), *Proc. ODP, Sci. Results*, 145: College Station, TX (Ocean Drilling Program), 577–596.
- Rea, D.K., and Leinen, M., 1985. Crustal subsidence and calcite deposition in the South Pacific Ocean. *In* Leinen, M., Rea, D.K., et al., *Init. Repts. DSDP*, 92: Washington (U.S. Govt. Printing Office), 299–303.
- Robert, C., and Kennett, J.P., 1994. Antarctic subtropical humid episode at the Paleocene–Eocene boundary: clay mineral evidence. *Geology*, 22:211–214.
- Shipboard Scientific Party, 1992a. Site 846. *In* Mayer, L., Pisias, N., Janacek, T., et al., *Proc. ODP, Init. Repts.*, 138: College Station, TX (Ocean Drilling Program), 265–333.
- , 1992b. Site 849. *In* Mayer, L., Pisias, N., Janacek, T., et al., *Proc. ODP, Init. Repts.*, 138: College Station, TX (Ocean Drilling Program), 735–807.

- , 1997. Sites 1008/1009. In Eberli, G.P., Swart, P.K., Malone, M.J., et al., *Proc. ODP, Init. Repts.*, 166: College Station, TX (Ocean Drilling Program), 347–373.
- Simoneit, B.R.T., 1978. The organic chemistry of marine sediments. In Riley, J.P., and Chester, R. (Eds.), *Chemical Oceanography* (2nd ed.) (Vol. 7): New York (Academic Press), 233–311.
- Sliter, W.V., and Brown, G.R., 1993. Shatsky Rise: seismic stratigraphy and sedimentary record of Pacific paleoceanography since the Early Cretaceous. In Natland, J.H., Storms, M.A., et al., *Proc. ODP, Sci. Results*, 132: College Station, TX (Ocean Drilling Program), 3–13.
- Storms, M.A., Natland, J.H., et al., 1991. *Proc. ODP, Init. Repts.*, 132: College Station, TX (Ocean Drilling Program).
- Taylor, B., Fujioka, K., et al., 1990. *Proc. ODP, Init. Repts.*, 126: College Station, TX (Ocean Drilling Program).
- Thomas, E., 1990. Late Cretaceous–early Eocene mass extinctions in the deep sea. In Sharpton, V.L., and Ward, P.D. (Eds.), *Global Catastrophes in Earth History: An Interdisciplinary Conference on Impacts, Volcanism, and Mass Mortality*. Spec. Pap.—Geol. Soc. Am., 247:481–495.
- Tjalsma, R.C., and Lohmann, G.P., 1983. *Paleocene–Eocene Bathyal and Abyssal Benthic Foraminifera from the Atlantic Ocean*. Spec. Publ.—Micropaleontology, 4.
- van Andel, T.H., 1977. Mesozoic/Cenozoic calcite compensation depth and the global distribution of calcareous sediments. *Earth Planet. Sci. Lett.*, 26:187–194.
- van Morkhoven, F.P.C.M., Berggren, W.A., and Edwards, A.S., 1986. Cenozoic cosmopolitan deep-water benthic foraminifera. *Bull. Cent. Rech. Explor.—Prod. Elf-Aquitaine*, 11.
- Woodruff, F., 1985. Changes in Miocene deep-sea benthic foraminiferal distribution in the Pacific Ocean: relationship to paleoceanography. In Kennett, J.P. (Ed.), *The Miocene Ocean: Paleoceanography and Biogeography*. Mem.—Geol. Soc. Am., 163:131–175.
- Young, J.R., 1998. Neogene. In Bown, P.R. (Ed.), *Calcareous Nannofossil Biostratigraphy*: London (Chapman and Hall), 225–265.
- Zachos, J.C., Lohmann, K.C., Walker, J.C.G., and Wise, S.W., Jr., 1993. Abrupt climate changes and transient climates during the Paleogene: a marine perspective. *J. Geol.*, 101:191–213.
- Zachos, J.C., Quinn, R.M., and Salamy, K., 1996. High resolution ( $10^4$  yr) deep-sea foraminiferal stable isotope records of the Eocene–Oligocene climate transition. *Paleoceanography*, 11:251–266.
- Zafiriou, O.C., Gagosian, R.B., Peltzer, E.T., Alford, J.B., and Loder, T., 1985. Air-to-sea fluxes of lipids at Enewetak Atoll. *J. Geophys. Res.*, 90:2409–2423.

Figure F1. Interpretation of seismic reflection profile across Site 1208. Mustard = middle Miocene to Holocene, light brown = lower Miocene and Paleogene, light green = Campanian, medium green = Albian. For details on the borehole depth to traveltime conversion, see “Depth-Traveltime Conversion,” p. 26, in “Physical Properties” in the “Explanatory Notes” chapter.

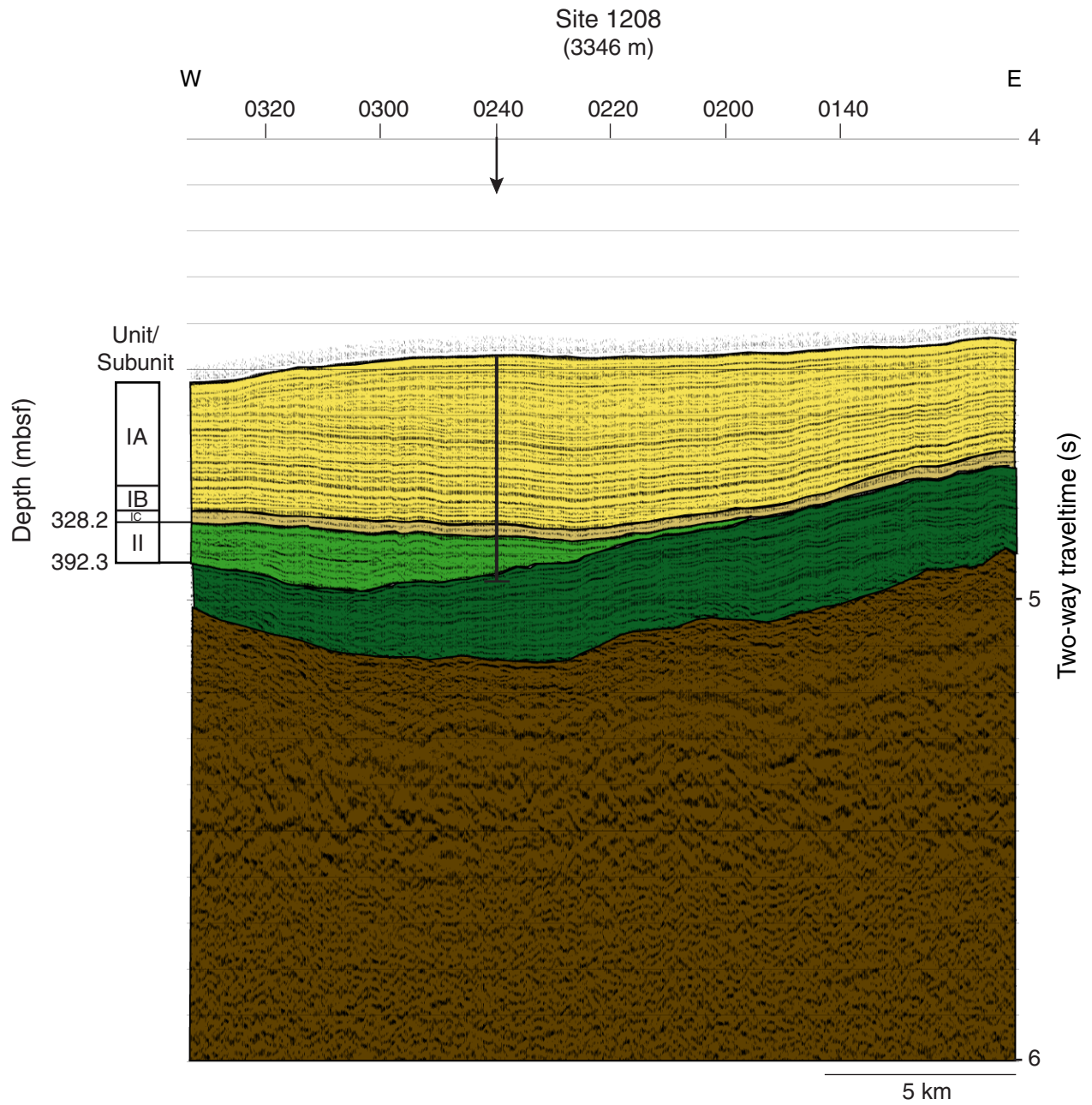


**Figure F2.** Summary diagram of coring results for Hole 1208A plotted on the meters below seafloor (mbsf) scale. The maximum penetration measured with the drill pipe was 392.3 mbsf. The accurate correction factor for the magnetic susceptibility raw instrument values is  $0.68 \times 10^{-5}$ . For details about figure symbols and descriptions see Figure F12, p. 101, in the “Leg 198 Summary” chapter.

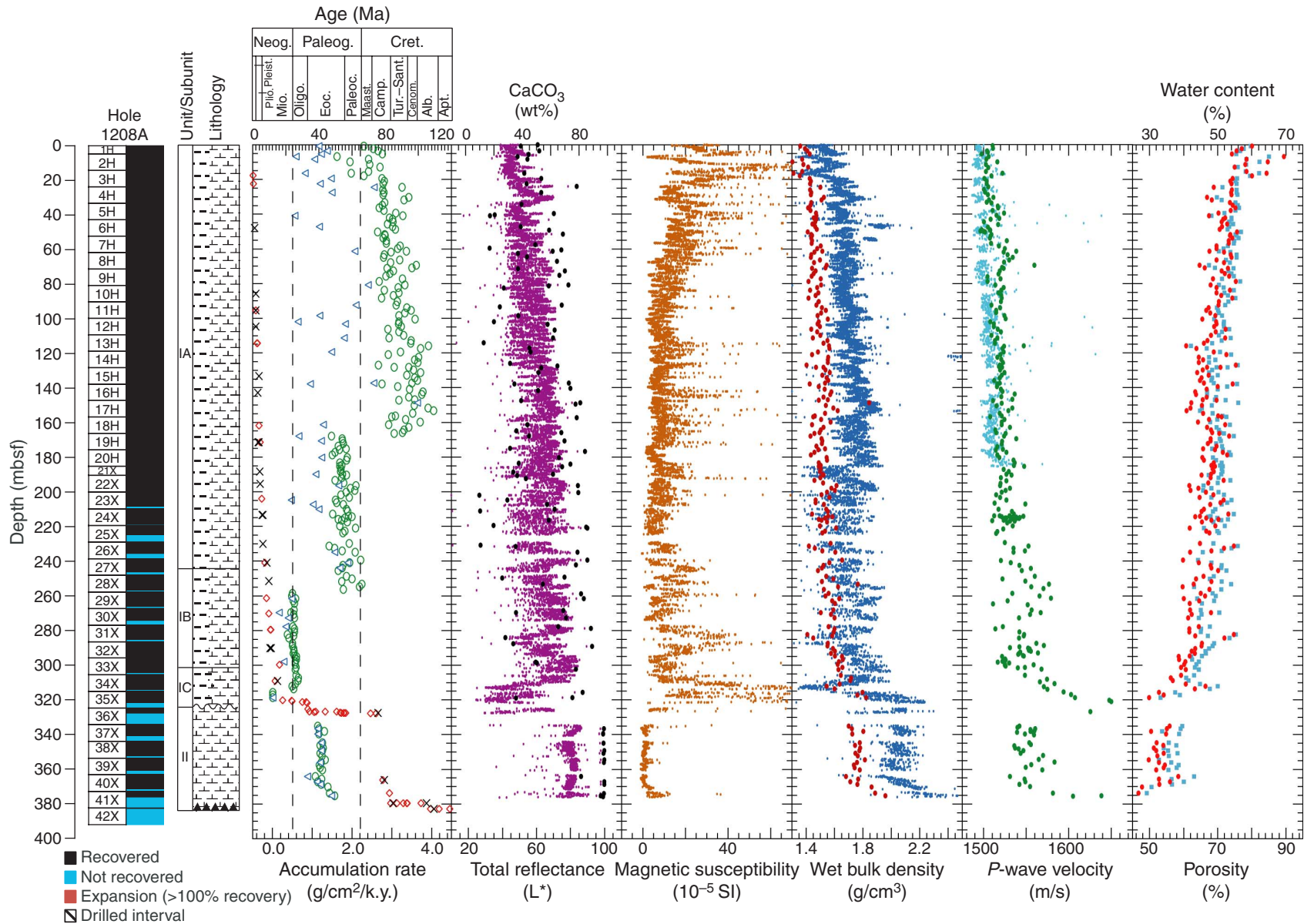


Figure F3. Change in circulation in North Pacific associated with the closure of the Indonesian Seaway. The size of arrows indicates intensity of currents (after Kennett et al., 1985). Gray circle = Site 1208.

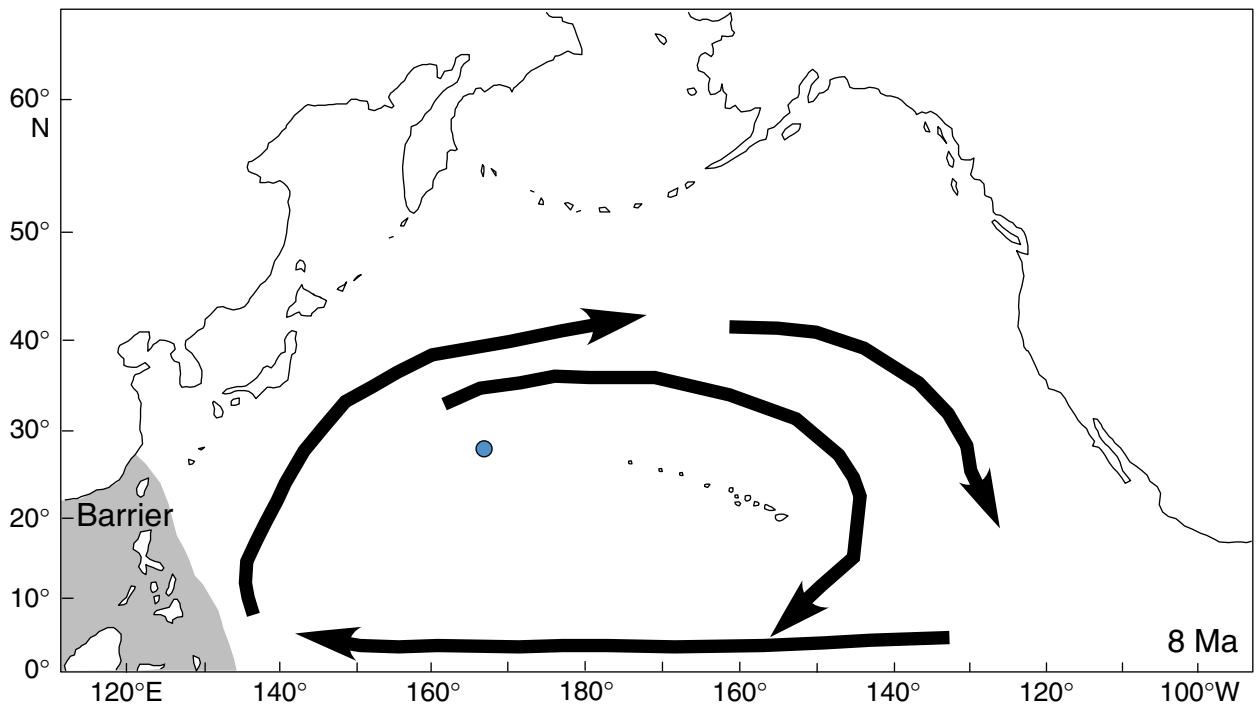
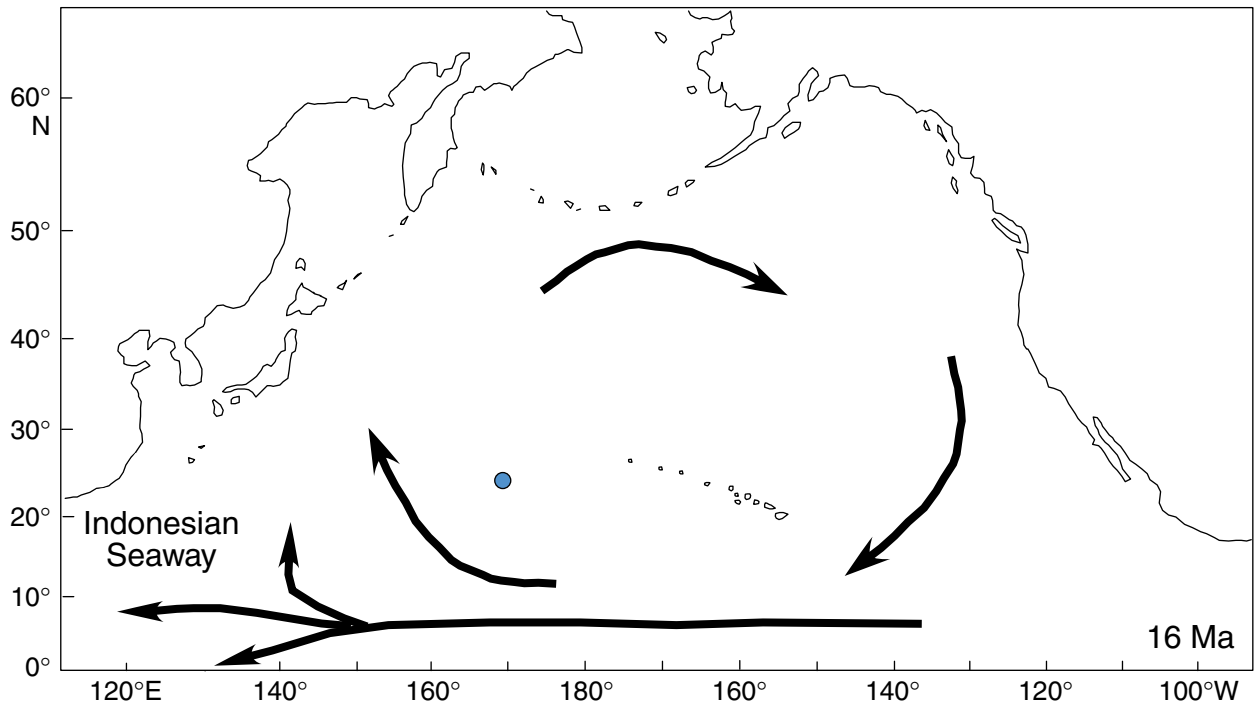
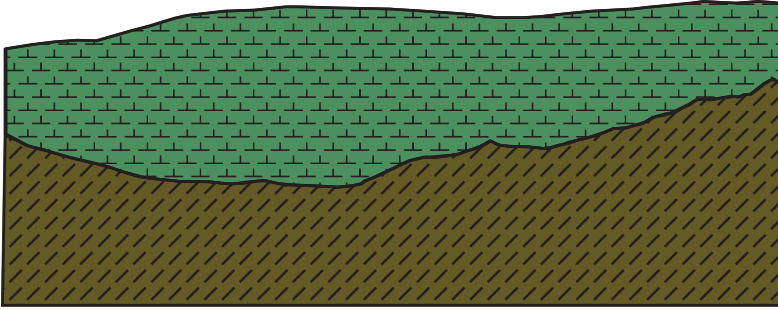
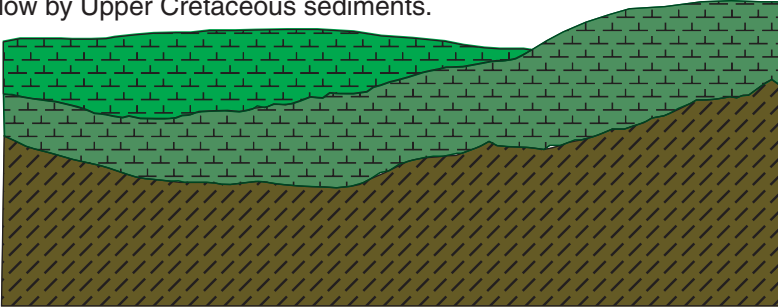


Figure F4. Interpretation of the evolution of the stratigraphic section at Site 1208 based on drilling results and seismic section.

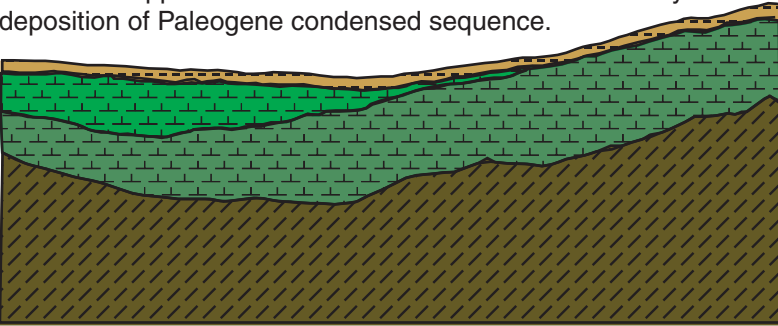
Deposition of Lower and mid-Cretaceous sediments above basement of Central High.



Erosion of Lower and mid-Cretaceous sediments and infilling of low by Upper Cretaceous sediments.



Erosion of Upper and mid-Cretaceous sediments and very slow deposition of Paleogene condensed sequence.



After short hiatus, deposition of Oligocene to mid-Miocene pelagic sediments followed by upper Miocene to Holocene drift.

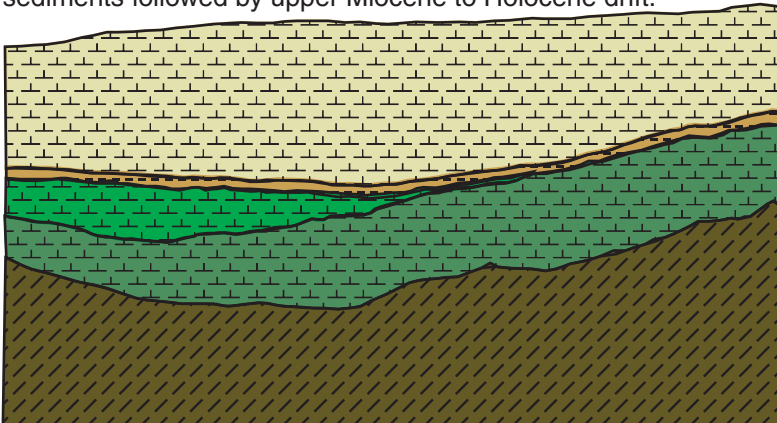


Figure F5. Core recovery, lithology, lithologic units, age with corresponding biostratigraphic zonation, color reflectance (at 550 nm), and percent carbonate for Hole 1208A. See "Lithostratigraphy," p. 4, in the "Explanatory Notes" chapter for the key to lithologic symbols. Foram. zn. = foraminiferal zone, nanno. zn. = nannofossil zone

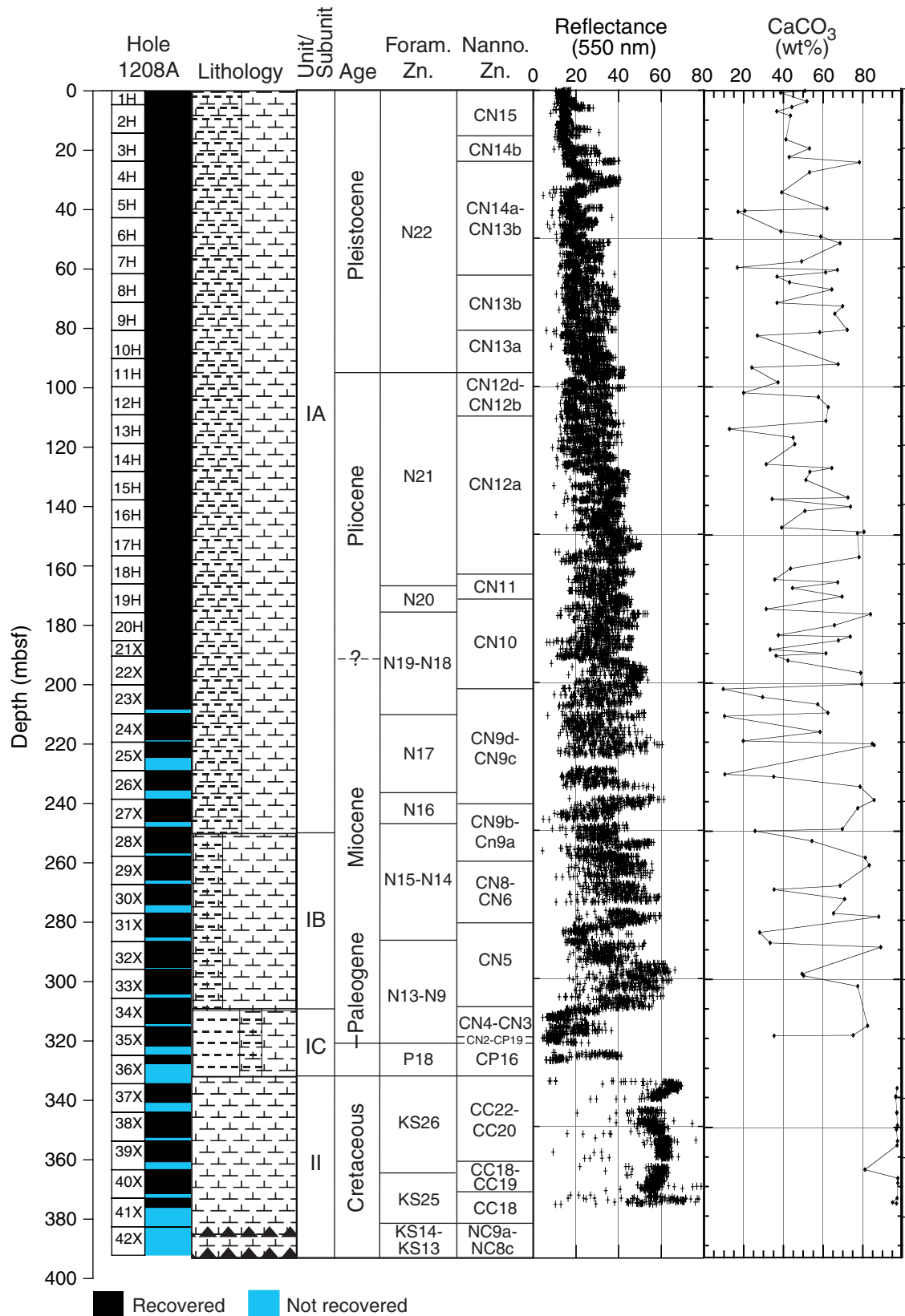
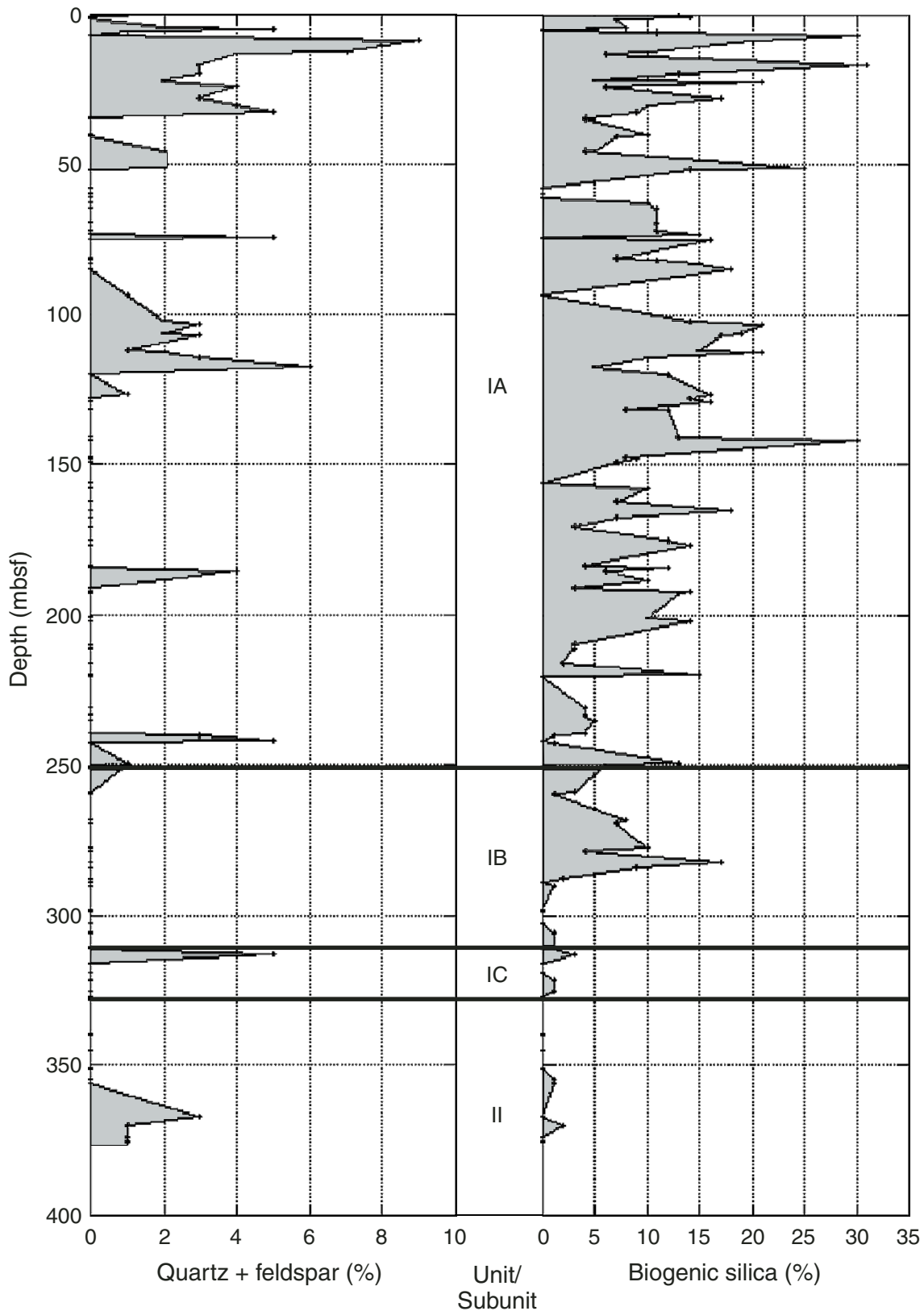
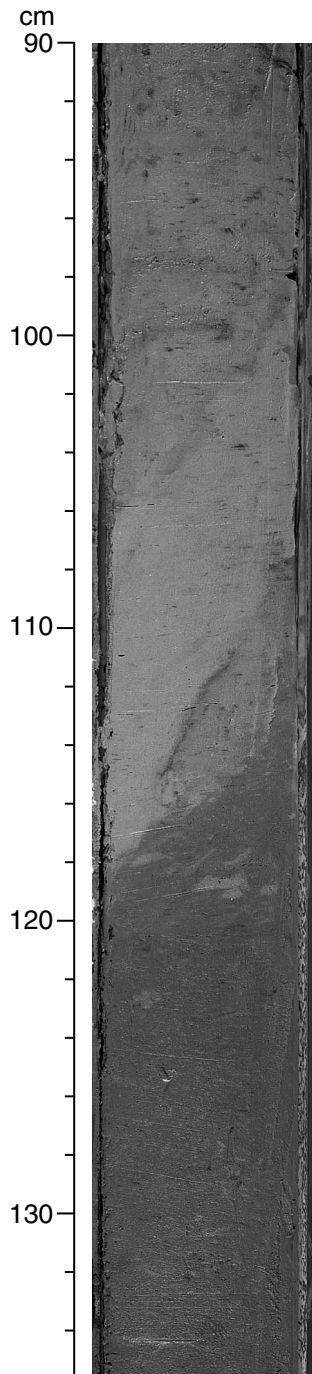


Figure F6. Downhole plots of smear slide estimates (see "Site 1208 Smear Slides," p. 43) of percent total biogenic silica (right) and percent total quartz and feldspar (left). Biogenic silica includes diatoms, radiolarians, sponge spicules, and silicoflagellates. The feldspar total may include some grains of volcanic origin as well. Note that these plots do not include "trace" amounts.



**Figure F7.** Close-up photograph of interval 198-1208A-3H-1, 90–135 cm, showing subparallel discontinuities at 98–118 cm, which could be the product of repeated erosion, faulting, or slumping. Darker (olive gray) nannofossil clay with diatoms is overlain by light olive-gray clayey nannofossil ooze. This interval is late Pleistocene in age.



**Figure F8.** Close-up photograph of interval 198-1208A-6H-6, 50–75 cm, showing subhorizontal, diffuse color bands at 66–73 cm just below a burrowed contact between underlying light greenish gray nannofossil ooze and overlying clayey nannofossil ooze with diatoms and radiolarians. Darker areas (e.g., at 53 cm) are pyrite pods and blebs. A carbonate analysis at 54 cm indicates that this sediment contains 59 wt% carbonate. This interval is Pleistocene in age.

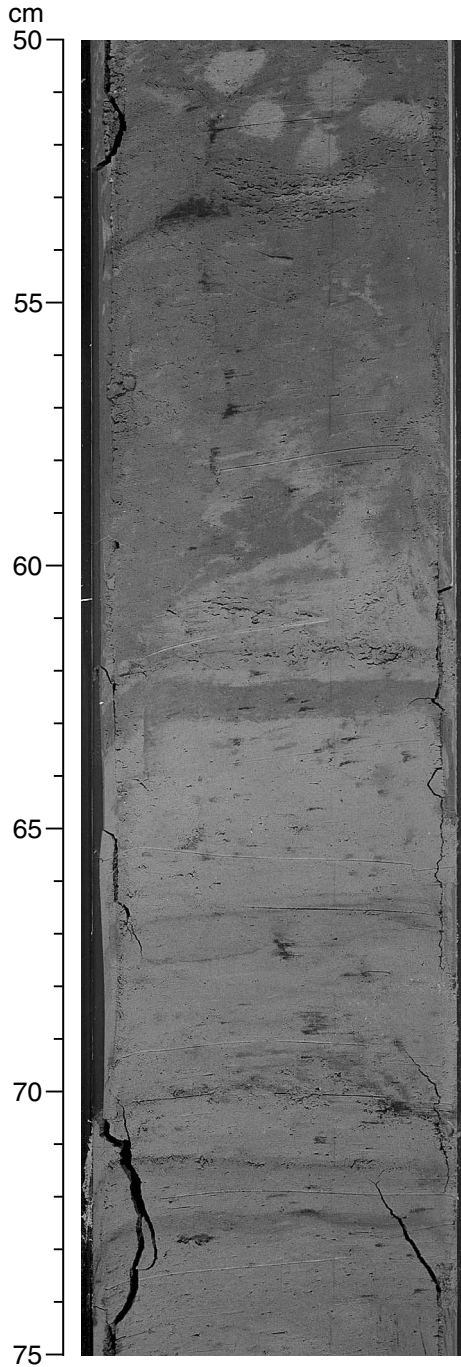


Figure F9. Composite digital photograph, color reflectance, and bulk density for Core 198-1208A-8H. This core is Pleistocene in age.

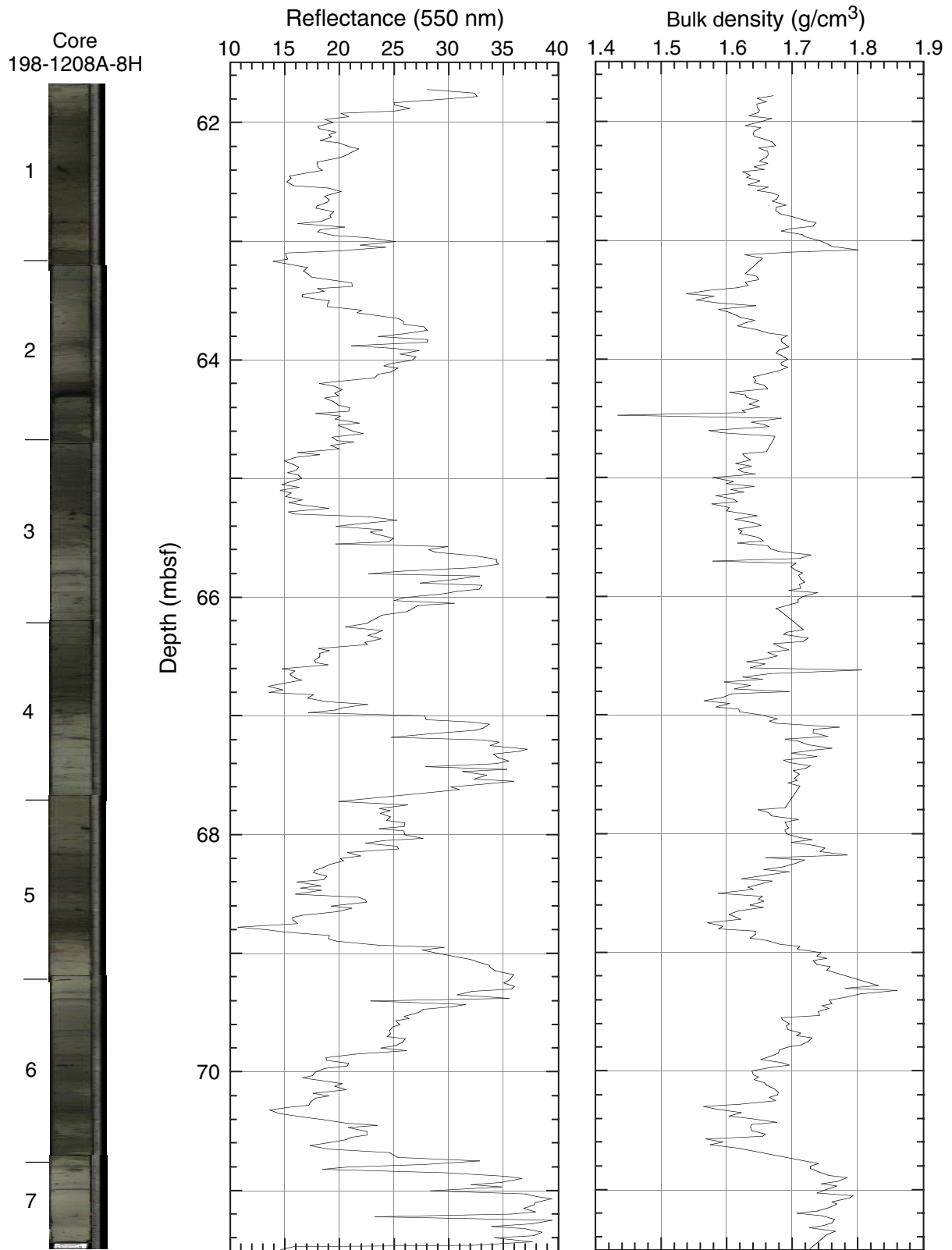
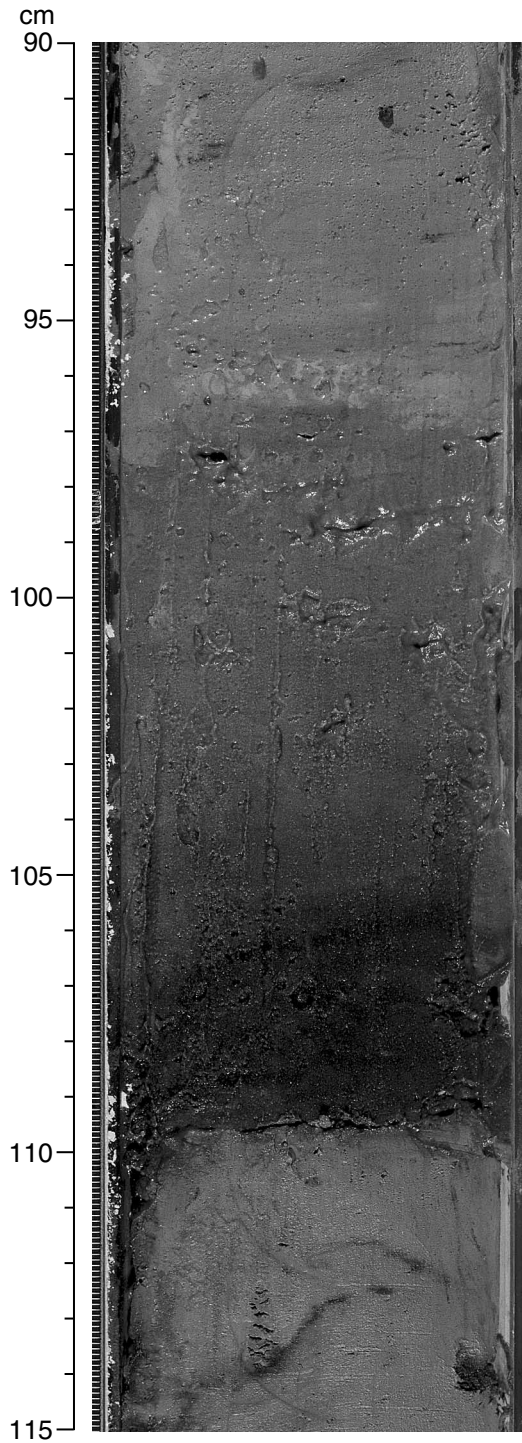


Figure F10. Close-up photograph of interval 198-1208A-6H-2, 90–115 cm, showing dark, greenish black (5G 2/1) ash overlying an abrupt contact with underlying light greenish gray nannofossil ooze. This interval is Pleistocene in age.



**Figure F11.** Close-up photograph of interval 198-1208A-2H-2, 0–50 cm, showing near-vertical burrow structure partly filled by dark pyrite that crosscuts the core diagonally from 19 to 47 cm. This interval is late Pleistocene in age.

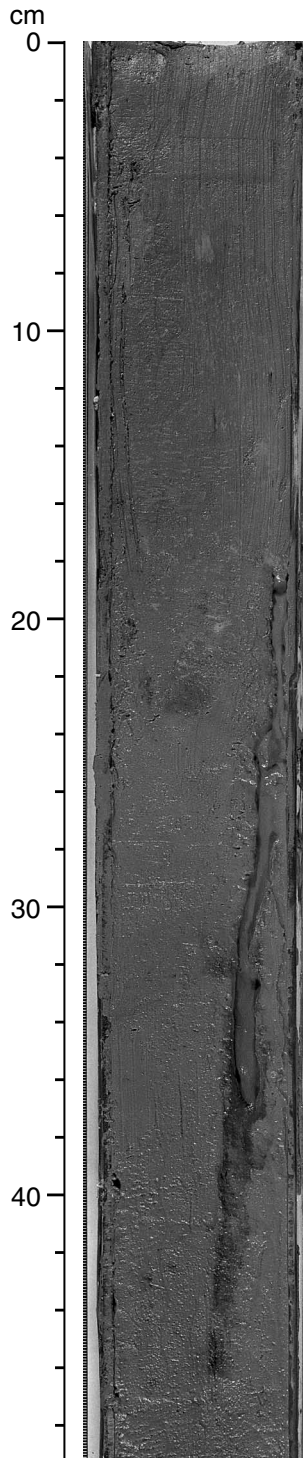


Figure F12. Close-up photograph of interval 198-1208A-30X-2, 70–95 cm, showing *Zoophycos*, *Chondrites*, and *Planolites* burrows. This interval is late Miocene in age.

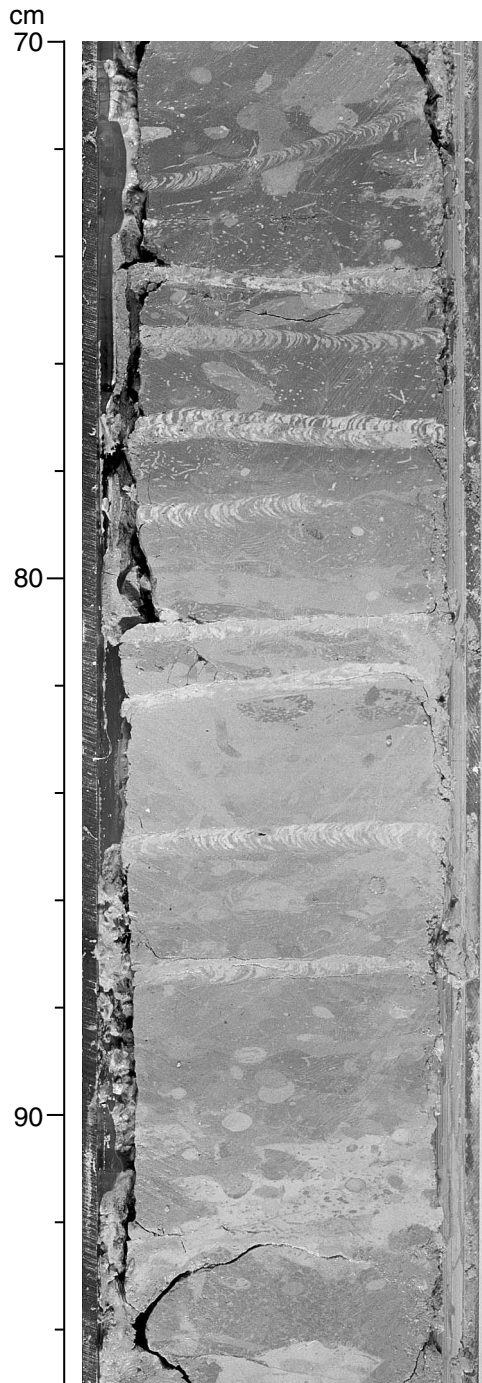


Figure F13. Close-up photograph of interval 198-1208A-32X-1, 126–145 cm, showing distinct *Planolites* burrows and an example of an “abundant” level of bioturbation where 100% of the surface is burrowed. The interval is middle Miocene in age.

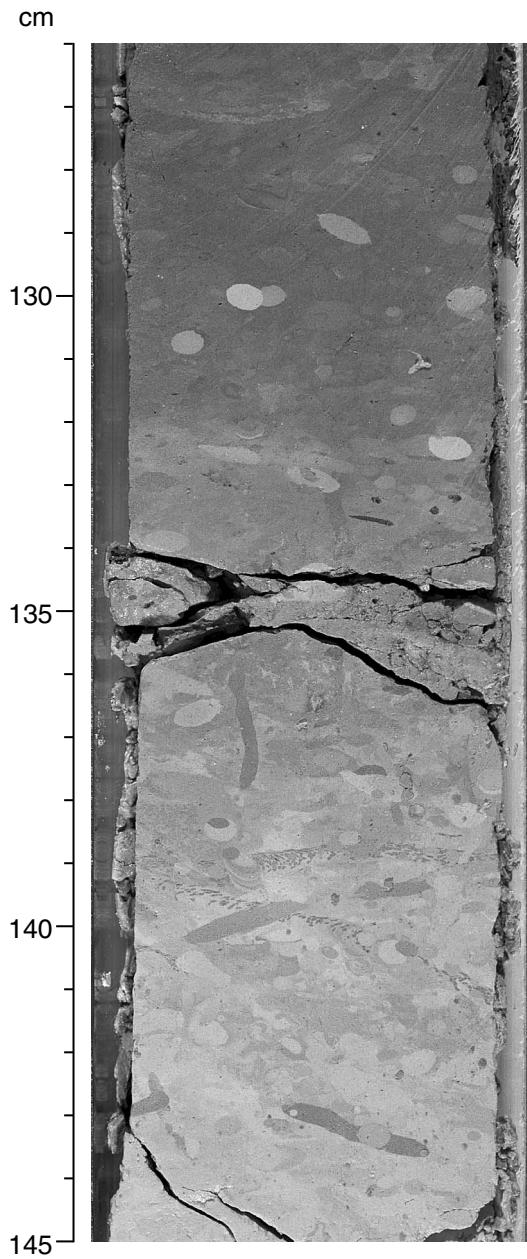


Figure F14. Close-up photograph of interval 198-1208A-31X-3, 0–26 cm, showing composite burrow and less distinct *Zoophycos* and *Planolites* burrows. The interval is late Miocene in age.

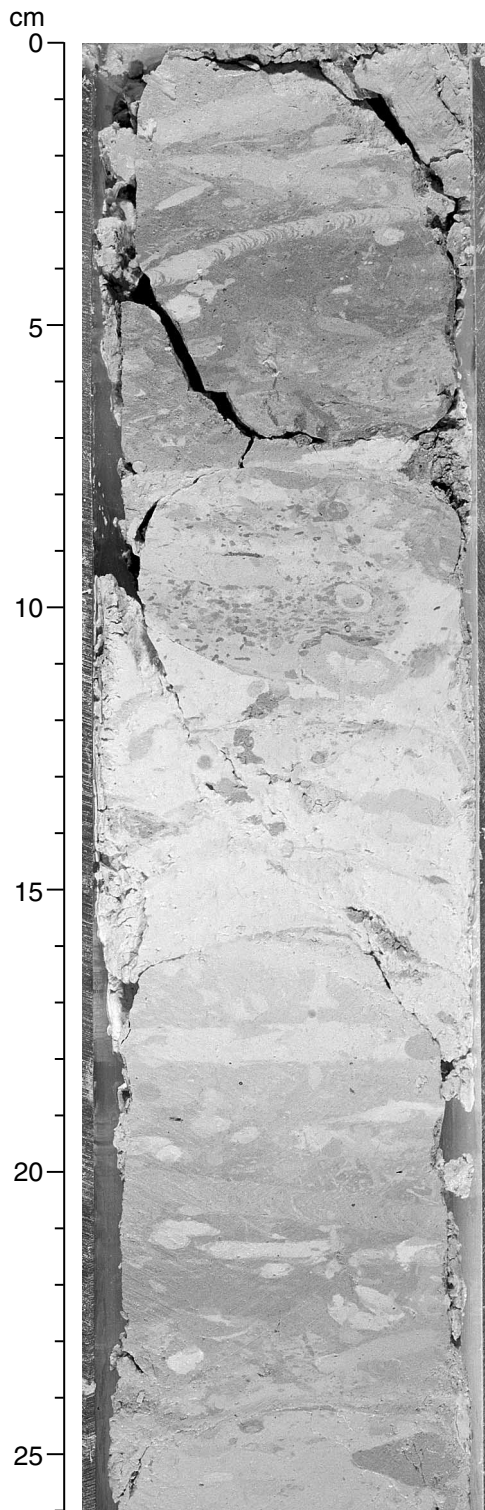


Figure F15. Composite digital photograph, color reflectance (solid circles), and magnetic susceptibility (crosses) for Core 198-1208A-36X. The accurate correction factor for the magnetic susceptibility raw instrument values is  $0.68 \times 10^{-6}$ .

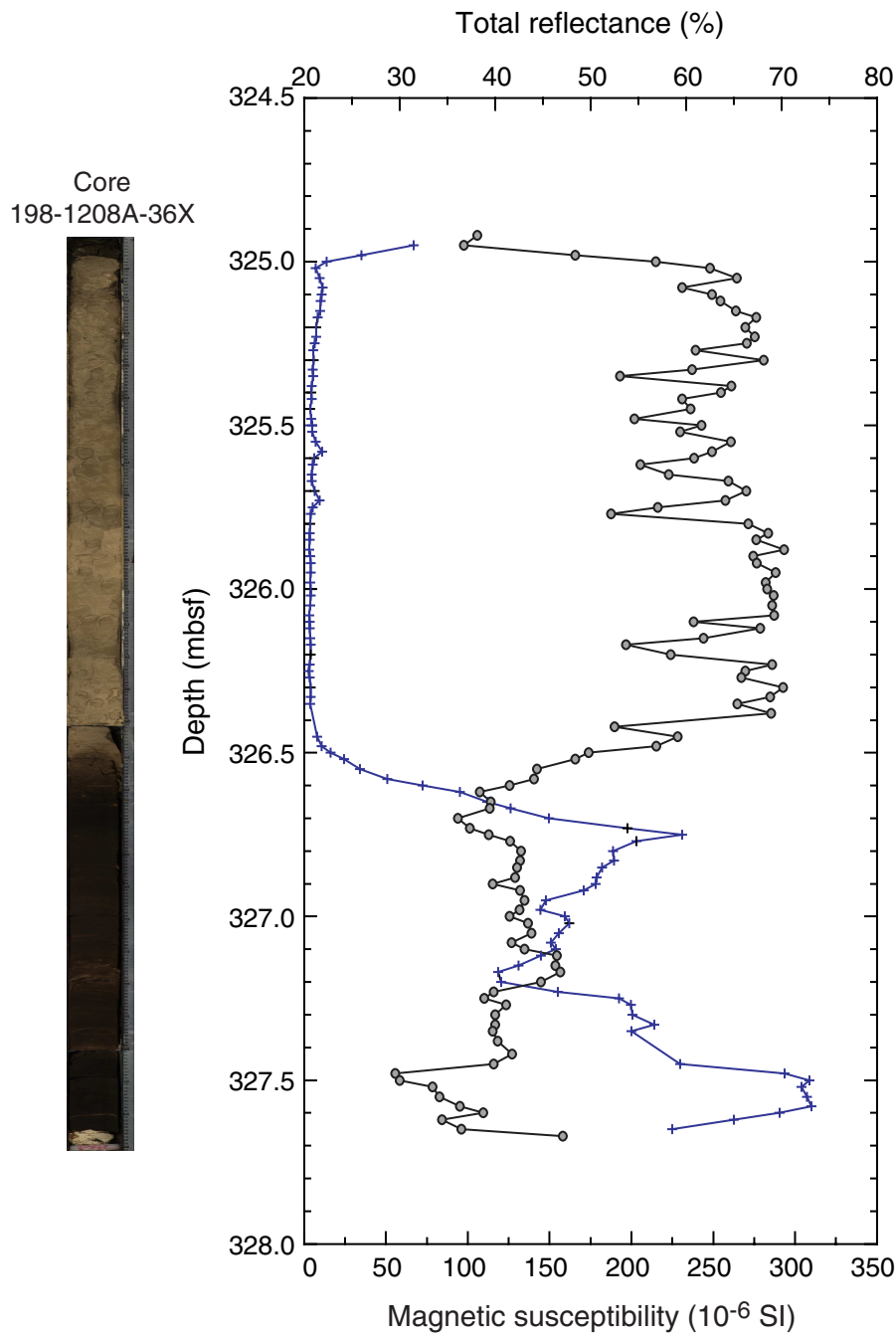


Figure F16. Color reflectance for Hole 1208A (1.25 to 2.5 Ma) plotted along with (A) obliquity and (B) precession as computed by Laskar (1990). The age model is based on an assumed constant sedimentation rate of 42 m/m.y.

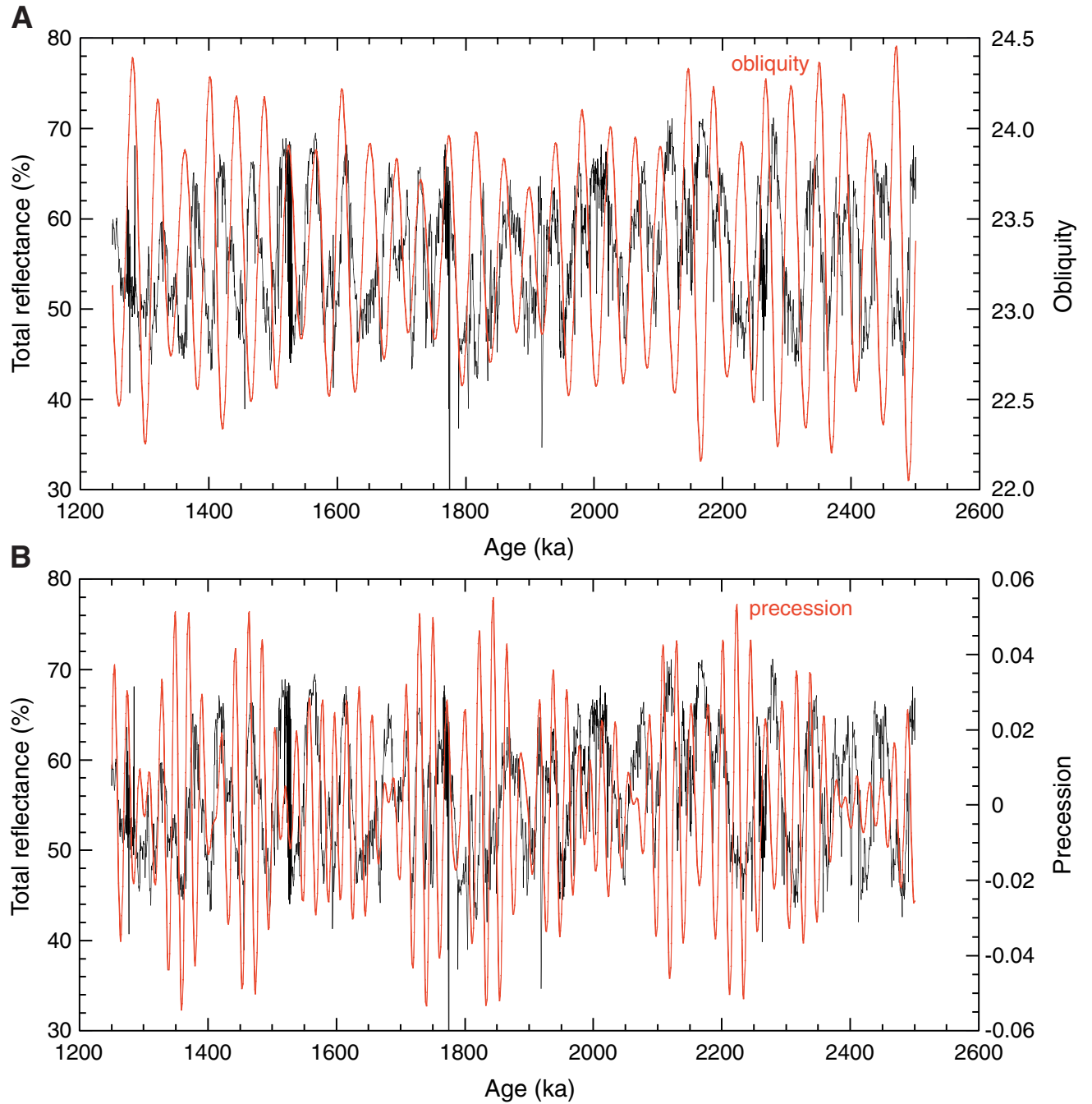


Figure F17. Digital photograph showing positions of nannofossil toothpick samples and age-diagnostic nannofossil datums (Sections 198-1208A-36X-2 and 36X-CC). The Eocene/Oligocene boundary is tentatively placed above the LO of the benthic foraminifer *Nuttalides truempyi*. LO = last occurrence, FO = first occurrence.

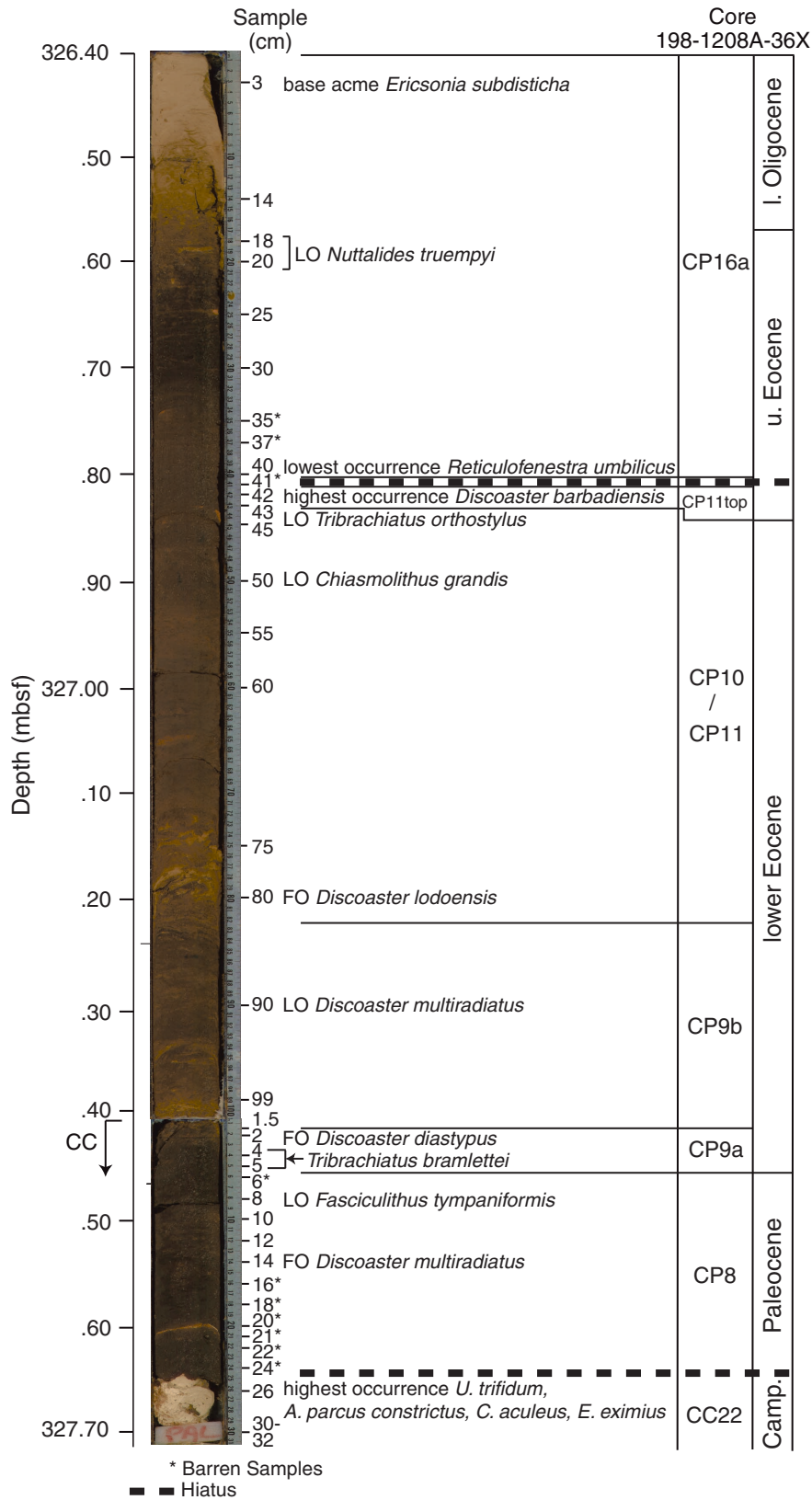


Figure F18. Hole 1208A archive-half magnetization intensities prior to demagnetization (open circles) and after AF demagnetization at peak fields of 20 mT (solid circles) as measured with the shipboard pass-through magnetometer.

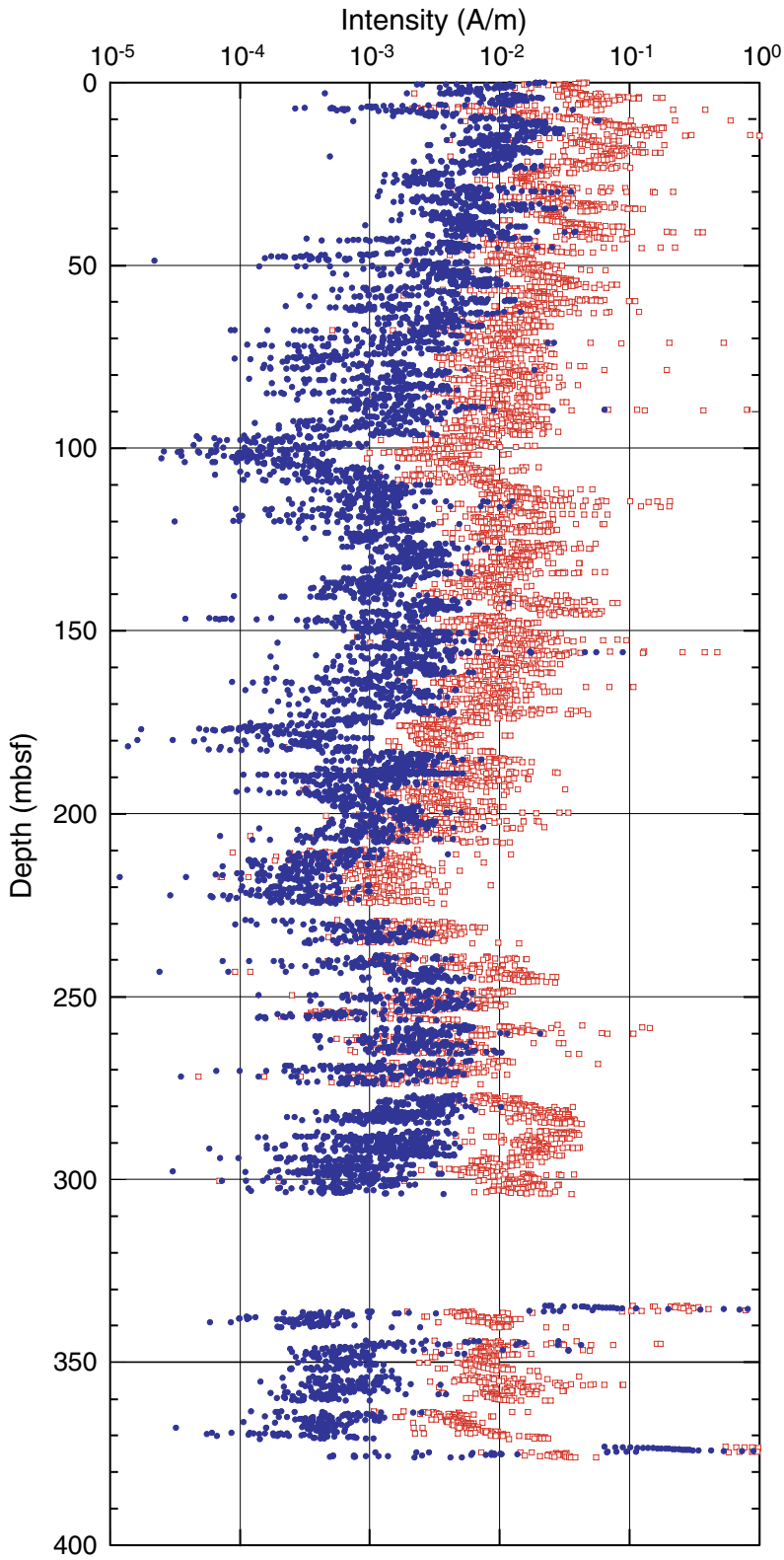


Figure F19. Inclination after AF demagnetization at peak fields of 20 mT as measured with the shipboard pass-through magnetometer at Hole 1208A. The column at the right of each plot shows interpreted zones of normal (black) and reversed (white) polarity. Gray intervals indicate zones in which no polarity interpretation is possible. Polarity zones at the top of the section and certain polarity zones farther downsection are tentatively correlated to polarity chrons.

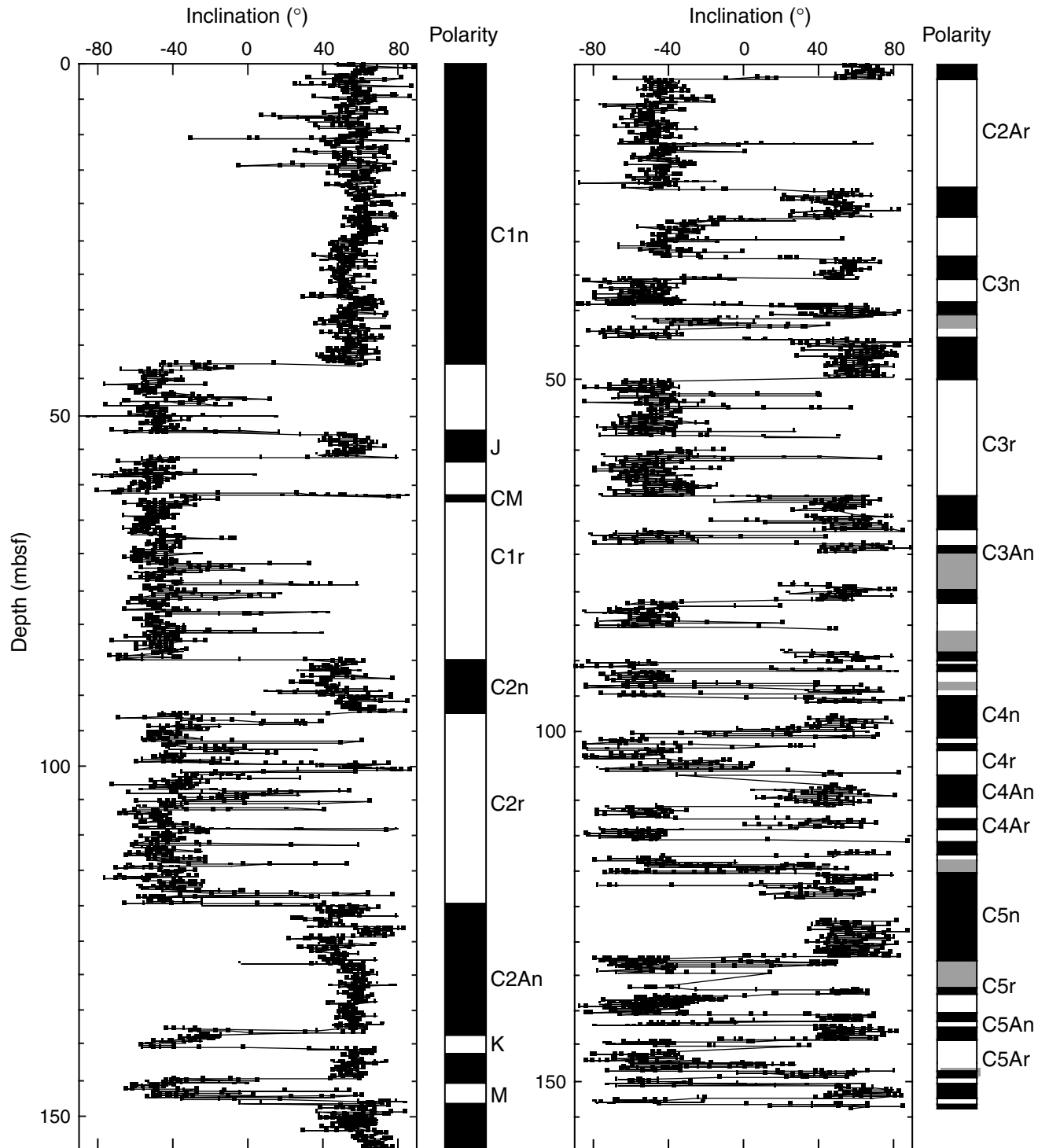
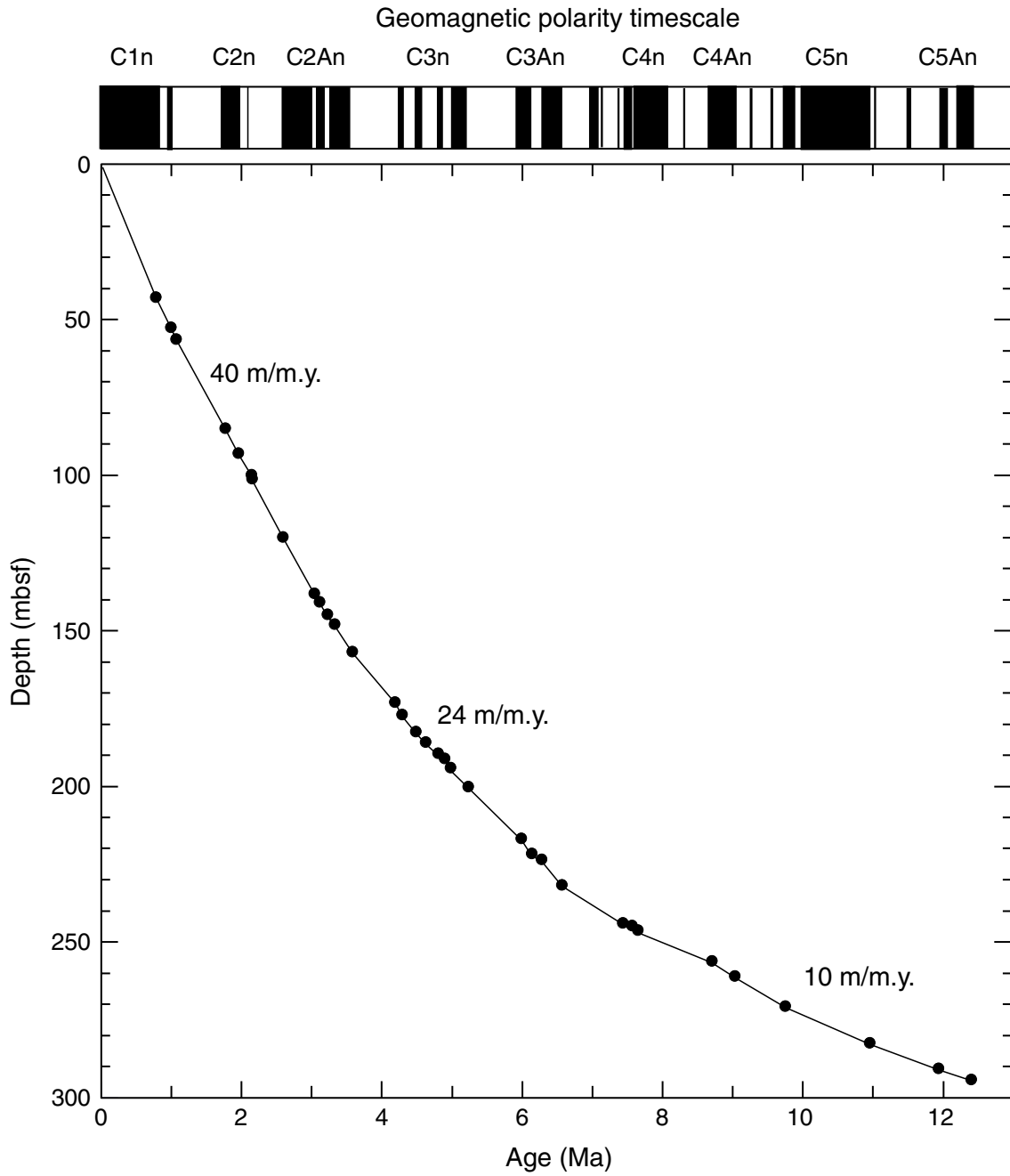


Figure F20. Age-depth curve for Site 1208 derived from the magnetic stratigraphy shown in Figure F19, p. 53, using the geomagnetic polarity timescale of Cande and Kent (1995). Average sedimentation rates in meters per million years are also plotted.



**Figure F21.** Age-depth plot of calcareous nannofossil (diamonds) and planktonic foraminiferal (crosses) datums in Hole 1208A. Datum ages and depths are presented in Tables T3, p. 80, and T4, p. 81.

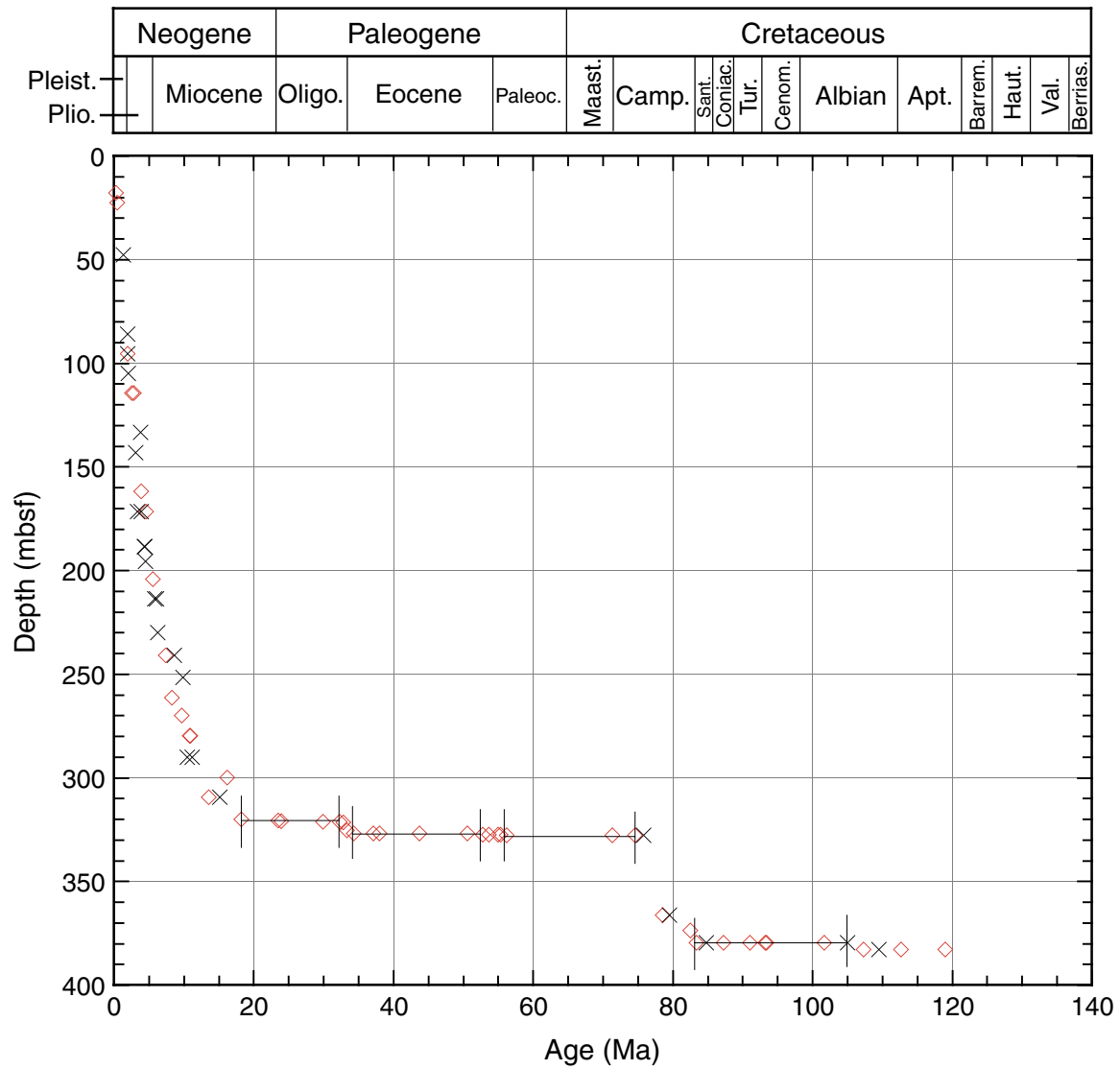


Figure F22. Age-depth plot of middle Eocene–late Paleocene calcareous nannofossil (diamonds) and planktonic foraminiferal (crosses) datums in Hole 1208A. Datum ages and depths are presented in Tables T3, p. 80, and T4, p. 81. FO = first occurrence, LO = last occurrence.

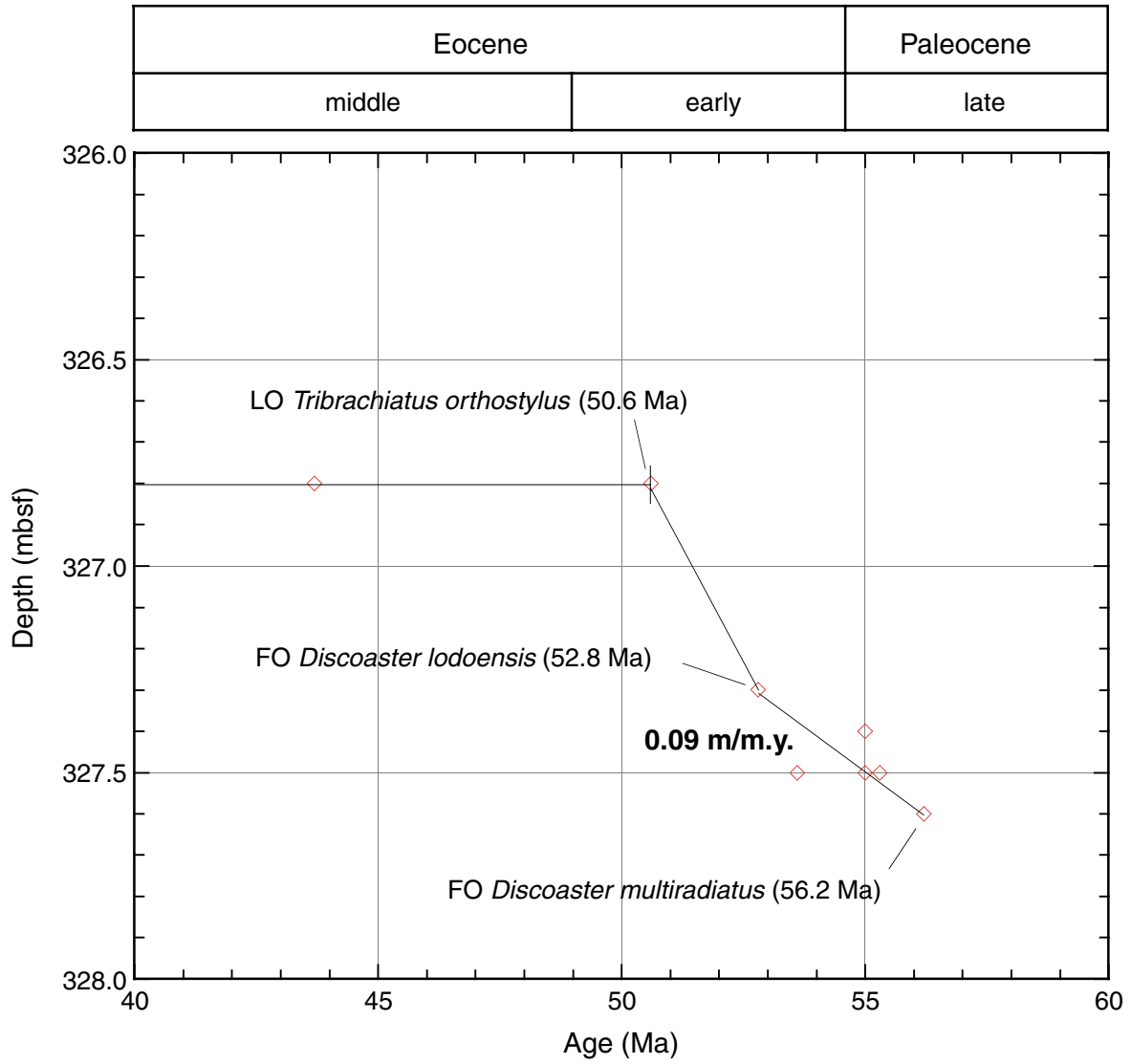


Figure F23. Age-depth plot of Neogene calcareous nannofossil (diamonds) and planktonic foraminiferal (crosses) datums in Hole 1208A. Datum ages and depths are presented in Tables T3, p. 80, and T4, p. 81. FO = first occurrence, LO = last occurrence.

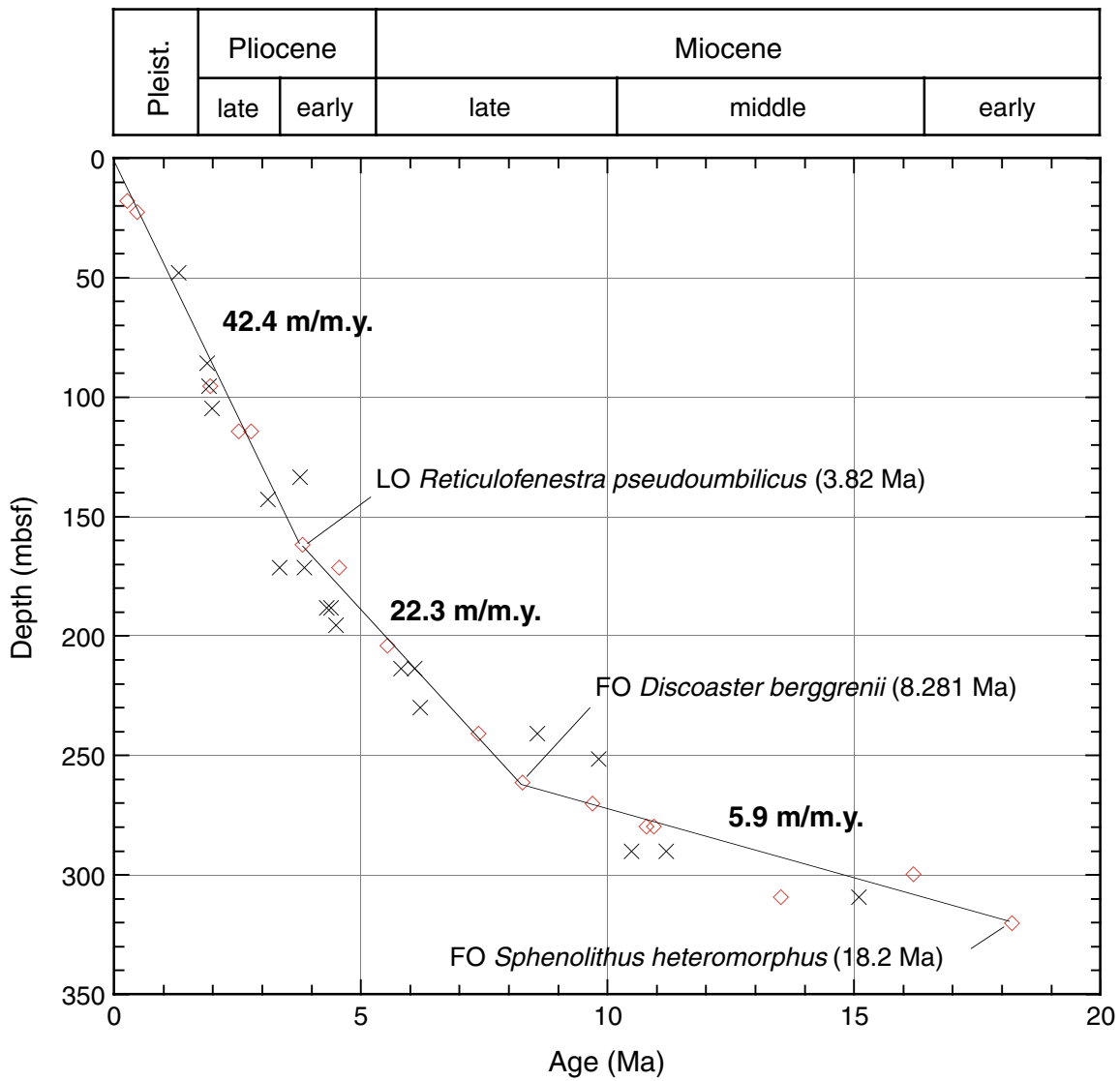


Figure F24. Age-depth plot of early Miocene–late Eocene calcareous nannofossil (diamonds) and planktonic foraminiferal (crosses) datums in Hole 1208A. Datum ages and depths are presented in Tables T3, p. 80, and T4, p. 81. FO = first occurrence, LO = last occurrence.

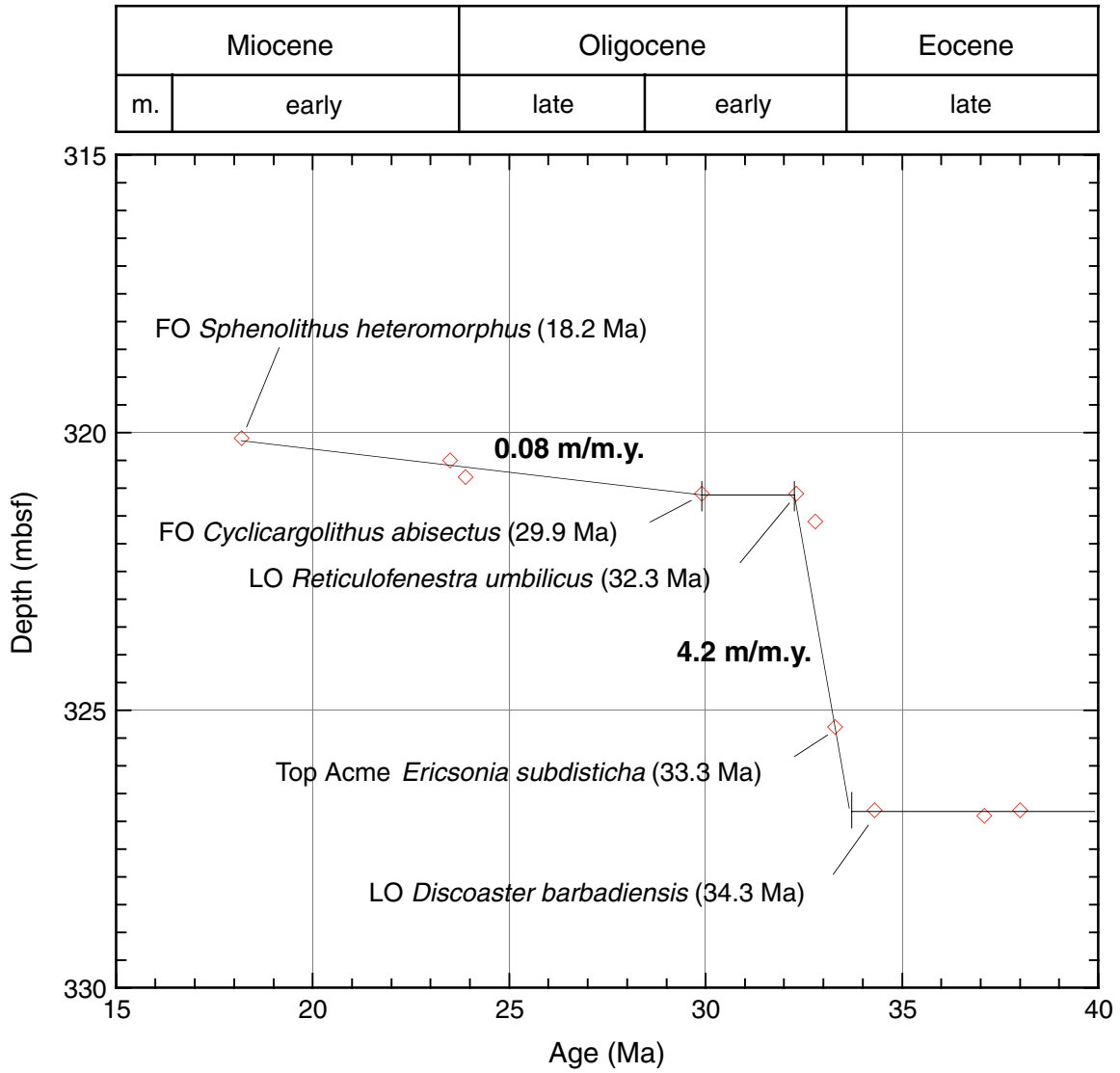


Figure F25. Age-depth plot of Cretaceous calcareous nannofossil (diamonds) and planktonic foraminiferal (crosses) datums in Hole 1208A. Datum ages and depths are presented in Tables T3, p. 80, and T4, p. 81. FO = first occurrence, LO = last occurrence.

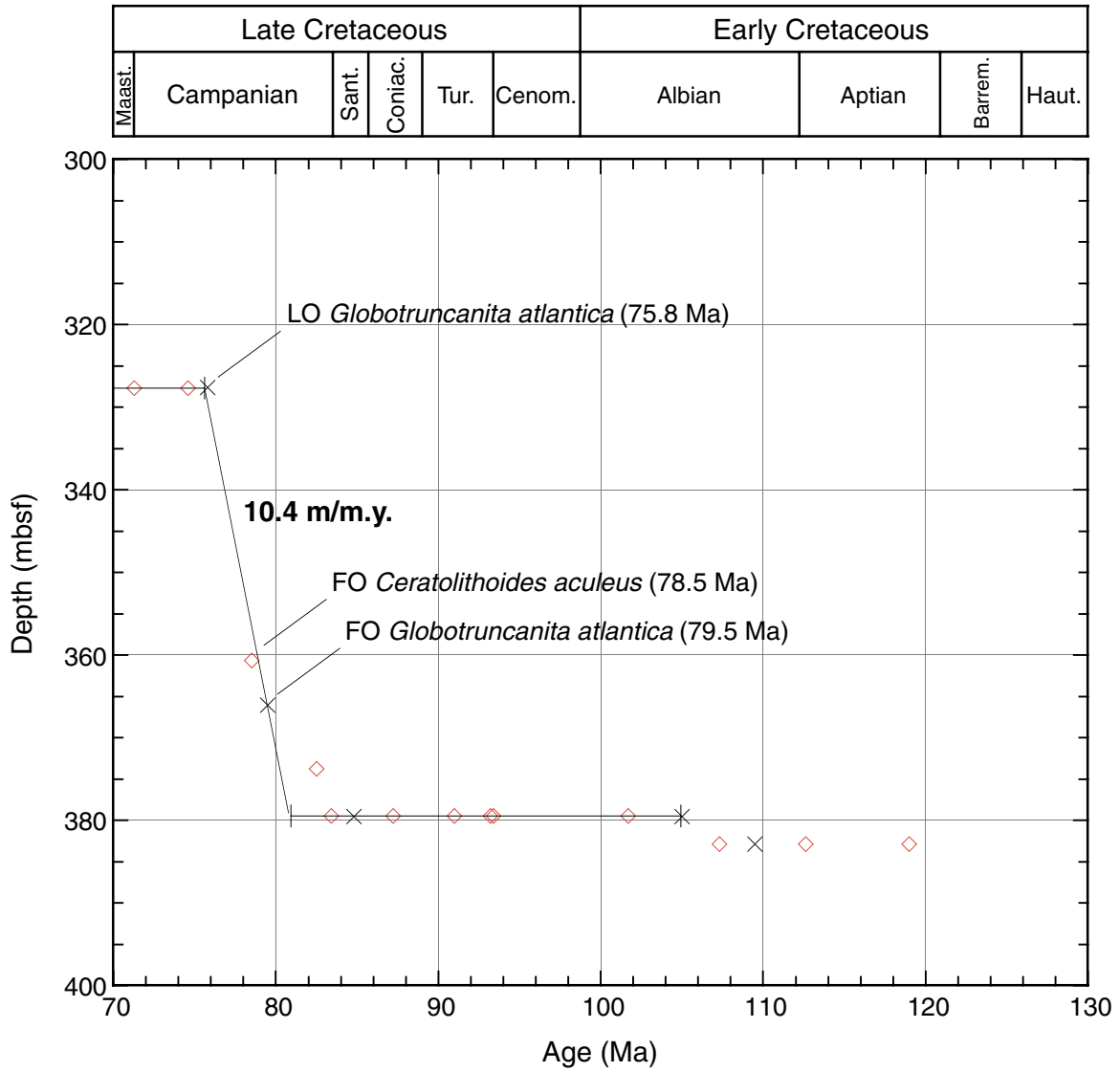


Figure F26. Mass accumulation rates for bulk sediment, carbonate fraction, and noncarbonate fraction vs. (A) depth and (B) age for the Neogene and Cretaceous of Hole 1208A.

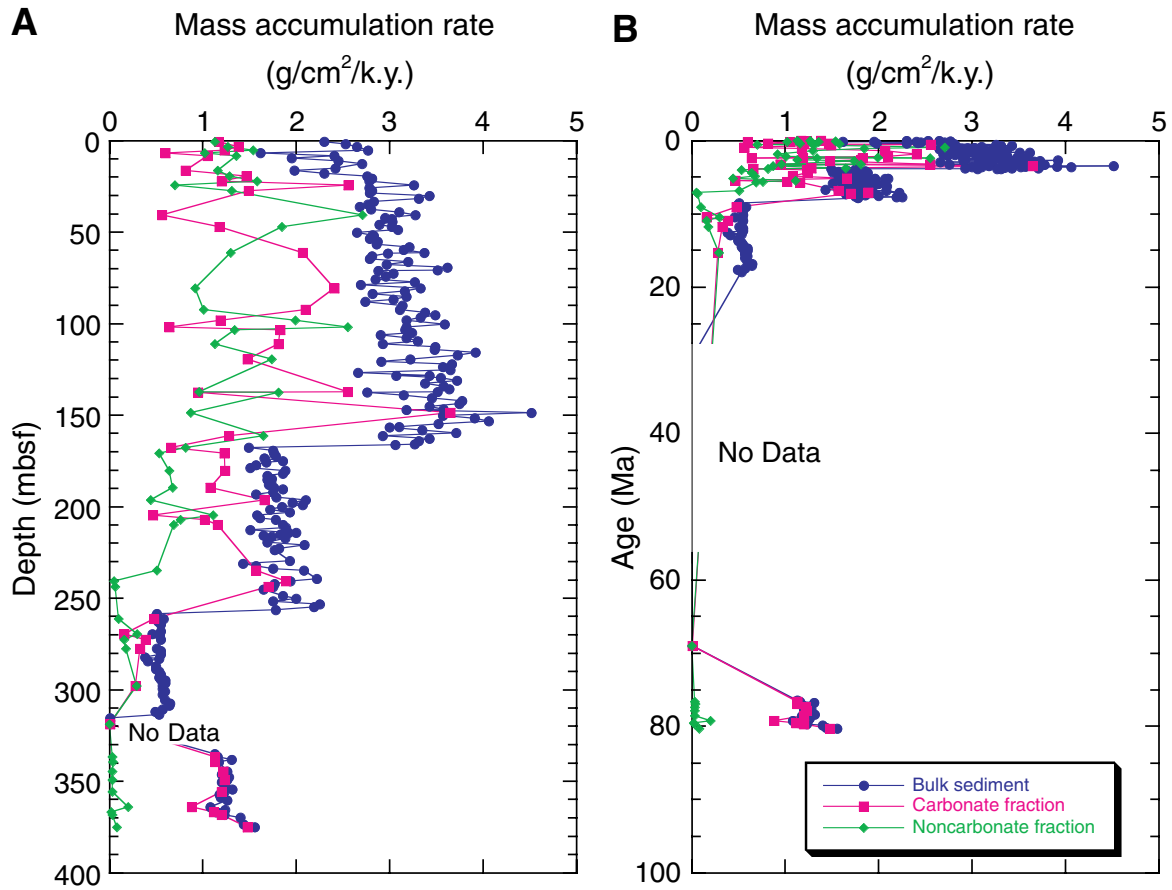
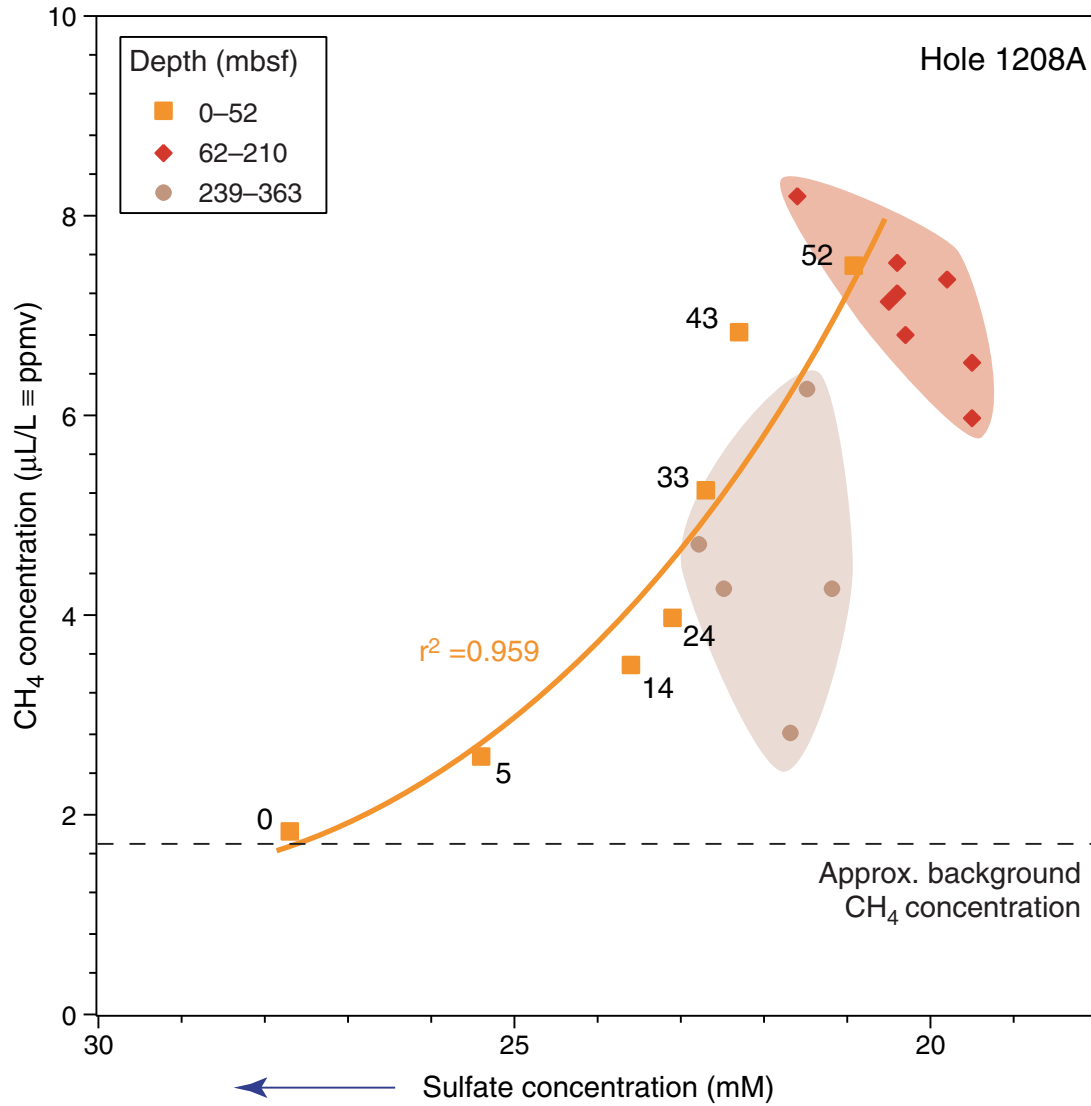


Figure F27. Plot of decreasing sulfate concentration vs. CH<sub>4</sub> concentration for Site 1208. The inverse exponential relationship for the upper 52 m and groupings to depth are shown.



**Figure F28.** Depth profiles of CH<sub>4</sub> and sulfate concentrations at Sites 1208, 846, 849, and 1009. Data are from Shipboard Scientific Party (1992a, 1992b, 1997).

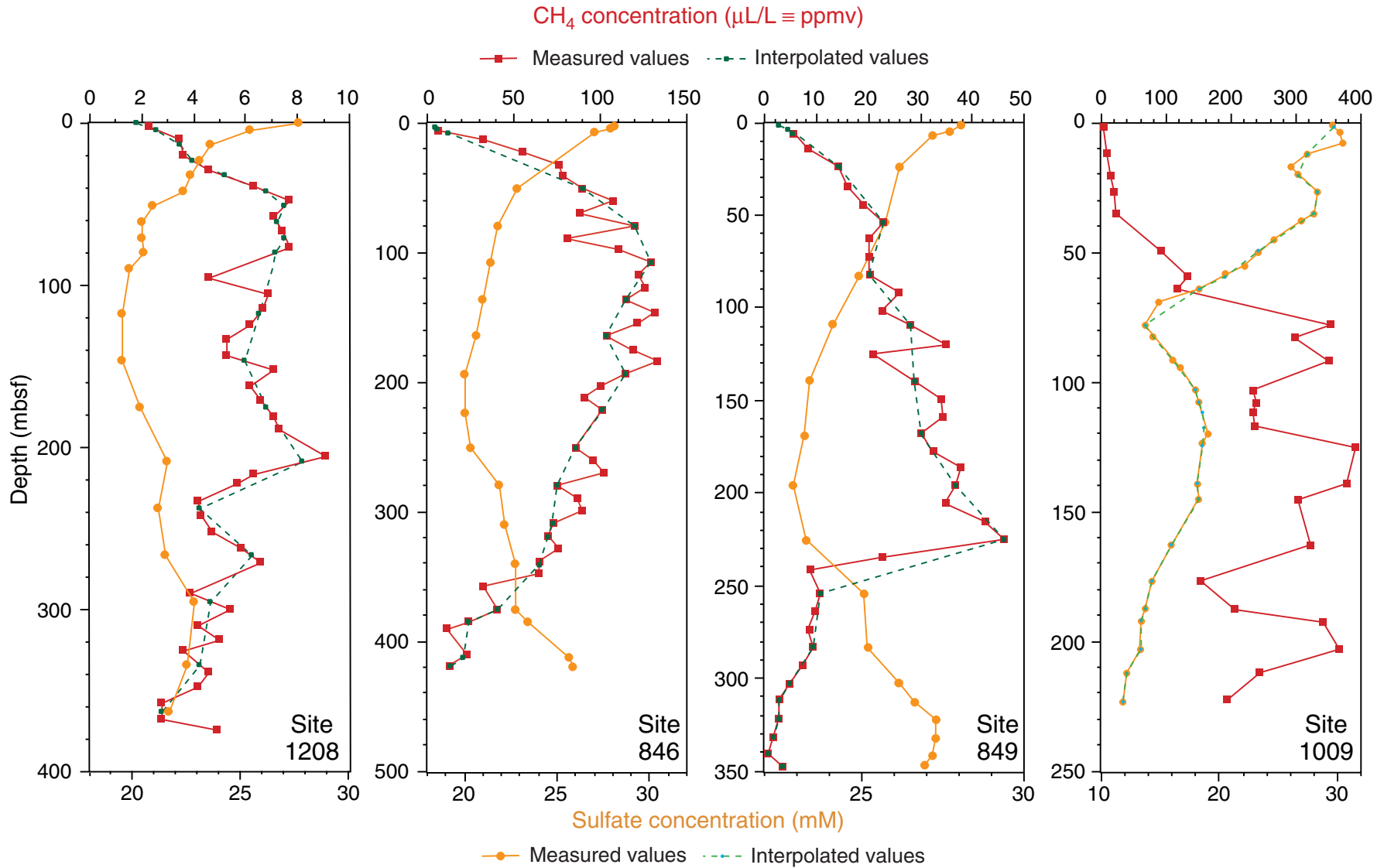
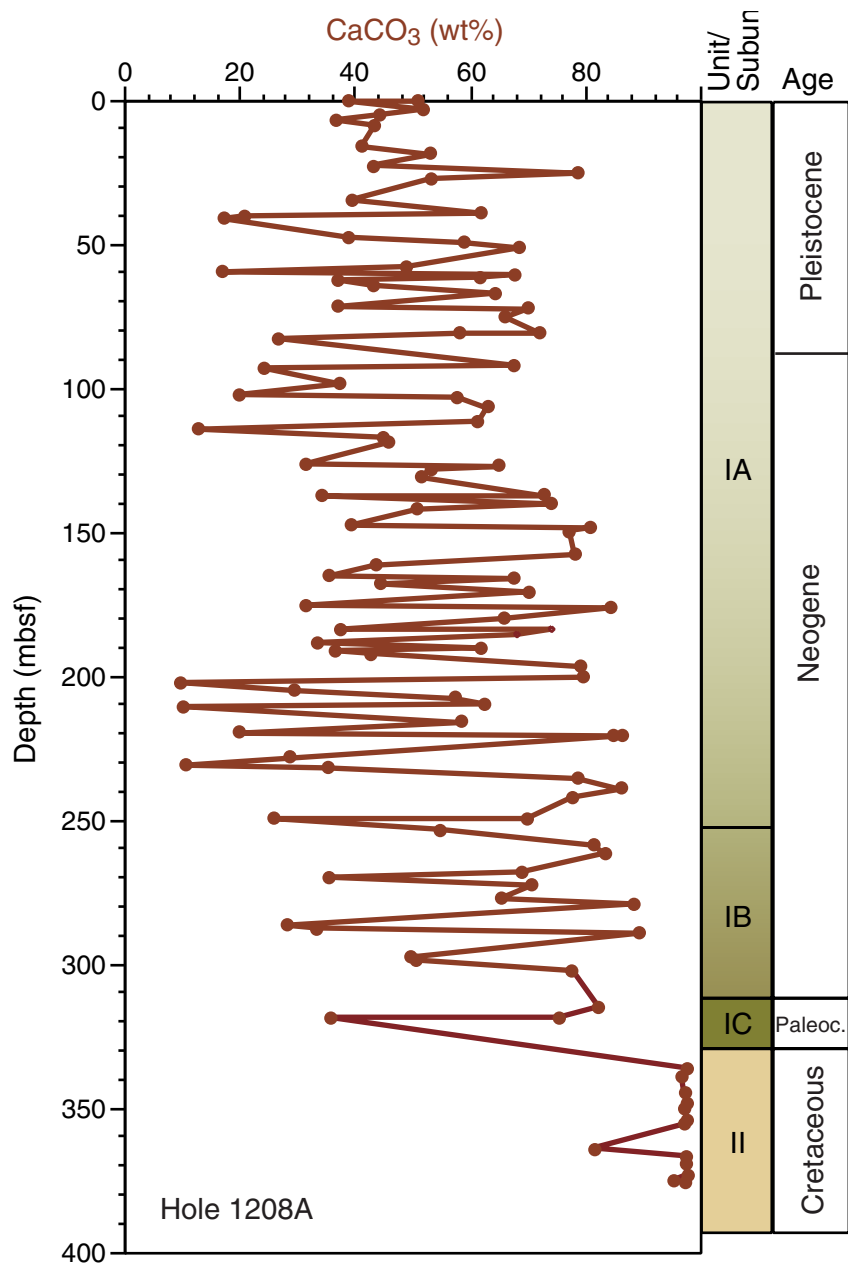
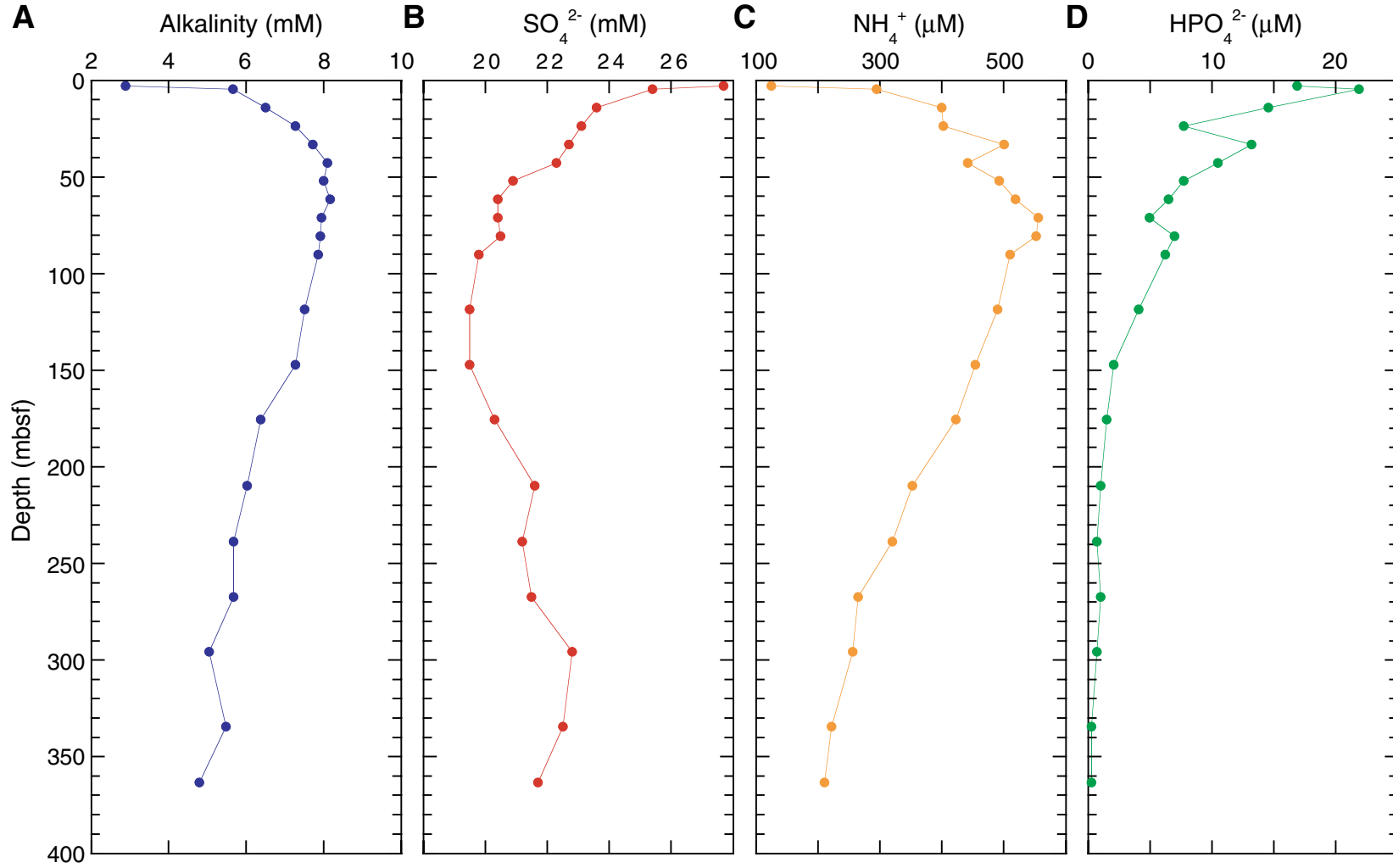


Figure F29. Downhole profiles of carbonate contents in Hole 1208A.



**Figure F30.** Site 1208 interstitial water profiles. **A.** Alkalinity. **B.** Sulfate. **C.** Ammonium. **D.** Phosphate. Alkalinity and sulfate profiles imply reducing conditions downcore, resulting in the degradation of organic matter and subsequent remobilization of ammonium and phosphate ions.



**Figure F31.** Crossplots implying related processes in Hole 1208A. **A.** Ammonium vs. alkalinity. **B.** Phosphate vs. alkalinity. **C.** Phosphate vs. calcium. The correlation of the alkalinity vs. ammonium implies that ammonia is being generated as a by-product of sulfate reduction. Downcore phosphate concentrations appear to be dominated by two different processes. Phosphate data for interstitial waters between 0.0 and 147.2 mbsf are correlated with calcium data ( $R^2 = 0.80$ ) to show that precipitation of calcium phosphate may be occurring. The correlation between phosphate and alkalinity below 147.2 mbsf implies that degradation of organic matter is the major influence on phosphate concentrations lower in the core.

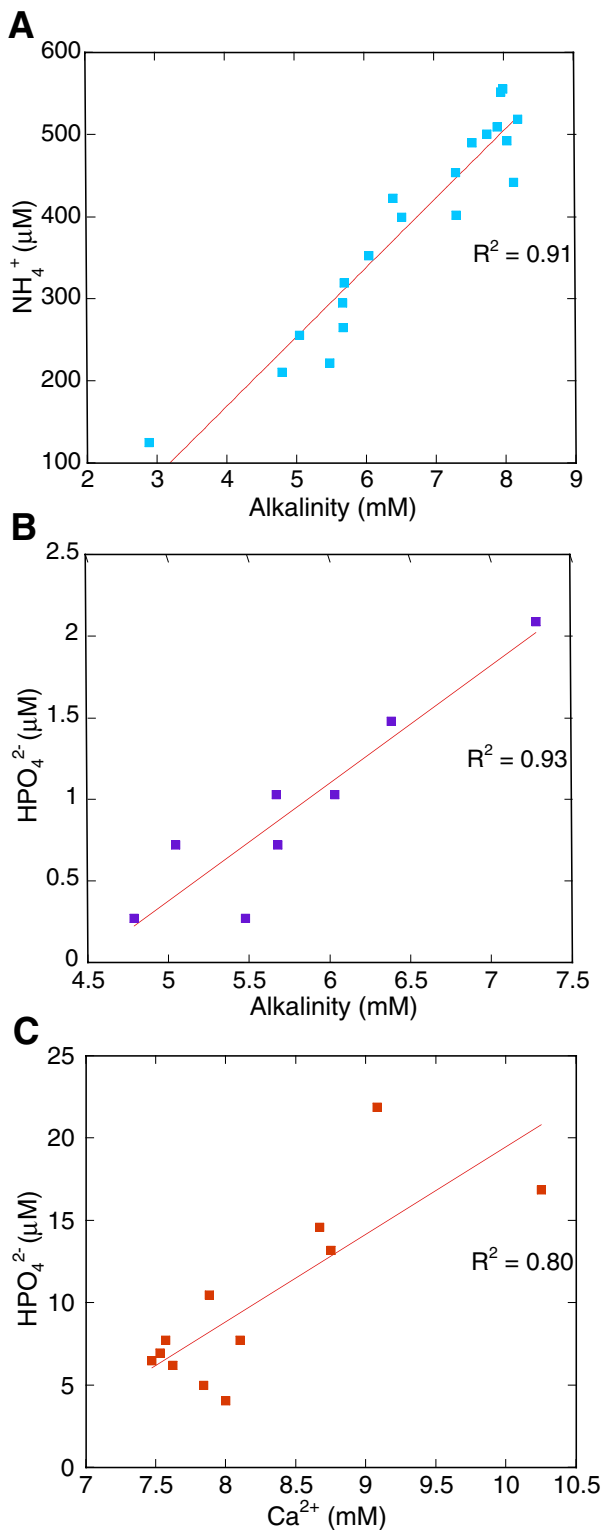
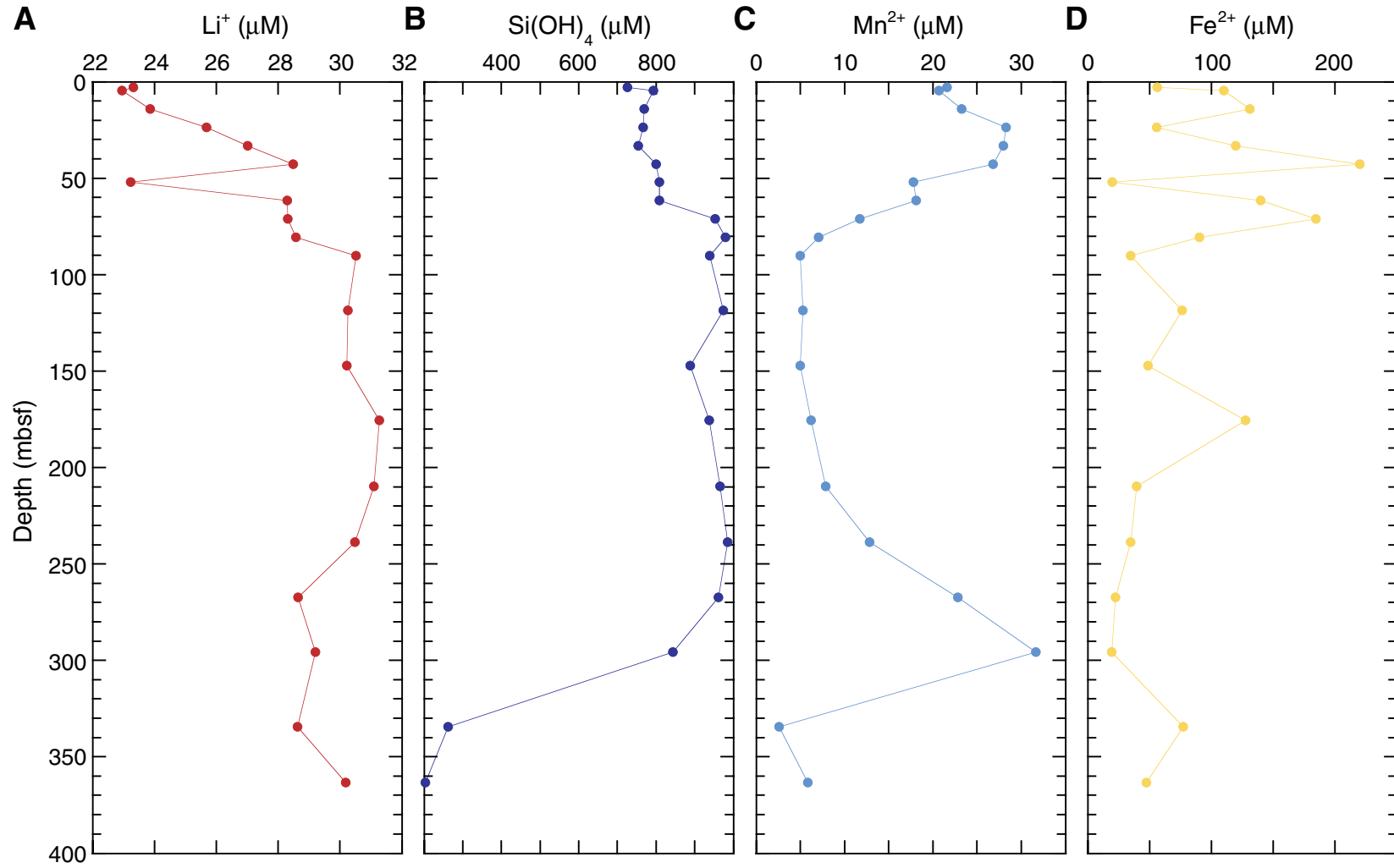


Figure F32. Hole 1208A pore water profiles. A. Lithium. B. Silicate. C. Manganese. D. Iron.



**Figure F33.** Interstitial water concentrations of major cations. **A.** Calcium. **B.** Sr and Sr/Ca ratio. **C.** Magnesium. **D.** Potassium. **E.** Magnesium vs. potassium. See “Calcium, Strontium, Magnesium, Boron, and Barium,” p. 27, in “Inorganic Geochemistry” for an explanation of the relationship.

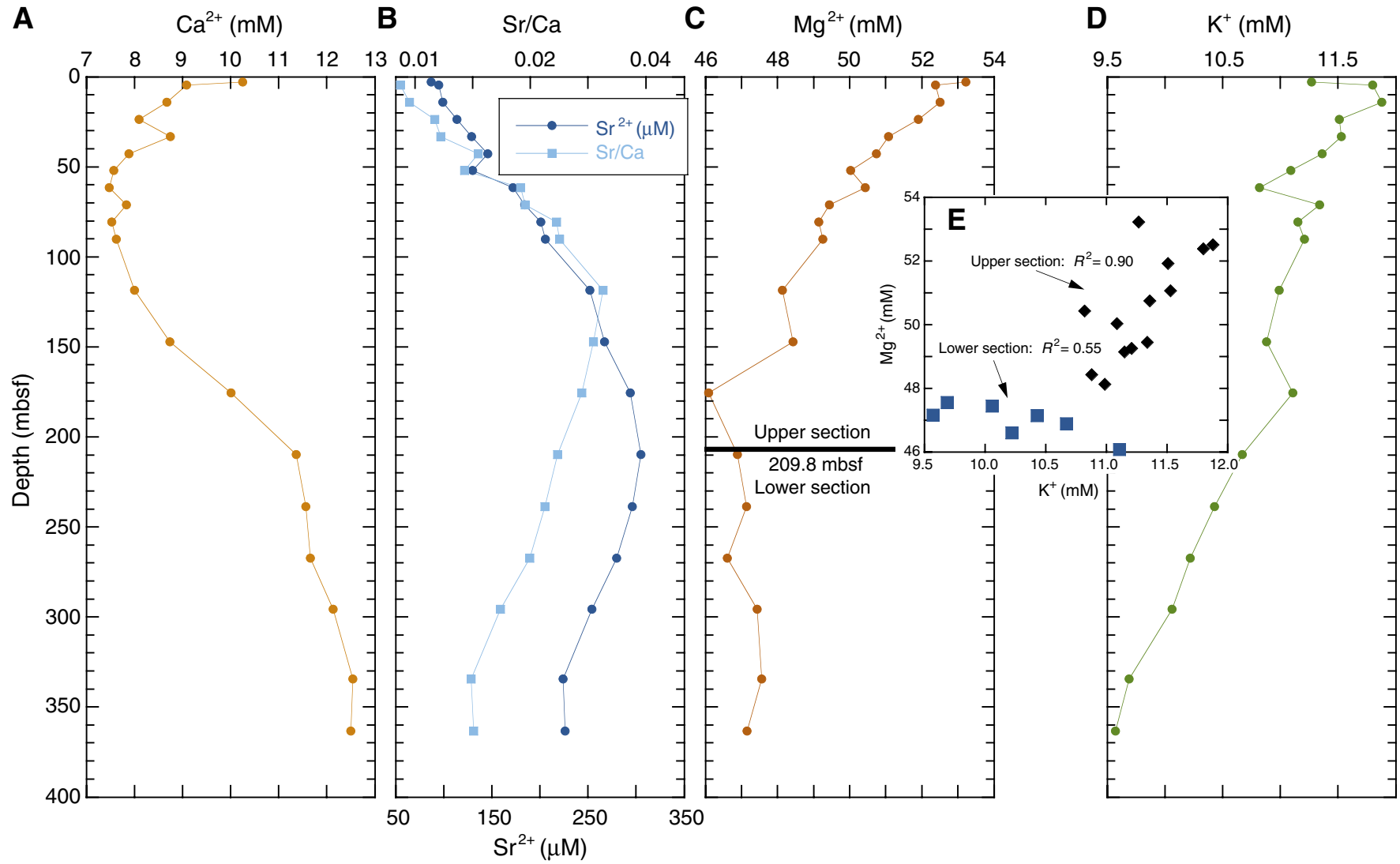


Figure F34. MST magnetic susceptibility measured in whole cores from Hole 1208A plotted vs. depth. Paleogene = Paleocene to early Oligocene. The accurate correction factor for the magnetic susceptibility raw instrument values is  $0.68 \times 10^{-5}$ .

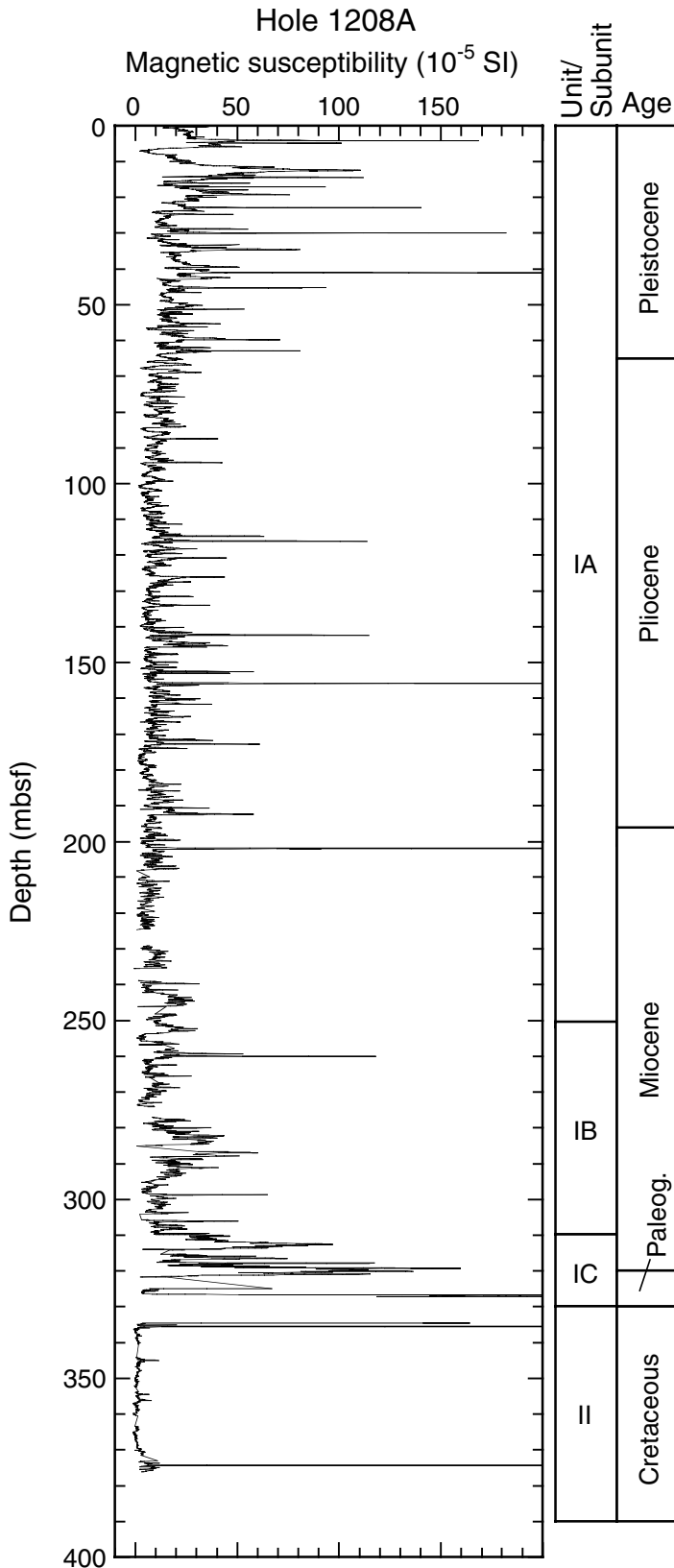


Figure F35. MST gamma ray attenuation (GRA) bulk density (lines) measured in whole cores from Hole 1208A plotted vs. depth. Discrete measurements of wet bulk density (see Table T9, p. 87) from Holes 1208A (solid circles) are plotted for comparison. Paleogene = Paleocene to early Oligocene.

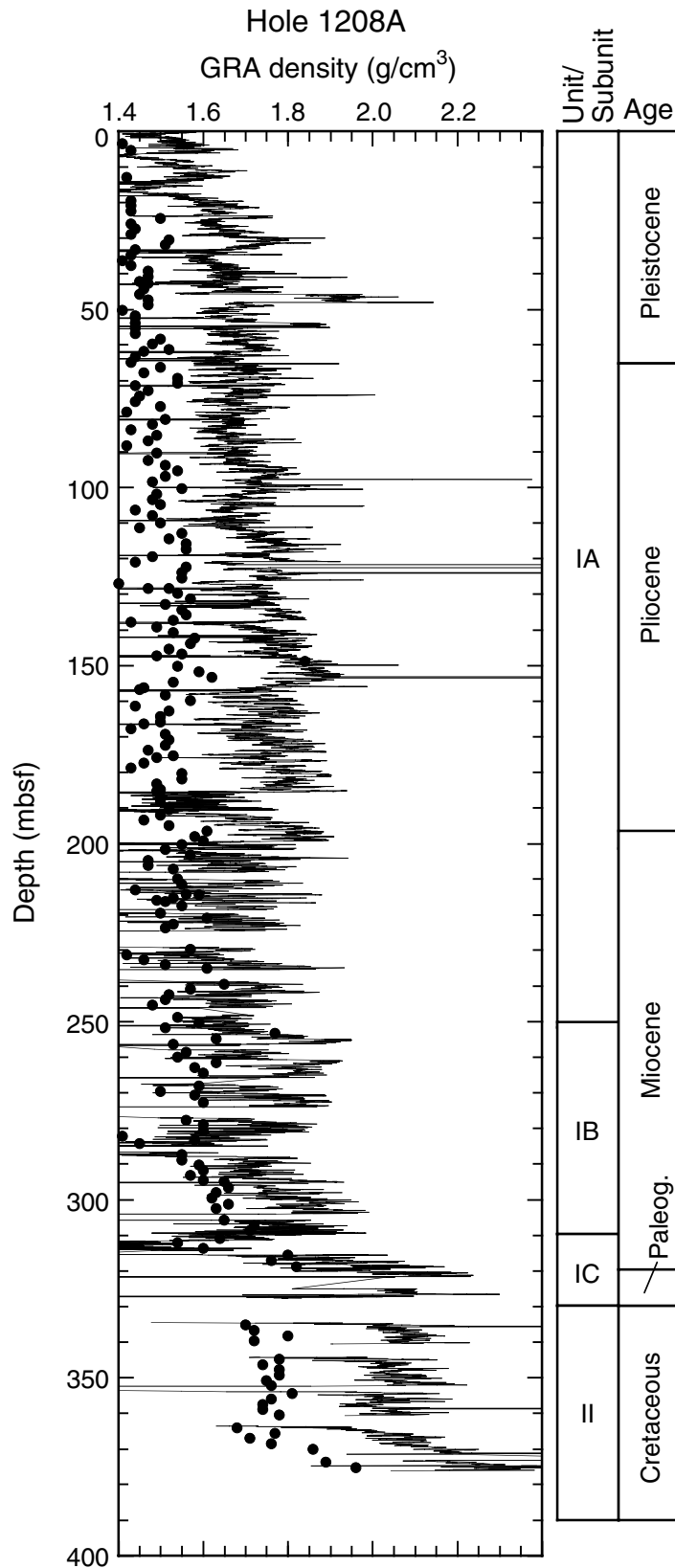


Figure F36. MST *P*-wave velocities measured in Hole 1208A whole cores (lines) plotted vs. depth. Discrete *P*-wave velocity (PWS3) data (solid circles) from the same intervals are also shown for comparison.

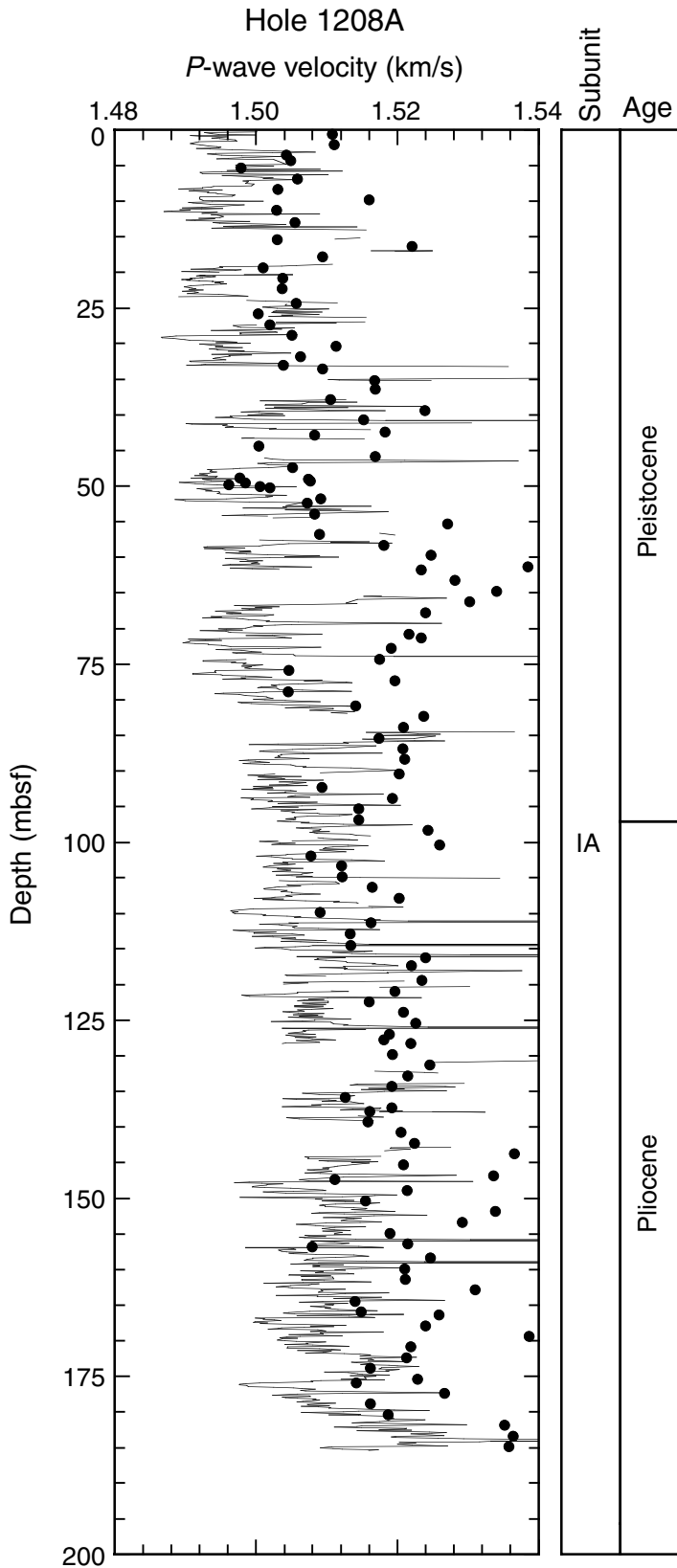


Figure F37. MST natural gamma radiation data for Hole 1208A plotted vs. depth. K = Cretaceous.

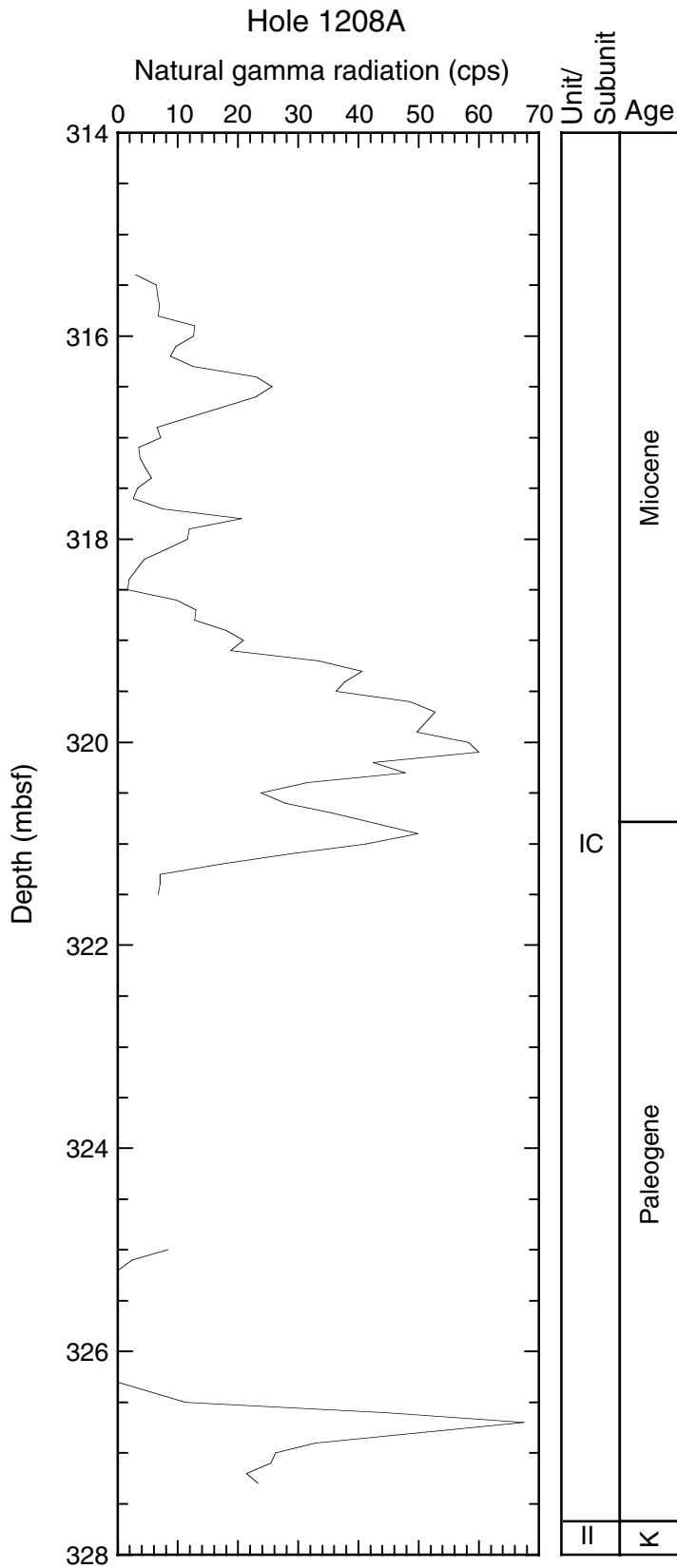


Figure F38. P-wave velocities for discrete samples from Holes 1208A plotted vs. depth. Paleogene = Paleocene to early Oligocene.

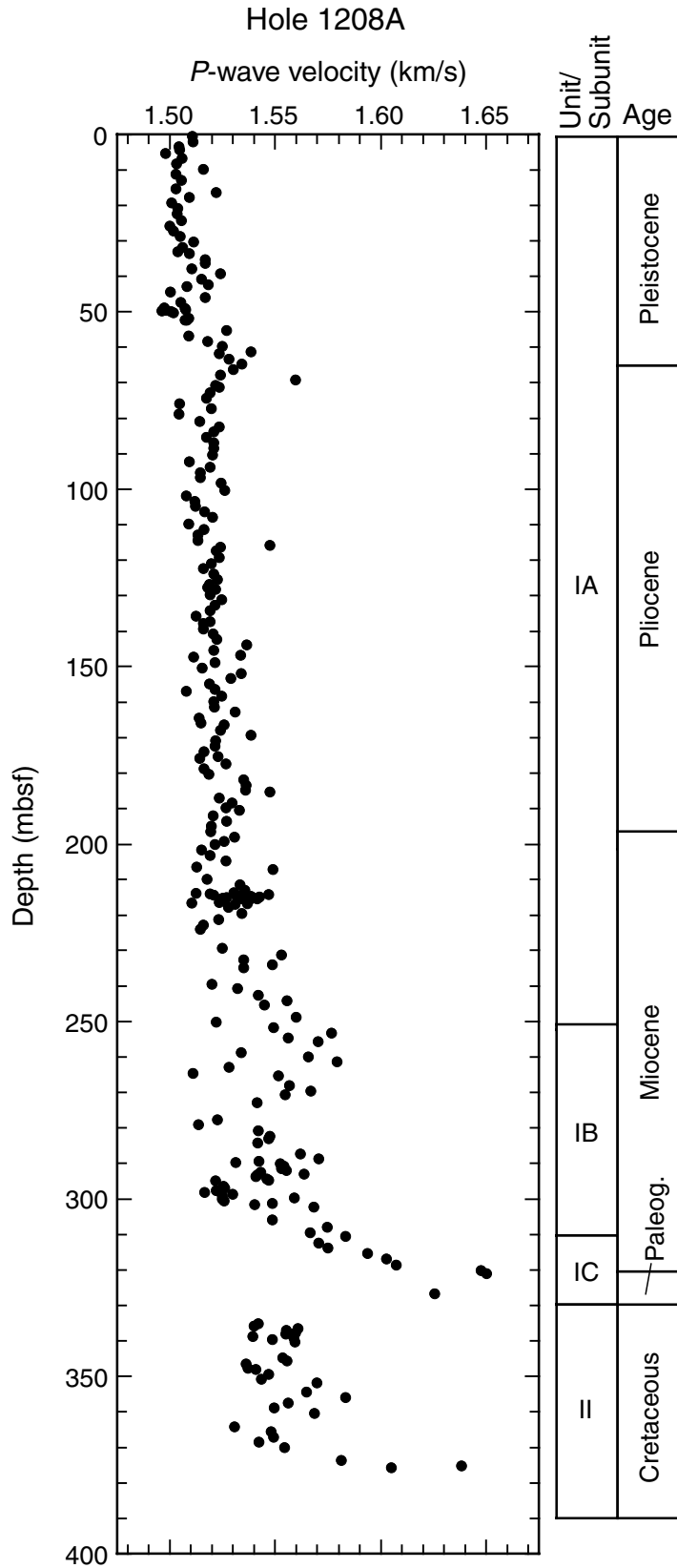


Figure F39. Discrete measurements of Hole 1208A *P*-wave velocities plotted vs. discrete wet bulk density measurements at comparable stratigraphic horizons.

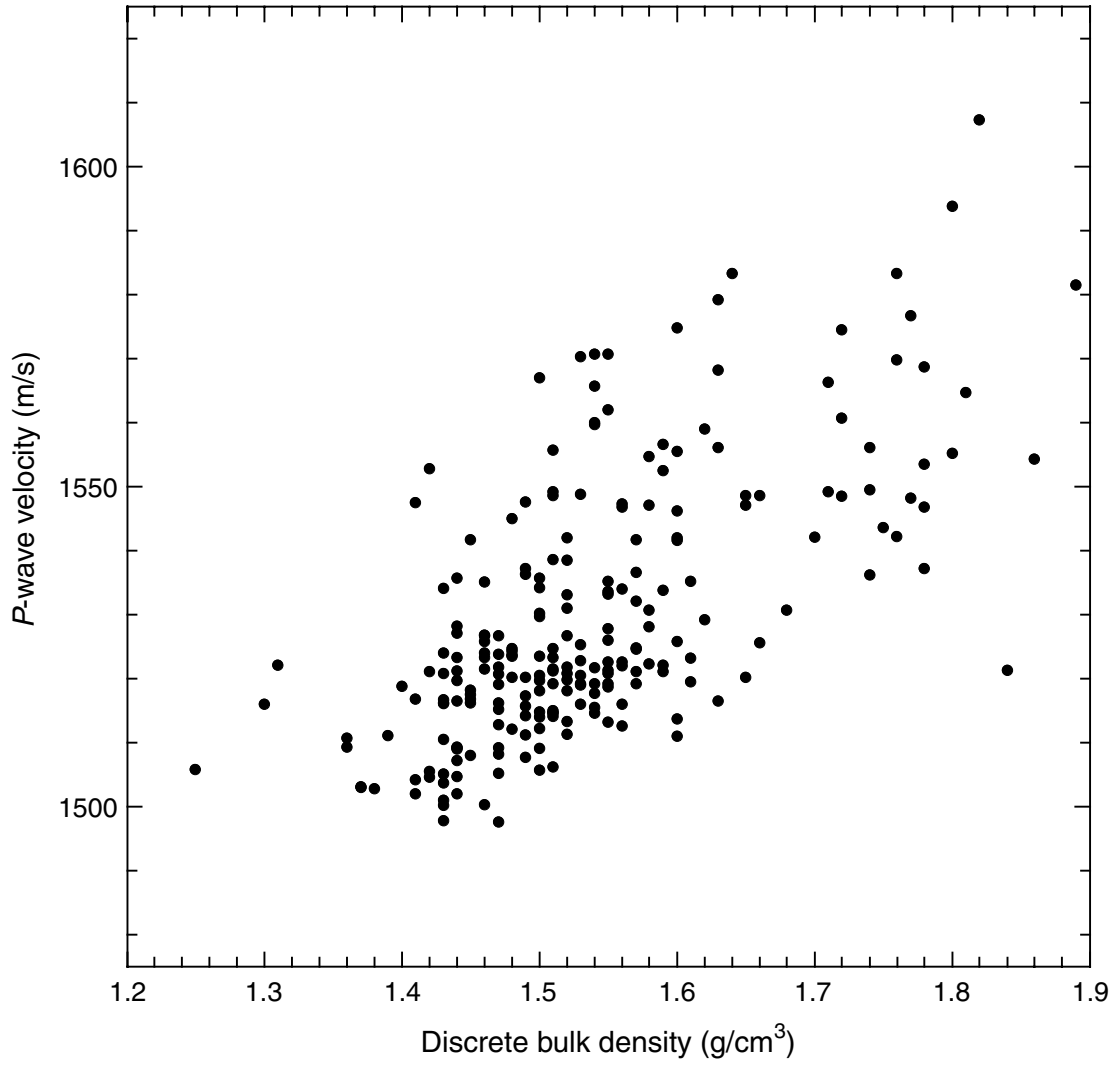


Figure F40. Thermal conductivity measured on Hole 1208A whole cores plotted vs. depth. Paleogene = Paleocene to early Oligocene.

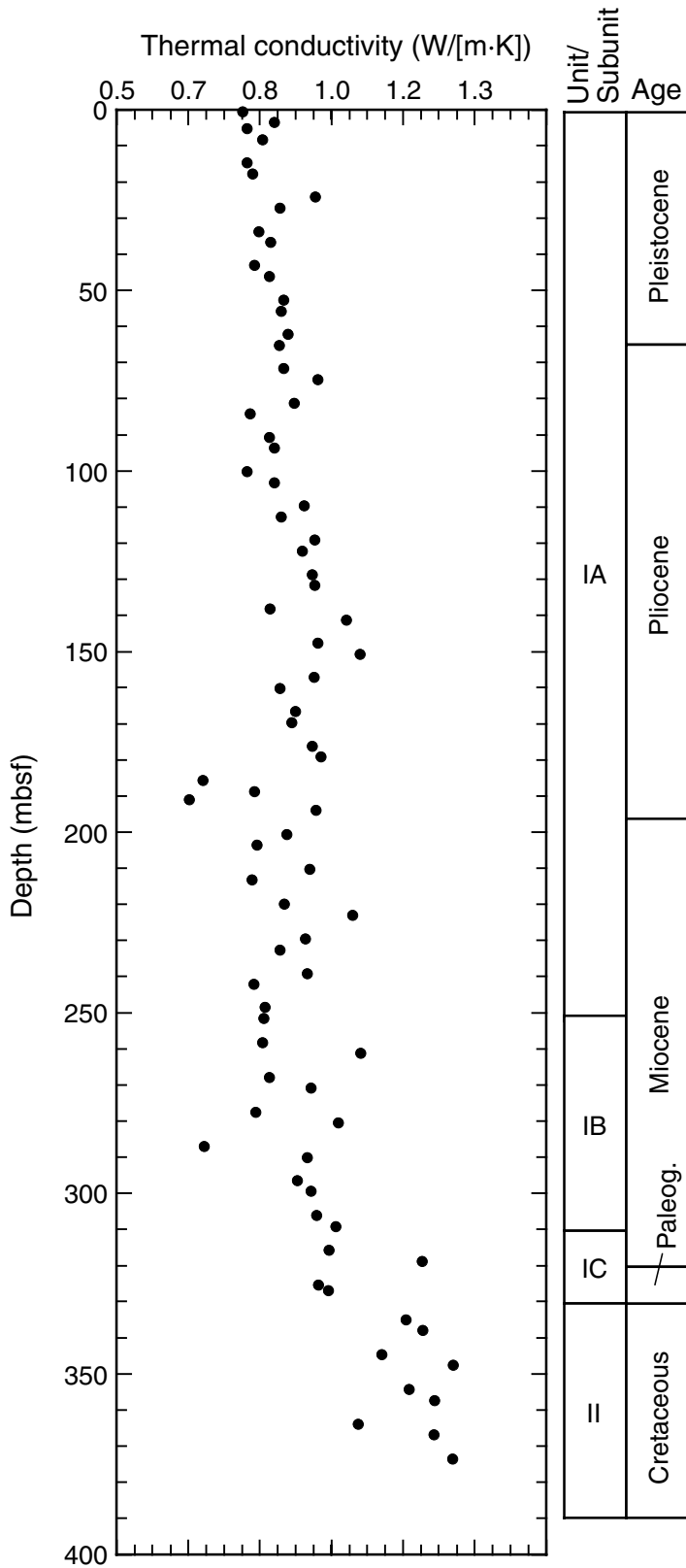


Figure F41. Hole 1208A whole-core thermal conductivity data plotted vs. discrete measurements of porosity for comparison.

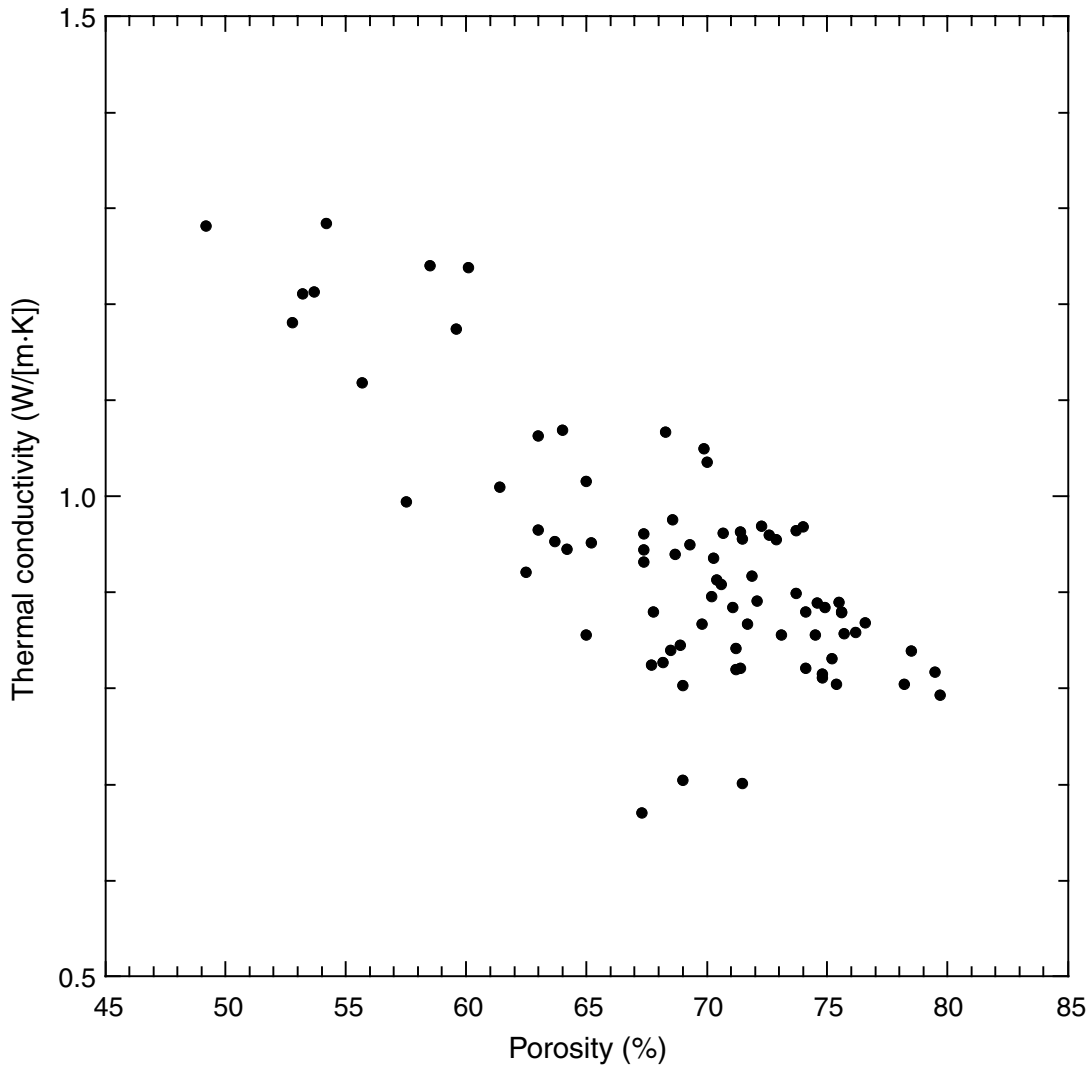


Figure F42. (A) Wet bulk density, (B) dry density, and (C) grain density determined for discrete samples from Hole 1208A plotted vs. depth. Paleogene = Paleocene to early Oligocene.

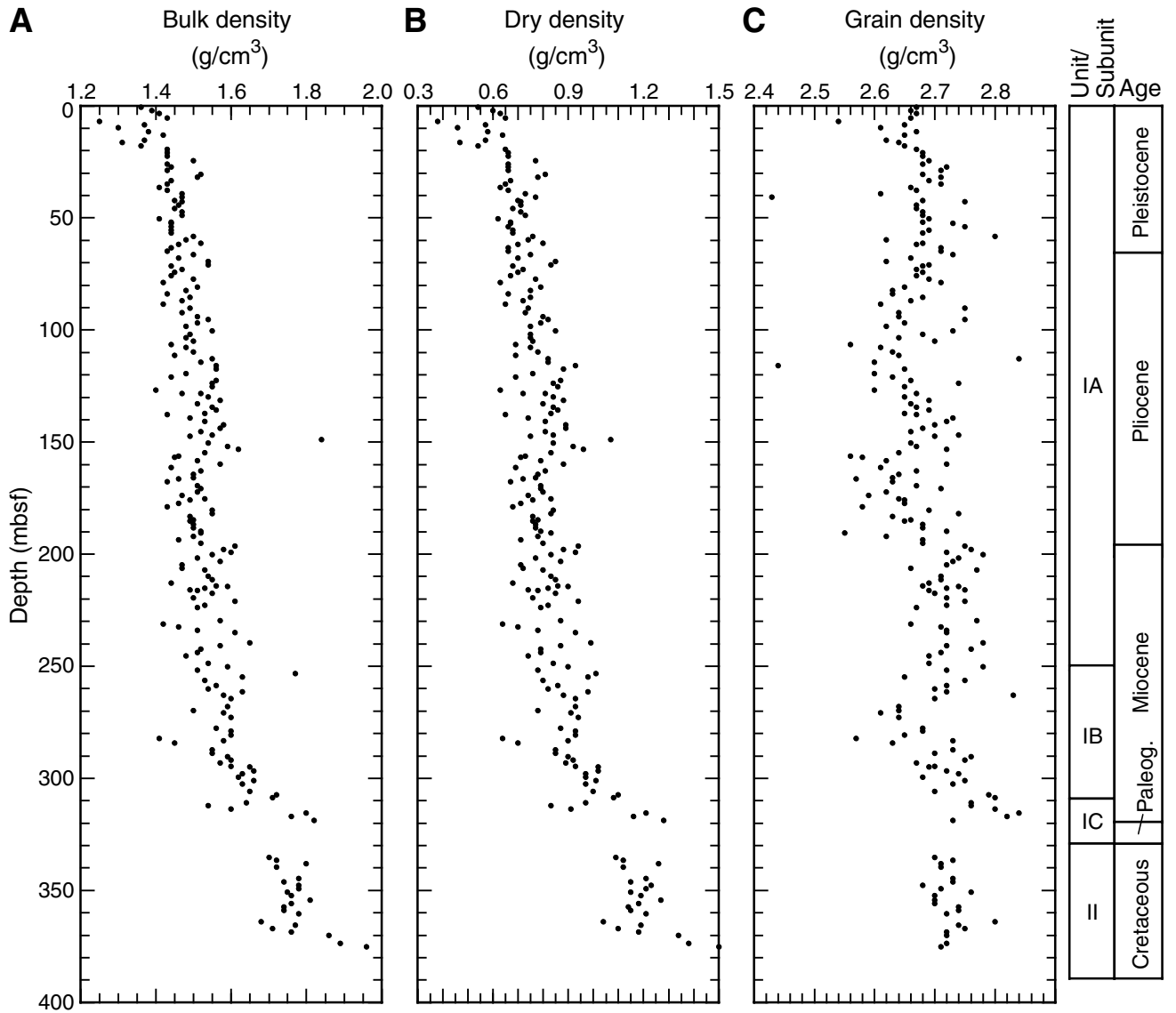
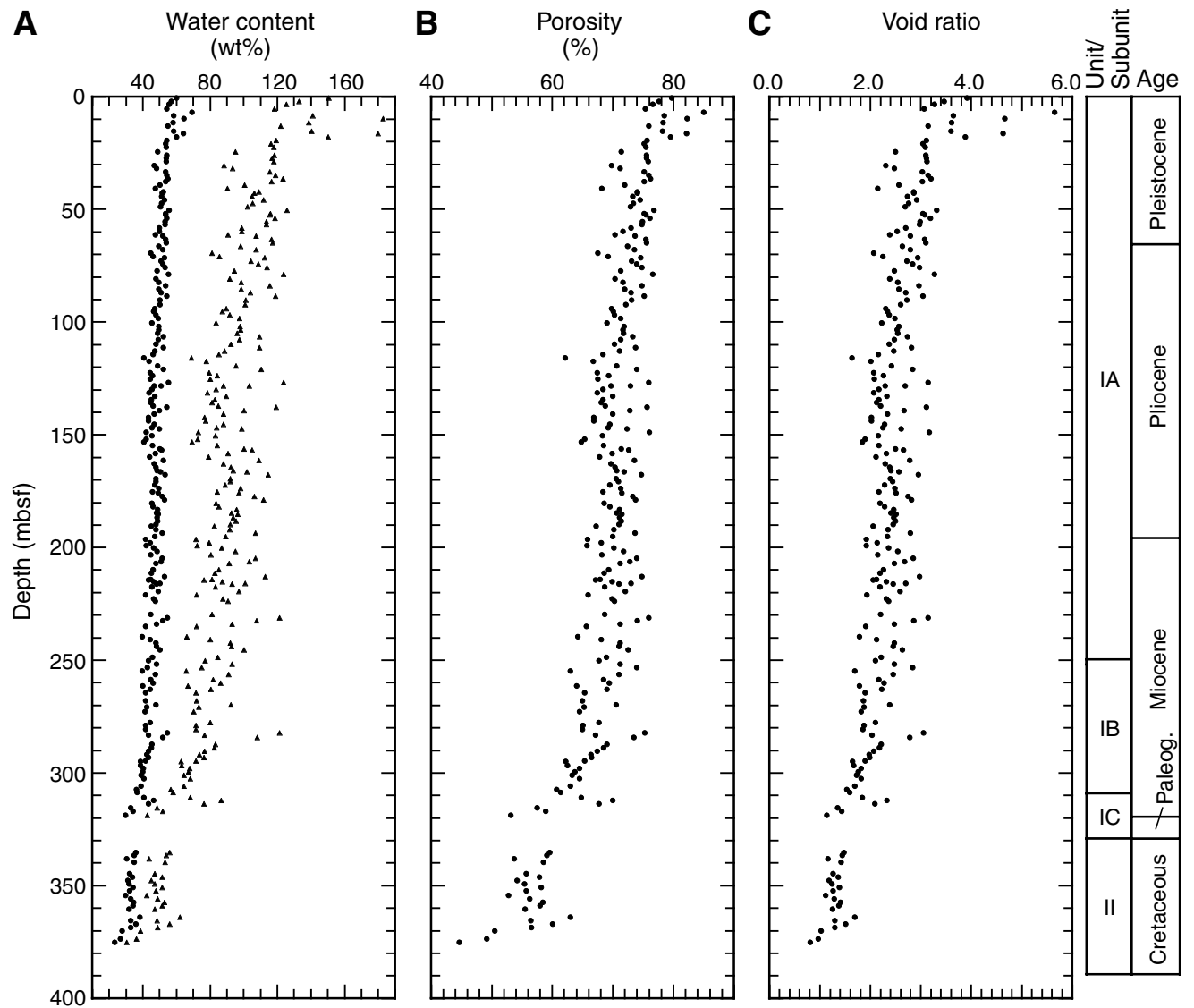


Figure F43. Water content (A) calculated relative to bulk sediment (circles) and solid phase (triangles), (B) porosity, and (C) void ratio determined for discrete samples from Hole 1208A plotted vs. depth. Paleogene = Paleocene to early Oligocene.



**Table T1.** Coring summary, Site 1208.

| <b>Hole 1208A</b>   |                    |                    |              |        |            |           |                 |
|---|--------------------|--------------------|--------------|--------|------------|-----------|-----------------|
| Latitude: 36°7.6301'N   |                    |                    |              |        |            |           |                 |
| Longitude: 158°12.0952'E  |                    |                    |              |        |            |           |                 |
| Time on site (hr): 62.25 (2315 hr, 14 Sep–1330 hr, 17 Sep 2001)   |                    |                    |              |        |            |           |                 |
| Time on hole (hr): 62.25 (2315 hr, 14 Sep–1330 hr, 17 Sep 2001)   |                    |                    |              |        |            |           |                 |
| Seafloor (drill pipe measurement from rig floor, mbrf): 3356.8    |                    |                    |              |        |            |           |                 |
| Distance between rig floor and sea level (m): 11.1                |                    |                    |              |        |            |           |                 |
| Water depth (drill pipe measurement from sea level, m): 3345.7    |                    |                    |              |        |            |           |                 |
| Total depth (drill pipe measurement from rig floor, mbrf): 3749.1 |                    |                    |              |        |            |           |                 |
| Total penetration (mbsf): 392.3                                   |                    |                    |              |        |            |           |                 |
| Total length of cored section (m): 392.3                          |                    |                    |              |        |            |           |                 |
| Total core recovered (m): 345.9                                   |                    |                    |              |        |            |           |                 |
| Core recovery (%): 88.17  |                    |                    |              |        |            |           |                 |
| Total number of cores: 42   |                    |                    |              |        |            |           |                 |
| Total number of drilled intervals: 0                              |                    |                    |              |        |            |           |                 |
| Core  | Date<br>(Sep 2001) | Local time<br>(hr) | Depth (mbsf) |        | Length (m) |           | Recovery<br>(%) |
|   |                    |                    | Top          | Bottom | Cored      | Recovered |                 |
| 198-1208A-  |                    |                    |              |        |            |           |                 |
| 1H  | 15                 | 0945               | 0.0          | 4.7    | 4.7        | 4.75      | 101.1           |
| 2H  | 15                 | 1035               | 4.7          | 14.2   | 9.5        | 9.59      | 100.9           |
| 3H  | 15                 | 1130               | 14.2         | 23.7   | 9.5        | 9.67      | 101.8           |
| 4H  | 15                 | 1235               | 23.7         | 33.2   | 9.5        | 9.82      | 103.4           |
| 5H  | 15                 | 1330               | 33.2         | 42.7   | 9.5        | 9.96      | 104.8           |
| 6H  | 15                 | 1430               | 42.7         | 52.2   | 9.5        | 9.97      | 104.9           |
| 7H  | 15                 | 1524               | 52.2         | 61.7   | 9.5        | 10.00     | 105.3           |
| 8H  | 15                 | 1625               | 61.7         | 71.2   | 9.5        | 9.95      | 104.7           |
| 9H  | 15                 | 1718               | 71.2         | 80.7   | 9.5        | 9.94      | 104.6           |
| 10H   | 15                 | 1824               | 80.7         | 90.2   | 9.5        | 9.97      | 104.9           |
| 11H   | 15                 | 1920               | 90.2         | 99.7   | 9.5        | 10.01     | 105.4           |
| 12H   | 15                 | 2015               | 99.7         | 109.2  | 9.5        | 9.85      | 103.7           |
| 13H   | 15                 | 2110               | 109.2        | 118.7  | 9.5        | 9.93      | 104.5           |
| 14H   | 15                 | 2205               | 118.7        | 128.2  | 9.5        | 10.05     | 105.8           |
| 15H   | 15                 | 2300               | 128.2        | 137.7  | 9.5        | 10.05     | 105.8           |
| 16H   | 15                 | 2355               | 137.7        | 147.2  | 9.5        | 10.12     | 106.5           |
| 17H   | 16                 | 0050               | 147.2        | 156.7  | 9.5        | 10.06     | 105.9           |
| 18H   | 16                 | 0145               | 156.7        | 166.2  | 9.5        | 10.01     | 105.4           |
| 19H   | 16                 | 0245               | 166.2        | 175.7  | 9.5        | 9.94      | 104.6           |
| 20H   | 16                 | 0425               | 175.7        | 185.2  | 9.5        | 10.00     | 105.3           |
| 21X   | 16                 | 0555               | 185.2        | 190.4  | 5.2        | 5.92      | 113.8           |
| 22X   | 16                 | 0700               | 190.4        | 200.1  | 9.7        | 9.64      | 99.4            |
| 23X   | 16                 | 0805               | 200.1        | 209.8  | 9.7        | 8.13      | 83.8            |
| 24X   | 16                 | 0910               | 209.8        | 219.4  | 9.6        | 8.99      | 93.6            |
| 25X   | 16                 | 1015               | 219.4        | 229.1  | 9.7        | 5.29      | 54.5            |
| 26X   | 16                 | 1120               | 229.1        | 238.7  | 9.6        | 6.52      | 67.9            |
| 27X   | 16                 | 1235               | 238.7        | 248.1  | 9.4        | 7.54      | 80.2            |
| 28X   | 16                 | 1345               | 248.1        | 257.8  | 9.7        | 8.77      | 90.4            |
| 29X   | 16                 | 1450               | 257.8        | 267.4  | 9.6        | 8.20      | 85.4            |
| 30X   | 16                 | 1555               | 267.4        | 277.0  | 9.6        | 6.84      | 71.2            |
| 31X   | 16                 | 1700               | 277.0        | 286.6  | 9.6        | 8.15      | 84.9            |
| 32X   | 16                 | 1750               | 286.6        | 295.9  | 9.3        | 8.87      | 95.4            |
| 33X   | 16                 | 1845               | 295.9        | 305.6  | 9.7        | 8.31      | 85.7            |
| 34X   | 16                 | 1940               | 305.6        | 315.3  | 9.7        | 8.62      | 88.9            |
| 35X   | 16                 | 2055               | 315.3        | 324.9  | 9.6        | 6.50      | 67.7            |
| 36X   | 16                 | 2250               | 324.9        | 334.5  | 9.6        | 2.81      | 29.3            |
| 37X   | 16                 | 2350               | 334.5        | 344.1  | 9.6        | 6.22      | 64.8            |
| 38X   | 17                 | 0040               | 344.1        | 353.8  | 9.7        | 8.44      | 87.0            |
| 39X   | 17                 | 0145               | 353.8        | 363.4  | 9.6        | 6.92      | 72.1            |
| 40X   | 17                 | 0245               | 363.4        | 373.1  | 9.7        | 8.18      | 84.3            |
| 41X   | 17                 | 0410               | 373.1        | 382.7  | 9.6        | 3.14      | 32.7            |
| 42X   | 17                 | 0545               | 382.7        | 392.3  | 9.6        | 0.25      | 2.6             |
| Cored totals:   |                    |                    |              |        | 392.3      | 345.89    | 88.2            |

**Table T2.** Summary of color and sedimentary features for Subunit IA, Site 1208.

|   | 198-1208A- |          |            |            |            |            |
|---|------------|----------|------------|------------|------------|------------|
|   | 1H to 4H   | 5H to 9H | 10H to 14H | 15H to 19H | 20H to 24X | 25X to 28X |
| <b>Colors:</b>                                  |            |          |            |            |            |            |
| <b>Lighter intervals</b>                        |            |          |            |            |            |            |
| 5B 9/1 bluish white                             |            |          |            |            |            | X          |
| 5B 7/1 light bluish gray                        |            |          |            |            |            | X          |
| N8 very light gray                              |            |          |            |            | X          | X          |
| N7 light gray                                   |            | X        |            | X          | X          |            |
| N6 medium light gray                            |            | X        | X          |            | X          |            |
| 5Y 8/1 yellowish gray                           |            |          |            |            | X          | X          |
| 5Y 5/2 light olive gray                         | X          | X        | X          |            |            | X          |
| 5Y 6/1 light olive gray                         | X          |          | X          | X          | X          | X          |
| 5GY 8/1 light greenish gray                     | X          | X        |            |            | X          |            |
| <b>Darker intervals</b>                         |            |          |            |            |            |            |
| 5G 6/1 greenish gray                            |            | X        |            |            | X          |            |
| 5GY 6/1 greenish gray                           | X          | X        | X          | X          | X          |            |
| 5Y 4/1 olive gray                               | X          | X        | X          | X          | X          |            |
| 5Y 3/2 olive gray                               |            |          | X          |            |            |            |
| 5GY 4/1 dark greenish gray                      |            |          | X          | X          | X          | X          |
| 5GY 6/1 dark greenish gray                      | X          | X        | X          | X          | X          | X          |
| <b>Sedimentary features:</b>                    |            |          |            |            |            |            |
| Color banding                                   | X          | X        | X          | X          | X          |            |
| Pyrite, blebs, pods, and burrow fills           | X          | X        | X          | X          | X          | X          |
| Abrupt, horizontal to vertical bedding contacts | X          |          |            |            |            |            |
| <b>Discrete burrows</b>                         |            |          |            |            |            |            |
| <i>Chondrites</i>                               | X          |          |            |            |            |            |
| Vertical  | X          |          | X          | X          |            |            |
| <i>Zoophycos</i>                                |            |          |            |            | X          | X          |
| Composite                                       |            |          |            |            |            | X          |
| <b>Volcaniclastics</b>                          |            |          |            |            |            |            |
| Volcanic ash (total number in cores)            | 2          | 6        | 9          | 1          | 0          | 3          |
| Pumice  |            |          | X          | X          |            |            |

Notes: X = presence. Numbers indicate frequency of ash beds in the core.

Table T3. Calcareous nannofossil datums, ages, and depths, Site 1208.

| Datum                                      | Zone/Subzone<br>(base) | Core, section, interval (cm) |               | Depth (mbsf) |        |       | Age<br>(Ma) |
|--|------------------------|------------------------------|---------------|--------------|--------|-------|-------------|
|  |                        | Top                          | Bottom        | Top          | Bottom | Mean  |             |
|  |                        | 198-1208A-                   | 198-1208A-    |              |        |       |             |
| FO <i>Emiliana huxleyi</i>                 | CN15                   | 2H-CC                        | 3H-5, 107-108 | 14.24        | 21.27  | 17.8  | 0.26        |
| LO <i>Pseudoemiliana lacunosa</i>          | CN14b                  | 3H-5, 107-108                | 3H-CC         | 21.27        | 23.82  | 22.5  | 0.46        |
| LO <i>Discoaster brouweri</i>              | CN13a/NN19             | 10H-CC                       | 11H-CC        | 90.62        | 100.16 | 95.4  | 1.95        |
| LO <i>Discoaster pentaradiatus</i>         | CN12d/NN18             | 12H-CC                       | 13H-CC        | 109.5        | 119.08 | 114.3 | 2.52        |
| LO <i>Discoaster tamalis</i>               | CN12b                  | 12H-CC                       | 13H-CC        | 109.5        | 119.08 | 114.3 | 2.78        |
| LO <i>Reticulofenestra pseudoumbilicus</i> | CN12a/NN16             | 17H-CC                       | 18H-CC        | 157.21       | 166.66 | 161.9 | 3.82        |
| LO <i>Amaurolithus</i> spp.                |                        | 18H-CC                       | 19H-CC        | 166.66       | 176.09 | 171.4 | 4.56        |
| LO <i>Discoaster quinqueramus</i>          | CN10a/NN12             | 22X-CC                       | 23X-CC        | 199.99       | 208.18 | 204.1 | 5.537       |
| FO <i>Amaurolithus</i> spp.                |                        | 26X-CC                       | 27X-CC        | 235.52       | 246.14 | 240.8 | 7.392       |
| FO <i>Discoaster berggrenii</i>            | CN9a/NN11a             | 28X-CC                       | 29X-CC        | 256.71       | 265.94 | 261.3 | 8.281       |
| LO <i>Catinaster coalitus</i>              |                        | 29X-CC                       | 30X-CC        | 265.94       | 274.2  | 270.1 | 9.694       |
| FO <i>Catinaster coalitus</i>              | CN6/NN8                | 30X-CC                       | 31X-CC        | 274.2        | 285.06 | 279.6 | 10.794      |
| LO <i>Coccolithus miopelagicus</i>         |                        | 30X-CC                       | 31X-CC        | 274.2        | 285.06 | 279.6 | 10.941      |
| LO <i>Sphenolithus heteromorphus</i>       | CN5a/NN6               | 33X-CC                       | 34X-CC        | 304.16       | 314.17 | 309.2 | 13.523      |
| Acme <i>Discoaster deflandrei</i>          |                        | 32X-CC                       | 33X-CC        | 295.41       | 304.16 | 299.8 | 16.2        |
| FO <i>Sphenolithus heteromorphus</i>       | CN3                    | 35X-4, 12                    | 35X-4, 50     | 319.92       | 320.3  | 320.1 | 18.2        |
| LO <i>Cyclicargolithus abisectus</i>       |                        | 35X-4, 50                    | 35X-4, 99     | 320.30       | 320.79 | 320.5 | 23.5        |
| LO <i>Reticulofenestra bisectus</i>        | CN1                    | 35X-4, 99                    | 35X-5, 10     | 320.79       | 320.9  | 320.8 | 23.9        |
| FO <i>Cyclicargolithus abisectus</i>       |                        | 35X-5, 10                    | 35X-5, 50     | 320.9        | 321.3  | 321.1 | 29.9        |
| LO <i>Reticulofenestra umbilicus</i>       | CP17                   | 35X-5, 10                    | 35X-5, 50     | 320.9        | 321.3  | 321.1 | 32.3        |
| LO <i>Ericsonia formosa</i>                | CP16c                  | 35X-5, 73                    | 35X-CC        | 321.53       | 321.75 | 321.6 | 32.8        |
| Acme <i>Ericsonia subdisticha</i>          | CP16b                  | 36X-1, 10                    | 36X-1, 70     | 325          | 325.6  | 325.3 | 33.3        |
| LO <i>Discoaster barbadiensis</i>          | CP16a                  | 36X-2, 40                    | 36X-2, 43     | 326.8        | 326.83 | 326.8 | 34.3        |
| LO <i>Chiasmolithus grandis</i>            | CP15                   | 36X-2, 45                    | 36X-2, 50     | 326.85       | 326.9  | 326.9 | 37.1        |
| FO <i>Reticulofenestra bisectus</i>        |                        | 36X-2, 40                    | 36X-2, 43     | 326.8        | 326.83 | 326.8 | 38.0        |
| FO <i>Reticulofenestra umbilicus</i>       | CP14a                  | 36X-2, 40                    | 36X-2, 43     | 326.8        | 326.83 | 326.8 | 43.7        |
| LO <i>Tribrachiatulus orthostylus</i>      |                        | 36X-2, 40                    | 36X-2, 43     | 326.8        | 326.83 | 326.8 | 50.6        |
| FO <i>Discoaster lodoensis</i>             | CP10                   | 36X-2, 80                    | 36X-2, 90     | 327.2        | 327.3  | 327.3 | 52.8        |
| FO <i>Tribrachiatulus orthostylus</i>      | CP9b                   | 36X-CC, 5                    | 36X-CC, 6     | 327.45       | 327.46 | 327.5 | 53.6        |
| FO <i>Tribrachiatulus bramlettei</i>       | CP9b                   | 36X-CC, 5                    | 36X-CC, 6     | 327.45       | 327.46 | 327.5 | 55.0        |
| FO <i>Discoaster diastypus</i>             | CP9b                   | 36X-CC, 4                    | 36X-CC, 5     | 327.44       | 327.45 | 327.4 | 55.0        |
| LO <i>Fasciculithus tympaniformis</i>      |                        | 36X-CC, 6                    | 36X-CC, 8     | 327.46       | 327.48 | 327.5 | 55.3        |
| FO <i>Discoaster multiradiatus</i>         | CP8                    | 36X-CC, 14                   | 36X-CC, 16    | 327.54       | 327.56 | 327.6 | 56.2        |
| LO <i>Uniplanarius trifidum</i>            |                        | 36X-CC                       | 36X-CC        | 327.6        | 327.7  | 327.7 | 71.3        |
| LO <i>Aspidolithus parvus constrictus</i>  | UC17                   | 36X-CC                       | 36X-CC        | 327.6        | 327.7  | 327.7 | 74.6        |
| FO <i>Ceratolithoides aculeus</i>          | CC20                   | 39X-CC                       | 40X-CC        | 360.62       | 371.53 | 366.1 | 78.5        |
| FO <i>Aspidolithus parvus constrictus</i>  |                        | 40X-CC                       | 41X-CC        | 371.53       | 376.14 | 373.8 | 82.5        |
| FO <i>Aspidolithus parvus</i>              | CC18/UC14              | 41X-CC                       | 42X-CC        | 376.14       | 382.9  | 379.5 | 83.4        |
| FO <i>Micula decussata</i>                 | CC14/UC10              | 41X-CC                       | 42X-CC        | 376.14       | 382.9  | 379.5 | 87.2        |
| FO <i>Eiffellithus eximius</i>             | CC12/UC8               | 41X-CC                       | 42X-CC        | 376.14       | 382.9  | 379.5 | 91.0        |
| FO <i>Quadrum gartneri</i>                 | CC11/UC7               | 41X-CC                       | 42X-CC        | 376.14       | 382.9  | 379.5 | 93.2        |
| LO <i>Helenea chiastia</i>                 | UC6                    | 41X-CC                       | 42X-CC        | 376.14       | 382.9  | 379.5 | 93.4        |
| FO <i>Eiffellithus turriseiffelii</i>      | NC10a                  | 41X-CC                       | 42X-CC        | 376.14       | 382.9  | 379.5 | 101.7       |
| FO <i>Tranolithus orionatus</i>            | NC8c                   | 42X-CC                       | 42XCC         | 382.9        | 382.9  | 382.9 | 107.3       |
| FO <i>Prediscosphaera columnata</i>        | NC8a                   | 42X-CC                       | 42XCC         | 382.9        | 382.9  | 382.9 | 112.6       |
| FO <i>Eprolithus floralis</i>              | NC7                    | 42X-CC                       | 42XCC         | 382.9        | 382.9  | 382.9 | 119.0       |

Notes: FO = first occurrence, LO = last occurrence. These data are presented in age vs. depth plots (see “[Sedimentation and Accumulation Rates](#),” p. 22, and Figs. [F21](#), p. 55, [F22](#), p. 56, [F23](#), p. 57, [F24](#), p. 58, [F25](#), p. 59).

**Table T4.** Planktonic foraminiferal datums, ages, and depths, Site 1208.

| Datum                                    | Zone<br>(base) | Core, section, interval (cm) |            | Depth (mbsf) |        |        | Age<br>(Ma) |
|--|----------------|------------------------------|------------|--------------|--------|--------|-------------|
|  |                | Top                          | Bottom     | Top          | Bottom | Mean   |             |
|  |                | 198-1208A-                   | 198-1208A- |              |        |        |             |
| LO <i>Globigerinoides obliquus</i>       |                | 5H-CC                        | 6H-CC      | 43.11        | 52.62  | 47.87  | 1.3         |
| LO <i>Globigerinoides fistulosus</i>     |                | 9H-CC                        | 10H-CC     | 81.09        | 90.62  | 85.86  | 1.88        |
| FO <i>Truncorotalia truncatulinoides</i> | N22            | 10H-CC                       | 11H-CC     | 90.62        | 100.16 | 95.39  | 1.92        |
| LO <i>Globigerinoides extremus</i>       |                | 11H-CC                       | 12H-CC     | 100.16       | 109.5  | 104.83 | 1.98        |
| FO <i>Truncorotalia tosaensis</i>        | N21            | 18H-CC                       | 19H-CC     | 166.66       | 176.09 | 171.38 | 3.35        |
| LO <i>Dentoglobigerina altispira</i>     |                | 15H-CC                       | 16H-CC     | 138.2        | 147.77 | 142.99 | 3.11        |
| LO <i>Sphaeroidinellopsis seminulina</i> |                | 15H-CC                       | 16H-CC     | 138.2        | 147.77 | 142.99 | 3.11        |
| LO <i>Globorotalia plesiotumida</i>      |                | 14H-CC                       | 15H-CC     | 128.7        | 138.2  | 133.45 | 3.77        |
| LO <i>Globorotalia margaritae</i>        |                | 18H-CC                       | 19H-CC     | 166.66       | 176.09 | 171.38 | 3.85        |
| FO <i>Truncorotalia crassaformis</i>     |                | 20H-CC                       | 21X-CC     | 185.65       | 191.07 | 188.36 | 4.31        |
| LO <i>Globoturborotalita nepenthes</i>   |                | 20H-CC                       | 21X-CC     | 185.65       | 191.07 | 188.36 | 4.39        |
| FO <i>Globorotalia puncticulata</i>      |                | 21X-CC                       | 22X-CC     | 191.07       | 199.99 | 195.53 | 4.5         |
| FO <i>Globorotalia tumida</i>            | N18            | 23X-CC                       | 24X-CC     | 208.18       | 218.74 | 213.46 | 5.82        |
| FO <i>Globorotalia margaritae</i>        |                | 23X-CC                       | 24X-CC     | 208.18       | 218.74 | 213.46 | 6.09        |
| FO <i>Globigerinoides conglobatus</i>    |                | 25X-CC                       | 26X-CC     | 224.59       | 235.52 | 230.06 | 6.2         |
| FO <i>Globorotalia plesiotumida</i>      | N17            | 26X-CC                       | 27X-CC     | 235.52       | 246.14 | 240.83 | 8.58        |
| FO <i>Neogloboquadrina acostaensis</i>   | N16            | 27X-CC                       | 28X-CC     | 246.14       | 256.71 | 251.43 | 9.82        |
| LO <i>Paragloborotalia mayeri</i>        | N15            | 31X-CC                       | 32X-CC     | 285.06       | 295.41 | 290.24 | 10.49       |
| FO <i>Globoturborotalita nepenthes</i>   | N14            | 31X-CC                       | 32X-CC     | 285.06       | 295.41 | 290.24 | 11.19       |
| FO <i>Orbulina universa</i>              | N9             | 33X-CC                       | 34X-CC     | 304.16       | 314.17 | 309.17 | 15.1        |
| LO <i>Globotruncanita atlantica</i>      |                | 36X-CC, 16                   | 36X-CC     | 327.56       | 327.7  | 327.63 | 75.8        |
| FO <i>Globotruncanita atlantica</i>      | KS26           | 39X-CC                       | 40X-CC     | 360.62       | 371.53 | 366.08 | 79.5        |
| FO <i>Globotruncanita elevata</i>        |                | 41X-CC                       | 42X-CC     | 376.14       | 382.9  | 379.52 | 84.8        |
| FO <i>Biticinella breggiensis</i>        | KS14           | 41X-CC                       | 42X-CC     | 376.14       | 382.9  | 379.52 | 105.0       |
| FO <i>Ticinella primula</i>              | KS13           | 42X-CC                       | 42X-CC     | 382.9        | 382.9  | 382.90 | 109.5       |

Notes: FO = first occurrence, LO = last occurrence. These data are presented in age vs. depth plots (see "Sedimentation and Accumulation Rates," p. 22, and Figs. F21, p. 55, F22, p. 56, F23, p. 57, F24, p. 58, and F25, p. 59).





**Table T6.** Concentrations of CH<sub>4</sub> in headspace gas, Site 1208.

| Core, section,<br>interval (cm) | Depth<br>(mbsf) | CH <sub>4</sub><br>(ppmv) |
|---------------------------------|-----------------|---------------------------|
| 198-1208A-                      |                 |                           |
| 1H-3, 0-5                       | 3.0             | 2.3                       |
| 2H-5, 0-5                       | 10.7            | 3.5                       |
| 3H-5, 0-5                       | 20.2            | 3.6                       |
| 4H-5, 0-5                       | 29.7            | 4.6                       |
| 5H-5, 0-5                       | 39.2            | 6.3                       |
| 6H-5, 0-5                       | 48.7            | 7.7                       |
| 7H-5, 0-5                       | 58.2            | 7.1                       |
| 8H-5, 0-5                       | 67.7            | 7.4                       |
| 9H-5, 0-5                       | 77.2            | 7.7                       |
| 11H-5, 0-5                      | 96.2            | 4.6                       |
| 12H-5, 0-5                      | 105.7           | 6.9                       |
| 13H-5, 0-5                      | 115.2           | 6.7                       |
| 14H-5, 0-5                      | 124.7           | 6.2                       |
| 15H-5, 0-5                      | 134.2           | 5.3                       |
| 16H-5, 0-5                      | 143.7           | 5.3                       |
| 17H-5, 0-5                      | 153.2           | 7.1                       |
| 18H-5, 0-5                      | 162.7           | 6.2                       |
| 19H-5, 0-5                      | 172.2           | 6.6                       |
| 20H-5, 0-5                      | 181.7           | 7.1                       |
| 21X-4, 0-5                      | 189.7           | 7.3                       |
| 23X-5, 0-5                      | 206.1           | 9.1                       |
| 24X-6, 0-5                      | 217.3           | 6.3                       |
| 25X-3, 0-5                      | 222.4           | 5.7                       |
| 26X-4, 0-5                      | 233.6           | 4.2                       |
| 27X-4, 0-5                      | 243.2           | 4.3                       |
| 28X-4, 0-5                      | 252.6           | 4.7                       |
| 29X-4, 0-5                      | 262.3           | 5.8                       |
| 30X-4, 0-5                      | 271.9           | 6.6                       |
| 32X-4, 0-5                      | 291.1           | 3.9                       |
| 33X-4, 0-5                      | 300.4           | 5.4                       |
| 34X-4, 0-5                      | 310.1           | 4.2                       |
| 35X-4, 0-5                      | 319.8           | 5.0                       |
| 36X-2, 0-5                      | 326.4           | 3.6                       |
| 37X-4, 0-5                      | 339.0           | 4.6                       |
| 38X-4, 0-5                      | 348.6           | 4.2                       |
| 39X-4, 0-5                      | 358.3           | 2.8                       |
| 40X-4, 0-5                      | 367.9           | 2.8                       |
| 41X-2, 0-5                      | 374.6           | 4.9                       |

**Table T7. Carbonate content, Site 1208.**

| Core, section,<br>interval (cm) | Depth<br>(mbsf) | Total<br>carbon<br>(wt%) | CaCO <sub>3</sub><br>(wt%) | Core, section,<br>interval (cm) | Depth<br>(mbsf) | Total<br>carbon<br>(wt%) | CaCO <sub>3</sub><br>(wt%) |
|---------------------------------|-----------------|--------------------------|----------------------------|---------------------------------|-----------------|--------------------------|----------------------------|
| 198-1208A-                      |                 |                          |                            | 20H-1, 110-111                  | 176.80          | 10.1                     | 84.1                       |
| 1H-1, 7-8                       | 0.07            | 6.1                      | 50.9                       | 20H-4, 16-17                    | 180.36          | 7.9                      | 65.9                       |
| 1H-1, 73-74                     | 0.73            | 4.7                      | 38.8                       | 20H-6, 51-52                    | 183.71          | 4.5                      | 37.5                       |
| 1H-3, 53-54                     | 3.53            | 6.2                      | 52.0                       | 20H-6, 101-102                  | 184.21          | 8.9                      | 73.9                       |
| 2H-1, 73-74                     | 5.43            | 5.3                      | 44.4                       | 21X-1, 36-37                    | 185.56          | 8.2                      | 67.9                       |
| 2H-2, 73-74                     | 6.93            | 4.4                      | 36.8                       | 21X-3, 40-41                    | 188.60          | 4.0                      | 33.5                       |
| 2H-3, 73-74                     | 8.43            | 5.2                      | 43.7                       | 21X-4, 17-18                    | 189.87          | 7.4                      | 61.6                       |
| 3H-2, 69-70                     | 16.39           | 5.0                      | 41.4                       | 22X-1, 38-39                    | 190.78          | 4.4                      | 36.5                       |
| 3H-4, 74-75                     | 19.44           | 6.4                      | 53.4                       | 22X-2, 41-42                    | 192.31          | 5.1                      | 42.4                       |
| 3H-6, 69-70                     | 22.39           | 5.2                      | 43.1                       | 22X-5, 13-14                    | 196.53          | 9.5                      | 79.1                       |
| 4H-1, 40-41                     | 24.10           | 9.4                      | 78.5                       | 23X-1, 30-31                    | 200.40          | 9.6                      | 79.6                       |
| 4H-3, 71-72                     | 27.41           | 6.4                      | 53.3                       | 23X-2, 37-38                    | 201.97          | 1.2                      | 9.8                        |
| 5H-1, 111-112                   | 34.31           | 4.7                      | 39.3                       | 23X-4, 13-14                    | 204.73          | 3.6                      | 29.6                       |
| 5H-5, 48-49                     | 39.68           | 7.5                      | 62.1                       | 23X-6, 10-11                    | 207.20          | 6.9                      | 57.4                       |
| 5H-5, 129-130                   | 40.49           | 2.5                      | 20.7                       | 24X-1, 20-21                    | 210.00          | 7.5                      | 62.6                       |
| 5H-6, 12-13                     | 40.82           | 2.1                      | 17.2                       | 24X-1, 127-128                  | 211.07          | 1.3                      | 10.4                       |
| 6H-4, 13-14                     | 47.33           | 4.7                      | 39.0                       | 24X-5, 63-64                    | 216.43          | 7.0                      | 58.6                       |
| 6H-5, 54-55                     | 49.24           | 7.1                      | 59.0                       | 25X-1, 12-13                    | 219.52          | 2.4                      | 19.8                       |
| 6H-6, 130-131                   | 51.50           | 8.3                      | 68.7                       | 25X-1, 98-99                    | 220.38          | 10.2                     | 84.9                       |
| 7H-4, 87-88                     | 57.57           | 5.9                      | 49.3                       | 25X-2, 8-9                      | 220.98          | 10.3                     | 85.9                       |
| 7H-5, 137-138                   | 59.57           | 2.0                      | 16.9                       | 26X-2, 11-12                    | 230.71          | 1.3                      | 10.6                       |
| 7H-6, 83-84                     | 60.53           | 8.1                      | 67.4                       | 26X-2, 94-95                    | 231.54          | 4.2                      | 35.3                       |
| 7H-7, 12-13                     | 61.32           | 7.4                      | 61.4                       | 26X-5, 34-35                    | 234.89          | 9.5                      | 78.8                       |
| 8H-1, 98-99                     | 62.68           | 4.4                      | 36.8                       | 27X-1, 79-80                    | 239.49          | 10.3                     | 86.0                       |
| 8H-2, 141-142                   | 64.61           | 5.2                      | 43.3                       | 27X-3, 47-48                    | 242.17          | 9.3                      | 77.7                       |
| 8H-4, 89-90                     | 67.09           | 7.8                      | 64.6                       | 28X-1, 114-115                  | 249.24          | 8.4                      | 69.8                       |
| 9H-1, 35-36                     | 71.55           | 4.4                      | 36.9                       | 28X-2, 24-25                    | 249.84          | 3.1                      | 25.8                       |
| 9H-2, 7-8                       | 72.77           | 8.4                      | 70.0                       | 28X-4, 69-70                    | 253.29          | 6.5                      | 54.5                       |
| 9H-3, 102-103                   | 75.22           | 7.9                      | 66.1                       | 29X-1, 103-104                  | 258.83          | 9.8                      | 81.4                       |
| 10H-1, 12-13                    | 80.82           | 8.7                      | 72.4                       | 29X-3, 73-74                    | 261.53          | 10.0                     | 83.4                       |
| 10H-1, 73-74                    | 81.43           | 7.0                      | 58.5                       | 30X-1, 101-102                  | 268.41          | 8.3                      | 68.8                       |
| 10H-2, 43-44                    | 82.63           | 3.2                      | 26.9                       | 30X-2, 74-75                    | 269.64          | 4.3                      | 35.5                       |
| 11H-2, 67-68                    | 92.37           | 8.1                      | 67.6                       | 30X-4, 95-96                    | 272.85          | 8.5                      | 71.0                       |
| 11H-3, 22-23                    | 93.42           | 2.9                      | 24.2                       | 31X-1, 74-75                    | 277.74          | 7.9                      | 65.4                       |
| 11H-6, 68-69                    | 98.38           | 4.5                      | 37.3                       | 31X-2, 24-25                    | 278.74          | 10.6                     | 88.3                       |
| 12H-2, 73-74                    | 101.93          | 2.4                      | 20.0                       | 31X-6, 13-14                    | 284.13          | 3.4                      | 28.1                       |
| 12H-3, 73-74                    | 103.43          | 6.9                      | 57.8                       | 32X-1, 103-104                  | 287.63          | 4.0                      | 33.5                       |
| 12H-5, 109-110                  | 106.79          | 7.5                      | 62.8                       | 32X-2, 104-105                  | 289.14          | 10.7                     | 89.3                       |
| 13H-2, 74-75                    | 111.44          | 7.4                      | 61.5                       | 33X-2, 73-74                    | 298.13          | 5.9                      | 49.5                       |
| 13H-4, 44-45                    | 114.14          | 1.6                      | 12.9                       | 33X-2, 132-133                  | 298.72          | 6.1                      | 50.4                       |
| 13H-6, 41-42                    | 117.11          | 5.4                      | 44.9                       | 33X-5, 42-43                    | 302.32          | 9.3                      | 77.7                       |
| 14H-1, 70-71                    | 119.40          | 5.5                      | 45.9                       | 35X-1, 44-45                    | 315.74          | 9.9                      | 82.5                       |
| 14H-5, 143-144                  | 126.13          | 3.8                      | 31.4                       | 35X-3, 48-49                    | 318.78          | 9.1                      | 75.4                       |
| 14H-6, 125-126                  | 127.45          | 7.8                      | 64.6                       | 35X-3, 65-66                    | 318.95          | 4.3                      | 35.5                       |
| 15H-1, 42-43                    | 128.62          | 6.4                      | 53.4                       | 37X-2, 74-75                    | 336.74          | 11.7                     | 97.6                       |
| 15H-3, 15-16                    | 131.35          | 6.2                      | 51.4                       | 37X-4, 42-43                    | 339.42          | 11.6                     | 96.9                       |
| 15H-7, 13-14                    | 137.33          | 8.7                      | 72.6                       | 37X-4, 72-73                    | 339.72          | 11.6                     | 96.8                       |
| 16H-1, 15-16                    | 137.85          | 4.1                      | 34.4                       | 38X-1, 75-76                    | 344.85          | 11.7                     | 97.3                       |
| 16H-2, 116-117                  | 140.36          | 8.9                      | 74.0                       | 38X-1, 94-95                    | 345.04          | 11.7                     | 97.3                       |
| 16H-3, 109-110                  | 141.79          | 6.1                      | 51.0                       | 38X-4, 72-73                    | 349.32          | 11.7                     | 97.7                       |
| 17H-1, 35-36                    | 147.55          | 4.7                      | 39.2                       | 38X-5, 62-63                    | 350.72          | 11.7                     | 97.2                       |
| 17H-2, 16-17                    | 148.86          | 9.7                      | 80.7                       | 39X-1, 72-73                    | 354.52          | 11.7                     | 97.8                       |
| 17H-2, 72-73                    | 149.42          | 9.3                      | 77.5                       | 39X-2, 73-74                    | 356.03          | 11.7                     | 97.4                       |
| 18H-1, 73-74                    | 157.43          | 9.4                      | 78.4                       | 40X-1, 70-71                    | 364.10          | 9.8                      | 81.3                       |
| 18H-4, 15-16                    | 161.35          | 5.2                      | 43.7                       | 40X-3, 72-73                    | 367.12          | 11.7                     | 97.8                       |
| 18H-6, 74-75                    | 164.94          | 4.3                      | 35.8                       | 40X-4, 72-73                    | 368.62          | 11.7                     | 97.8                       |
| 18H-7, 19-20                    | 165.89          | 8.1                      | 67.5                       | 41X-1, 83-84                    | 373.93          | 11.7                     | 97.6                       |
| 19H-2, 15-16                    | 167.85          | 5.4                      | 44.7                       | 41X-2, 69-70                    | 375.29          | 11.4                     | 95.2                       |
| 19H-4, 8-9                      | 170.78          | 8.4                      | 69.7                       | 41X-2, 107-108                  | 375.67          | 11.7                     | 97.1                       |
| 19H-6, 134-135                  | 175.04          | 3.8                      | 31.4                       |                                 |                 |                          |                            |

**Table T8.** Results of geochemical analyses, Site 1208.

| Core, section,<br>interval (cm) | Depth<br>(mbsf) | Alkalinity |          | Cl <sup>-</sup><br>(mM) | SO <sub>4</sub> <sup>2-</sup><br>(mM) | Na <sup>+</sup><br>(mM) | Mg <sup>2+</sup><br>(mM) | Ca <sup>2+</sup><br>(mM) | K <sup>+</sup><br>(mM) | H <sub>4</sub> SiO <sub>4</sub><br>(μM) | NH <sub>4</sub> <sup>+</sup><br>(μM) | HPO <sub>4</sub> <sup>2-</sup><br>(μM) | Sr <sup>2+</sup><br>(μM) | Fe <sup>2+</sup><br>(μM) | Mn <sup>2+</sup><br>(μM) | Li <sup>+</sup><br>(μM) | Ba <sup>2+</sup><br>(μM) | H <sub>3</sub> BO <sub>3</sub><br>(μM) |     |
|---------------------------------|-----------------|------------|----------|-------------------------|---------------------------------------|-------------------------|--------------------------|--------------------------|------------------------|---|--------------------------------------|--|--------------------------|--------------------------|--------------------------|-------------------------|--------------------------|--|-----|
|                                 |                 | pH         | Salinity |                         |                                       |                         |                          |                          |                        |   |                                      |  |                          |                          |                          |                         |                          |  |     |
| 198-1208A-                      |                 |            |          |                         |                                       |                         |                          |                          |                        |   |                                      |  |                          |                          |                          |                         |                          |  |     |
| 1H-2, 145-150                   | 2.95            | 7.51       | 2.89     | 34.5                    | 558                                   | 27.7                    | 478                      | 53.2                     | 10.3                   | 11.3                                    | 726                                  | 125                                    | 16.9                     | 87                       | 56                       | 22                      | 23                       | 0.7                                    | 442 |
| 2H-4, 145-150                   | 10.65           | 7.45       | 5.66     | 34.5                    | 559                                   | 25.4                    | 481                      | 52.4                     | 9.1                    | 11.8                                    | 793                                  | 295                                    | 21.9                     | 95                       | 110                      | 21                      | 23                       | 0.4                                    | 478 |
| 3H-4, 145-150                   | 20.15           | 7.37       | 6.50     | 35.0                    | 559                                   | 23.6                    | 478                      | 52.5                     | 8.7                    | 11.9                                    | 769                                  | 400                                    | 14.6                     | 99                       | 131                      | 23                      | 24                       | 0.3                                    | 462 |
| 4H-4, 145-150                   | 29.65           | 7.49       | 7.28     | 35.0                    | 559                                   | 23.1                    | 481                      | 51.9                     | 8.1                    | 11.5                                    | 767                                  | 402                                    | 7.7                      | 114                      | 56                       | 28                      | 26                       | 0.6                                    | 454 |
| 5H-4, 145-150                   | 39.15           | 7.36       | 7.72     | 35.0                    | 560                                   | 22.7                    | 482                      | 51.1                     | 8.8                    | 11.5                                    | 754                                  | 501                                    | 13.2                     | 129                      | 120                      | 28                      | 27                       | 0.8                                    | 460 |
| 6H-4, 145-150                   | 48.65           | 7.33       | 8.11     | 35.0                    | 557                                   | 22.3                    | 481                      | 50.8                     | 7.9                    | 11.4                                    | 800                                  | 442                                    | 10.5                     | 146                      | 220                      | 27                      | 28                       | 0.3                                    | 450 |
| 7H-4, 145-150                   | 58.15           | 7.31       | 8.01     | 35.0                    | 555                                   | 20.9                    | 478                      | 50.0                     | 7.6                    | 11.1                                    | 808                                  | 493                                    | 7.7                      | 130                      | 20                       | 18                      | 23                       | 1.3                                    | 374 |
| 8H-4, 145-150                   | 67.65           | 7.25       | 8.17     | 35.0                    | 559                                   | 20.4                    | 481                      | 50.4                     | 7.5                    | 10.8                                    | 808                                  | 519                                    | 6.5                      | 172                      | 140                      | 18                      | 28                       | 0.3                                    | 440 |
| 9H-4, 145-150                   | 77.15           | 7.25       | 7.95     | 34.5                    | 559                                   | 20.4                    | 482                      | 49.4                     | 7.8                    | 11.3                                    | 953                                  | 556                                    | 5.0                      | 184                      | 185                      | 12                      | 28                       | 0.3                                    | 460 |
| 10H-4, 145-150                  | 86.65           | 7.20       | 7.92     | 34.5                    | 559                                   | 20.5                    | 483                      | 49.1                     | 7.5                    | 11.2                                    | 979                                  | 552                                    | 7.0                      | 201                      | 90                       | 7                       | 29                       | 0.7                                    | 458 |
| 11H-4, 145-150                  | 96.15           | 7.24       | 7.87     | 34.5                    | 563                                   | 19.8                    | 486                      | 49.3                     | 7.6                    | 11.2                                    | 940                                  | 510                                    | 6.2                      | 206                      | 35                       | 5                       | 31                       | 1.5                                    | 451 |
| 14H-4, 145-150                  | 124.65          | 7.23       | 7.51     | 34.5                    | 560                                   | 19.5                    | 483                      | 48.1                     | 8.0                    | 11.0                                    | 974                                  | 490                                    | 4.1                      | 252                      | 77                       | 5                       | 30                       | 0.3                                    | 458 |
| 17H-4, 145-150                  | 153.15          | 7.19       | 7.28     | 34.5                    | 561                                   | 19.5                    | 482                      | 48.4                     | 8.7                    | 10.9                                    | 888                                  | 454                                    | 2.1                      | 267                      | 49                       | 5                       | 30                       | 0.5                                    | 434 |
| 20H-4, 145-150                  | 181.65          | 7.47       | 6.38     | 34.5                    | 560                                   | 20.3                    | 483                      | 46.1                     | 10.0                   | 11.1                                    | 938                                  | 423                                    | 1.5                      | 294                      | 128                      | 6                       | 31                       | 1.8                                    | 436 |
| 24X-5, 135-150                  | 217.15          | 7.32       | 6.03     | 34.5                    | 557                                   | 21.6                    | 479                      | 46.9                     | 11.4                   | 10.7                                    | 966                                  | 353                                    | 1.0                      | 305                      | 39                       | 8                       | 31                       | 0.4                                    | 425 |
| 27X-3, 135-150                  | 243.05          | 7.20       | 5.68     | 34.5                    | 554                                   | 21.2                    | 474                      | 47.1                     | 11.6                   | 10.4                                    | 985                                  | 320                                    | 0.7                      | 296                      | 35                       | 13                      | 30                       | 0.7                                    | 428 |
| 30X-3, 135-150                  | 271.75          | 7.19       | 5.67     | 34.5                    | 557                                   | 21.5                    | 478                      | 46.6                     | 11.7                   | 10.2                                    | 962                                  | 265                                    | 1.0                      | 280                      | 22                       | 23                      | 29                       | 0.4                                    | 436 |
| 33X-3, 135-150                  | 300.25          | 7.24       | 5.04     | 34.5                    | 557                                   | 22.8                    | 478                      | 47.4                     | 12.1                   | 10.1                                    | 843                                  | 256                                    | 0.7                      | 254                      | 19                       | 32                      | 29                       | 1.8                                    | 446 |
| 37X-3, 145-150                  | 338.95          | 7.27       | 5.48     | 34.5                    | 561                                   | 22.5                    | 482                      | 47.6                     | 12.5                   | 9.7                                     | 262                                  | 222                                    | 0.3                      | 224                      | 77                       | 3                       | 29                       | 0.9                                    | 444 |
| 40X-3, 145-150                  | 367.85          | 7.21       | 4.79     | 34.5                    | 572                                   | 21.7                    | 491                      | 47.2                     | 12.5                   | 9.6                                     | 204                                  | 211                                    | 0.3                      | 226                      | 47                       | 6                       | 30                       | 0.6                                    | 460 |

**Table T9.** Discrete index properties measurements for Site 1208.  
(Continued on next three pages.)

| Core, section,<br>interval (cm) | Depth<br>(mbsf) | Water content (wt%) |          | Density (g/cm <sup>3</sup> ) |      |       | Porosity<br>(%) | Void<br>ratio |
|---------------------------------|-----------------|---------------------|----------|------------------------------|------|-------|-----------------|---------------|
|                                 |                 | Bulk mass           | Dry mass | Bulk                         | Dry  | Grain |                 |               |
| 198-1208A-                      |                 |                     |          |                              |      |       |                 |               |
| 1H-1, 70-72                     | 0.70            | 60.1                | 150.6    | 1.36                         | 0.54 | 2.67  | 79.7            | 3.92          |
| 1H-2, 70-72                     | 2.20            | 57.1                | 133.0    | 1.39                         | 0.60 | 2.66  | 77.6            | 3.46          |
| 1H-3, 55-57                     | 3.55            | 55.6                | 125.4    | 1.41                         | 0.63 | 2.67  | 76.6            | 3.27          |
| 2H-1, 70-72                     | 5.40            | 54.2                | 118.2    | 1.43                         | 0.65 | 2.66  | 75.4            | 3.06          |
| 2H-2, 70-72                     | 6.90            | 69.5                | 227.7    | 1.25                         | 0.38 | 2.54  | 85.0            | 5.65          |
| 2H-3, 70-72                     | 8.40            | 58.5                | 141.2    | 1.37                         | 0.57 | 2.65  | 78.5            | 3.65          |
| 2H-4, 70-72                     | 9.90            | 64.7                | 183.0    | 1.30                         | 0.46 | 2.61  | 82.3            | 4.66          |
| 2H-5, 70-72                     | 11.40           | 58.1                | 138.8    | 1.38                         | 0.58 | 2.67  | 78.3            | 3.61          |
| 2H-6, 73-75                     | 12.93           | 55.0                | 122.0    | 1.42                         | 0.64 | 2.65  | 75.9            | 3.15          |
| 3H-1, 118-120                   | 15.38           | 58.4                | 140.3    | 1.37                         | 0.57 | 2.62  | 78.2            | 3.60          |
| 3H-2, 70-72                     | 16.40           | 64.3                | 180.0    | 1.31                         | 0.47 | 2.64  | 82.2            | 4.63          |
| 3H-3, 70-72                     | 17.90           | 60.1                | 150.3    | 1.36                         | 0.54 | 2.65  | 79.5            | 3.88          |
| 3H-4, 70-72                     | 19.40           | 54.4                | 119.2    | 1.43                         | 0.65 | 2.67  | 75.7            | 3.11          |
| 3H-5, 70-72                     | 20.90           | 53.7                | 116.2    | 1.43                         | 0.66 | 2.68  | 75.2            | 3.04          |
| 3H-6, 70-72                     | 22.40           | 54.1                | 117.9    | 1.43                         | 0.66 | 2.68  | 75.5            | 3.09          |
| 4H-1, 70-72                     | 24.40           | 48.8                | 95.1     | 1.50                         | 0.77 | 2.69  | 71.4            | 2.50          |
| 4H-2, 70-72                     | 25.90           | 54.2                | 118.2    | 1.43                         | 0.66 | 2.68  | 75.6            | 3.10          |
| 4H-3, 70-72                     | 27.40           | 53.9                | 116.9    | 1.44                         | 0.66 | 2.72  | 75.6            | 3.11          |
| 4H-4, 70-72                     | 28.90           | 54.1                | 118.1    | 1.43                         | 0.66 | 2.71  | 75.8            | 3.12          |
| 4H-5, 70-72                     | 30.40           | 46.9                | 88.4     | 1.52                         | 0.81 | 2.68  | 69.8            | 2.31          |
| 4H-6, 70-72                     | 31.90           | 48.3                | 93.4     | 1.51                         | 0.78 | 2.71  | 71.2            | 2.47          |
| 5H-1, 10-12                     | 33.30           | 53.6                | 115.4    | 1.44                         | 0.67 | 2.69  | 75.2            | 3.03          |
| 5H-2, 10-12                     | 34.80           | 54.4                | 119.1    | 1.43                         | 0.65 | 2.71  | 75.9            | 3.15          |
| 5H-3, 10-12                     | 36.30           | 55.2                | 123.4    | 1.41                         | 0.63 | 2.66  | 76.2            | 3.20          |
| 5H-4, 10-12                     | 37.80           | 53.8                | 116.5    | 1.43                         | 0.66 | 2.67  | 75.2            | 3.03          |
| 5H-5, 10-12                     | 39.30           | 50.2                | 100.6    | 1.47                         | 0.73 | 2.61  | 72.0            | 2.57          |
| 5H-6, 12-14                     | 40.82           | 47.5                | 90.4     | 1.47                         | 0.77 | 2.43  | 68.2            | 2.15          |
| 5H-7, 8-10                      | 42.28           | 52.2                | 109.2    | 1.45                         | 0.70 | 2.68  | 74.1            | 2.86          |
| 6H-1, 13-15                     | 42.83           | 51.6                | 106.5    | 1.47                         | 0.71 | 2.75  | 74.1            | 2.86          |
| 6H-2, 13-15                     | 44.33           | 51.2                | 105.1    | 1.46                         | 0.71 | 2.67  | 73.3            | 2.74          |
| 6H-3, 13-15                     | 45.83           | 52.8                | 111.8    | 1.45                         | 0.68 | 2.67  | 74.5            | 2.92          |
| 6H-4, 13-15                     | 47.33           | 51.3                | 105.3    | 1.47                         | 0.71 | 2.68  | 73.4            | 2.76          |
| 6H-5, 13-15                     | 48.83           | 50.6                | 102.5    | 1.47                         | 0.73 | 2.68  | 72.9            | 2.69          |
| 6H-6, 13-15                     | 50.33           | 55.7                | 125.9    | 1.41                         | 0.62 | 2.69  | 76.8            | 3.31          |
| 6H-7, 13-15                     | 51.83           | 53.7                | 115.9    | 1.44                         | 0.67 | 2.68  | 75.2            | 3.04          |
| 7H-1, 13-15                     | 52.33           | 53.6                | 115.7    | 1.44                         | 0.67 | 2.73  | 75.5            | 3.08          |
| 7H-2, 13-15                     | 53.83           | 54.3                | 118.7    | 1.44                         | 0.66 | 2.75  | 76.1            | 3.19          |
| 7H-3, 13-15                     | 55.33           | 53.2                | 113.5    | 1.44                         | 0.68 | 2.69  | 74.9            | 2.99          |
| 7H-4, 13-15                     | 56.83           | 53.2                | 113.5    | 1.44                         | 0.68 | 2.68  | 74.8            | 2.97          |
| 7H-5, 13-15                     | 58.33           | 49.7                | 98.9     | 1.50                         | 0.76 | 2.80  | 73.0            | 2.70          |
| 7H-6, 8-10                      | 59.78           | 49.7                | 98.8     | 1.48                         | 0.74 | 2.62  | 71.7            | 2.53          |
| 7H-7, 13-15                     | 61.33           | 47.6                | 90.7     | 1.52                         | 0.80 | 2.68  | 70.4            | 2.38          |
| 8H-1, 12-14                     | 61.82           | 51.8                | 107.3    | 1.46                         | 0.70 | 2.67  | 73.7            | 2.80          |
| 8H-2, 13-15                     | 63.33           | 53.8                | 116.6    | 1.44                         | 0.66 | 2.71  | 75.5            | 3.08          |
| 8H-3, 13-15                     | 64.83           | 54.0                | 117.4    | 1.43                         | 0.66 | 2.71  | 75.6            | 3.10          |
| 8H-4, 15-17                     | 66.35           | 49.6                | 98.3     | 1.50                         | 0.75 | 2.73  | 72.4            | 2.63          |
| 8H-5, 13-15                     | 67.83           | 51.8                | 107.5    | 1.46                         | 0.70 | 2.66  | 73.6            | 2.79          |
| 8H-6, 16-18                     | 69.36           | 44.7                | 81.0     | 1.54                         | 0.85 | 2.62  | 67.5            | 2.07          |
| 8H-7, 15-17                     | 70.85           | 46.2                | 85.7     | 1.54                         | 0.83 | 2.69  | 69.2            | 2.25          |
| 9H-1, 13-15                     | 71.33           | 53.0                | 112.6    | 1.44                         | 0.68 | 2.68  | 74.6            | 2.94          |
| 9H-2, 13-15                     | 72.83           | 51.1                | 104.4    | 1.47                         | 0.72 | 2.67  | 73.1            | 2.72          |
| 9H-3, 13-15                     | 74.33           | 52.1                | 108.7    | 1.45                         | 0.70 | 2.68  | 74.0            | 2.84          |
| 9H-4, 13-15                     | 75.83           | 53.3                | 113.9    | 1.44                         | 0.67 | 2.67  | 74.8            | 2.97          |
| 9H-5, 13-15                     | 77.33           | 48.6                | 94.6     | 1.50                         | 0.77 | 2.69  | 71.3            | 2.48          |
| 9H-6, 13-15                     | 78.83           | 55.3                | 123.7    | 1.42                         | 0.63 | 2.71  | 76.6            | 3.27          |
| 10H-1, 13-15                    | 80.83           | 47.9                | 91.8     | 1.51                         | 0.79 | 2.65  | 70.4            | 2.38          |
| 10H-2, 13-15                    | 82.33           | 49.6                | 98.6     | 1.48                         | 0.75 | 2.63  | 71.7            | 2.54          |
| 10H-3, 13-15                    | 83.83           | 53.6                | 115.4    | 1.43                         | 0.66 | 2.63  | 74.8            | 2.96          |
| 10H-4, 13-15                    | 85.33           | 49.6                | 98.4     | 1.49                         | 0.75 | 2.68  | 72.0            | 2.57          |
| 10H-5, 13-15                    | 86.83           | 51.0                | 104.1    | 1.47                         | 0.72 | 2.66  | 73.0            | 2.71          |
| 10H-6, 13-15                    | 88.33           | 54.3                | 119.0    | 1.42                         | 0.65 | 2.61  | 75.2            | 3.04          |
| 11H-1, 13-15                    | 90.33           | 50.3                | 101.1    | 1.49                         | 0.74 | 2.75  | 73.1            | 2.72          |
| 11H-2, 70-72                    | 92.40           | 50.2                | 100.8    | 1.47                         | 0.73 | 2.64  | 72.2            | 2.60          |
| 11H-3, 70-72                    | 93.90           | 47.3                | 89.6     | 1.51                         | 0.80 | 2.64  | 69.8            | 2.31          |
| 11H-4, 70-72                    | 95.40           | 46.6                | 87.3     | 1.54                         | 0.82 | 2.75  | 70.1            | 2.34          |
| 11H-5, 70-72                    | 96.90           | 47.8                | 91.6     | 1.51                         | 0.79 | 2.65  | 70.3            | 2.37          |

Table T9 (continued).

| Core, section,<br>interval (cm) | Depth<br>(mbsf) | Water content (wt%) |          | Density (g/cm <sup>3</sup> ) |      |       | Porosity<br>(%) | Void<br>ratio |
|---------------------------------|-----------------|---------------------|----------|------------------------------|------|-------|-----------------|---------------|
|                                 |                 | Bulk mass           | Dry mass | Bulk                         | Dry  | Grain |                 |               |
| 11H-6, 70-72                    | 98.40           | 49.3                | 97.4     | 1.48                         | 0.75 | 2.62  | 71.3            | 2.49          |
| 12H-1, 70-72                    | 100.40          | 45.5                | 83.6     | 1.55                         | 0.85 | 2.73  | 69.0            | 2.23          |
| 12H-2, 70-72                    | 101.90          | 49.5                | 98.0     | 1.49                         | 0.75 | 2.68  | 71.9            | 2.56          |
| 12H-3, 70-72                    | 103.40          | 49.6                | 98.3     | 1.48                         | 0.75 | 2.64  | 71.7            | 2.53          |
| 12H-4, 70-72                    | 104.90          | 49.0                | 96.3     | 1.50                         | 0.76 | 2.70  | 71.8            | 2.54          |
| 12H-5, 70-72                    | 106.40          | 52.3                | 109.5    | 1.44                         | 0.69 | 2.56  | 73.3            | 2.74          |
| 12H-6, 70-72                    | 107.90          | 49.4                | 97.5     | 1.48                         | 0.75 | 2.61  | 71.3            | 2.48          |
| 13H-1, 70-72                    | 109.90          | 48.0                | 92.5     | 1.50                         | 0.78 | 2.63  | 70.3            | 2.37          |
| 13H-2, 70-72                    | 111.40          | 52.2                | 109.3    | 1.45                         | 0.69 | 2.64  | 73.8            | 2.82          |
| 13H-3, 70-72                    | 112.90          | 47.0                | 88.6     | 1.55                         | 0.82 | 2.84  | 71.1            | 2.46          |
| 13H-4, 72-74                    | 114.42          | 46.0                | 85.3     | 1.52                         | 0.82 | 2.60  | 68.4            | 2.16          |
| 13H-5, 70-72                    | 115.90          | 40.7                | 68.8     | 1.56                         | 0.93 | 2.44  | 62.1            | 1.64          |
| 13H-6, 70-72                    | 117.40          | 43.7                | 77.8     | 1.56                         | 0.88 | 2.65  | 66.8            | 2.01          |
| 14H-1, 70-72                    | 119.40          | 48.8                | 95.3     | 1.48                         | 0.76 | 2.60  | 70.7            | 2.42          |
| 14H-2, 70-72                    | 120.90          | 52.5                | 110.3    | 1.44                         | 0.69 | 2.63  | 73.9            | 2.84          |
| 14H-3, 70-72                    | 122.40          | 44.4                | 79.7     | 1.56                         | 0.87 | 2.66  | 67.4            | 2.07          |
| 14H-4, 70-72                    | 123.90          | 45.7                | 84.2     | 1.55                         | 0.84 | 2.74  | 69.3            | 2.26          |
| 14H-5, 70-72                    | 125.40          | 44.5                | 80.2     | 1.55                         | 0.86 | 2.65  | 67.5            | 2.08          |
| 14H-6, 70-72                    | 126.90          | 55.3                | 123.8    | 1.40                         | 0.63 | 2.60  | 75.9            | 3.14          |
| 14H-7, 70-72                    | 128.40          | 46.9                | 88.2     | 1.52                         | 0.81 | 2.67  | 69.7            | 2.30          |
| 15H-1, 13-15                    | 128.33          | 50.8                | 103.3    | 1.47                         | 0.72 | 2.67  | 72.9            | 2.69          |
| 15H-2, 13-15                    | 129.83          | 45.6                | 83.7     | 1.54                         | 0.84 | 2.65  | 68.4            | 2.17          |
| 15H-3, 7-9                      | 131.27          | 44.0                | 78.6     | 1.57                         | 0.88 | 2.69  | 67.4            | 2.07          |
| 15H-4, 13-15                    | 132.83          | 47.3                | 89.8     | 1.51                         | 0.80 | 2.66  | 70.0            | 2.33          |
| 15H-5, 13-15                    | 134.33          | 45.3                | 83.0     | 1.55                         | 0.84 | 2.67  | 68.4            | 2.17          |
| 15H-6, 13-15                    | 135.83          | 44.8                | 81.2     | 1.56                         | 0.86 | 2.69  | 68.1            | 2.13          |
| 15H-7, 13-15                    | 137.33          | 46.0                | 85.1     | 1.53                         | 0.83 | 2.65  | 68.8            | 2.20          |
| 16H-1, 13-15                    | 137.83          | 54.4                | 119.3    | 1.43                         | 0.65 | 2.67  | 75.7            | 3.11          |
| 16H-2, 13-15                    | 139.33          | 50.0                | 100.2    | 1.49                         | 0.74 | 2.73  | 72.8            | 2.67          |
| 16H-3, 13-15                    | 140.83          | 46.8                | 88.1     | 1.53                         | 0.81 | 2.72  | 70.0            | 2.34          |
| 16H-4, 13-15                    | 142.33          | 43.4                | 76.8     | 1.58                         | 0.89 | 2.70  | 66.9            | 2.02          |
| 16H-5, 13-15                    | 143.83          | 43.6                | 77.4     | 1.57                         | 0.89 | 2.68  | 66.9            | 2.02          |
| 16H-6, 15-17                    | 145.35          | 46.8                | 88.0     | 1.52                         | 0.81 | 2.66  | 69.5            | 2.28          |
| 16H-7, 15-17                    | 146.85          | 45.6                | 84.0     | 1.55                         | 0.84 | 2.74  | 69.2            | 2.25          |
| 17H-1, 11-13                    | 147.31          | 49.7                | 98.9     | 1.49                         | 0.75 | 2.70  | 72.3            | 2.61          |
| 17H-2, 13-15                    | 148.83          | 42.2                | 73.1     | 1.84                         | 1.07 | 4.45  | 76.0            | 3.17          |
| 17H-3, 13-15                    | 150.33          | 45.4                | 83.3     | 1.54                         | 0.84 | 2.66  | 68.3            | 2.16          |
| 17H-4, 13-15                    | 151.83          | 42.0                | 72.6     | 1.59                         | 0.92 | 2.67  | 65.4            | 1.89          |
| 17H-5, 13-15                    | 153.33          | 40.9                | 69.3     | 1.62                         | 0.96 | 2.72  | 64.8            | 1.84          |
| 17H-6, 13-15                    | 154.83          | 45.7                | 84.3     | 1.53                         | 0.83 | 2.64  | 68.5            | 2.17          |
| 17H-7, 13-15                    | 156.33          | 50.1                | 100.2    | 1.46                         | 0.73 | 2.56  | 71.4            | 2.50          |
| 18H-1, 13-15                    | 156.83          | 51.2                | 105.1    | 1.45                         | 0.71 | 2.58  | 72.6            | 2.65          |
| 18H-2, 13-15                    | 158.33          | 47.5                | 90.6     | 1.51                         | 0.79 | 2.62  | 69.9            | 2.32          |
| 18H-3, 13-15                    | 159.83          | 44.2                | 79.2     | 1.57                         | 0.88 | 2.72  | 67.8            | 2.11          |
| 18H-4, 13-15                    | 161.33          | 52.2                | 109.2    | 1.44                         | 0.69 | 2.61  | 73.6            | 2.78          |
| 18H-5, 13-15                    | 162.83          | 46.9                | 88.2     | 1.52                         | 0.81 | 2.67  | 69.7            | 2.30          |
| 18H-6, 13-15                    | 164.33          | 48.0                | 92.3     | 1.50                         | 0.78 | 2.64  | 70.4            | 2.38          |
| 18H-7, 16-18                    | 165.86          | 48.4                | 93.8     | 1.50                         | 0.77 | 2.63  | 70.7            | 2.41          |
| 19H-1, 13-15                    | 166.33          | 50.5                | 101.9    | 1.46                         | 0.72 | 2.57  | 71.9            | 2.56          |
| 19H-2, 13-15                    | 167.83          | 53.4                | 114.7    | 1.43                         | 0.67 | 2.63  | 74.7            | 2.95          |
| 19H-3, 13-15                    | 169.33          | 47.9                | 92.1     | 1.51                         | 0.79 | 2.67  | 70.6            | 2.40          |
| 19H-4, 13-15                    | 170.83          | 47.9                | 92.1     | 1.52                         | 0.79 | 2.71  | 70.9            | 2.44          |
| 19H-5, 13-15                    | 172.33          | 47.1                | 89.2     | 1.51                         | 0.80 | 2.62  | 69.5            | 2.28          |
| 19H-6, 13-15                    | 173.83          | 49.6                | 98.3     | 1.47                         | 0.74 | 2.59  | 71.3            | 2.49          |
| 19H-7, 13-15                    | 175.33          | 45.7                | 84.2     | 1.53                         | 0.83 | 2.64  | 68.4            | 2.17          |
| 20H-1, 13-15                    | 175.83          | 49.2                | 97.0     | 1.49                         | 0.76 | 2.65  | 71.5            | 2.51          |
| 20H-2, 13-15                    | 177.33          | 51.5                | 106.4    | 1.46                         | 0.71 | 2.65  | 73.3            | 2.75          |
| 20H-3, 13-15                    | 178.83          | 52.8                | 111.8    | 1.43                         | 0.68 | 2.58  | 73.8            | 2.82          |
| 20H-4, 13-15                    | 180.33          | 45.5                | 83.5     | 1.55                         | 0.84 | 2.69  | 68.6            | 2.19          |
| 20H-5, 13-15                    | 181.83          | 46.0                | 85.3     | 1.55                         | 0.83 | 2.74  | 69.5            | 2.28          |
| 20H-6, 13-16                    | 183.33          | 48.9                | 95.9     | 1.49                         | 0.76 | 2.63  | 71.1            | 2.46          |
| 20H-7, 13-15                    | 184.83          | 48.1                | 92.8     | 1.50                         | 0.78 | 2.66  | 70.7            | 2.41          |
| 21X-1, 15-17                    | 185.35          | 49.2                | 96.7     | 1.49                         | 0.76 | 2.65  | 71.5            | 2.51          |
| 21X-2, 20-22                    | 186.90          | 48.5                | 94.0     | 1.50                         | 0.77 | 2.68  | 71.1            | 2.46          |
| 21X-3, 13-15                    | 188.33          | 48.8                | 95.5     | 1.50                         | 0.77 | 2.68  | 71.4            | 2.50          |
| 21X-4, 13-15                    | 189.83          | 48.0                | 92.1     | 1.52                         | 0.79 | 2.72  | 71.0            | 2.45          |
| 22X-1, 13-15                    | 190.53          | 45.3                | 82.7     | 1.52                         | 0.83 | 2.55  | 67.3            | 2.06          |
| 22X-2, 13-15                    | 192.03          | 47.9                | 91.8     | 1.50                         | 0.78 | 2.62  | 70.2            | 2.35          |
| 22X-3, 13-15                    | 193.53          | 51.7                | 107.0    | 1.46                         | 0.71 | 2.68  | 73.7            | 2.80          |

Table T9 (continued).

| Core, section,<br>interval (cm) | Depth<br>(mbsf) | Water content (wt%) |          | Density (g/cm <sup>3</sup> ) |      |       | Porosity<br>(%) | Void<br>ratio |
|---------------------------------|-----------------|---------------------|----------|------------------------------|------|-------|-----------------|---------------|
|                                 |                 | Bulk mass           | Dry mass | Bulk                         | Dry  | Grain |                 |               |
| 22X-4, 13-15                    | 195.03          | 47.2                | 89.4     | 1.52                         | 0.80 | 2.68  | 70.0            | 2.34          |
| 22X-5, 13-15                    | 196.53          | 41.7                | 71.6     | 1.61                         | 0.94 | 2.75  | 65.8            | 1.92          |
| 22X-6, 13-15                    | 198.03          | 44.3                | 79.4     | 1.58                         | 0.88 | 2.76  | 68.1            | 2.14          |
| 22X-7, 13-15                    | 199.23          | 42.0                | 72.4     | 1.60                         | 0.93 | 2.72  | 65.7            | 1.92          |
| 23X-1, 11-13                    | 200.21          | 46.5                | 86.9     | 1.55                         | 0.83 | 2.78  | 70.2            | 2.36          |
| 23X-2, 11-13                    | 201.71          | 48.7                | 95.1     | 1.51                         | 0.77 | 2.74  | 71.8            | 2.55          |
| 23X-3, 11-13                    | 203.21          | 44.7                | 80.7     | 1.57                         | 0.87 | 2.73  | 68.2            | 2.15          |
| 23X-4, 11-13                    | 204.71          | 51.7                | 107.0    | 1.47                         | 0.71 | 2.72  | 74.0            | 2.85          |
| 23X-5, 11-13                    | 206.21          | 50.8                | 103.4    | 1.47                         | 0.72 | 2.66  | 72.8            | 2.68          |
| 23X-6, 11-13                    | 207.21          | 47.8                | 91.4     | 1.53                         | 0.80 | 2.77  | 71.2            | 2.47          |
| 24X-1, 18-20                    | 209.98          | 46.0                | 85.2     | 1.54                         | 0.83 | 2.71  | 69.3            | 2.26          |
| 24X-2, 13-15                    | 211.43          | 45.3                | 82.8     | 1.55                         | 0.85 | 2.71  | 68.6            | 2.19          |
| 24X-3, 13-15                    | 212.93          | 53.1                | 113.0    | 1.44                         | 0.68 | 2.69  | 74.8            | 2.97          |
| 24X-3, 146-148                  | 214.26          | 44.8                | 81.0     | 1.56                         | 0.86 | 2.68  | 67.9            | 2.12          |
| 24X-4, 13-15                    | 214.43          | 43.4                | 76.5     | 1.59                         | 0.90 | 2.74  | 67.2            | 2.05          |
| 24X-4, 88-90                    | 215.18          | 46.6                | 87.4     | 1.53                         | 0.82 | 2.72  | 69.9            | 2.32          |
| 24X-5, 12-14                    | 215.92          | 50.2                | 100.8    | 1.49                         | 0.74 | 2.75  | 73.0            | 2.70          |
| 24X-5, 53-55                    | 216.33          | 48.2                | 93.2     | 1.51                         | 0.78 | 2.69  | 71.0            | 2.45          |
| 24X-6, 18-20                    | 217.48          | 45.4                | 83.3     | 1.55                         | 0.85 | 2.70  | 68.7            | 2.19          |
| 25X-1, 21-23                    | 219.61          | 49.3                | 97.2     | 1.50                         | 0.76 | 2.72  | 72.1            | 2.59          |
| 25X-2, 8-10                     | 220.98          | 41.8                | 72.0     | 1.61                         | 0.94 | 2.75  | 65.9            | 1.93          |
| 25X-3, 33-35                    | 222.73          | 46.7                | 87.6     | 1.53                         | 0.82 | 2.72  | 69.9            | 2.32          |
| 25X-4, 14-16                    | 223.74          | 47.6                | 90.7     | 1.51                         | 0.79 | 2.67  | 70.3            | 2.36          |
| 26X-1, 65-67                    | 229.75          | 44.8                | 81.2     | 1.57                         | 0.87 | 2.77  | 68.7            | 2.20          |
| 26X-2, 68-70                    | 231.28          | 54.8                | 121.2    | 1.42                         | 0.64 | 2.66  | 75.9            | 3.15          |
| 26X-3, 51-53                    | 232.61          | 51.9                | 107.8    | 1.46                         | 0.70 | 2.71  | 74.1            | 2.86          |
| 26X-4, 45-47                    | 234.05          | 48.2                | 93.0     | 1.51                         | 0.78 | 2.72  | 71.2            | 2.47          |
| 26X-5, 40-42                    | 234.95          | 41.9                | 72.0     | 1.61                         | 0.93 | 2.72  | 65.6            | 1.91          |
| 27X-1, 78-80                    | 239.48          | 39.8                | 66.1     | 1.65                         | 0.99 | 2.78  | 64.2            | 1.79          |
| 27X-2, 68-70                    | 240.88          | 44.5                | 80.3     | 1.57                         | 0.87 | 2.72  | 68.1            | 2.13          |
| 27X-3, 69-71                    | 242.39          | 47.9                | 92.0     | 1.52                         | 0.79 | 2.76  | 71.2            | 2.48          |
| 27X-4, 70-72                    | 243.90          | 48.1                | 92.7     | 1.51                         | 0.79 | 2.71  | 71.0            | 2.45          |
| 27X-5, 70-72                    | 245.40          | 50.1                | 100.2    | 1.48                         | 0.74 | 2.69  | 72.5            | 2.63          |
| 28X-1, 68-70                    | 248.78          | 45.8                | 84.5     | 1.54                         | 0.84 | 2.69  | 68.9            | 2.22          |
| 28X-2, 68-70                    | 250.28          | 43.6                | 77.2     | 1.59                         | 0.90 | 2.78  | 67.7            | 2.10          |
| 28X-3, 66-68                    | 251.76          | 48.2                | 93.1     | 1.51                         | 0.78 | 2.72  | 71.2            | 2.47          |
| 28X-4, 68-70                    | 253.28          | 42.9                | 75.1     | 1.77                         | 1.01 | 3.87  | 73.9            | 2.84          |
| 28X-5, 69-71                    | 254.79          | 39.7                | 65.9     | 1.63                         | 0.98 | 2.65  | 63.0            | 1.70          |
| 28X-6, 71-73                    | 256.31          | 47.6                | 91.0     | 1.53                         | 0.80 | 2.75  | 71.0            | 2.45          |
| 29X-1, 78-80                    | 258.58          | 45.0                | 81.9     | 1.56                         | 0.86 | 2.72  | 68.5            | 2.17          |
| 29X-2, 75-77                    | 260.05          | 46.3                | 86.3     | 1.54                         | 0.82 | 2.70  | 69.4            | 2.27          |
| 29X-3, 73-75                    | 261.53          | 40.1                | 67.0     | 1.63                         | 0.98 | 2.72  | 64.0            | 1.78          |
| 29X-4, 68-70                    | 262.98          | 44.6                | 80.6     | 1.58                         | 0.88 | 2.83  | 69.0            | 2.23          |
| 29X-5, 64-66                    | 264.44          | 41.8                | 71.7     | 1.60                         | 0.93 | 2.70  | 65.4            | 1.89          |
| 30X-1, 68-70                    | 268.08          | 41.9                | 72.0     | 1.59                         | 0.93 | 2.64  | 65.0            | 1.86          |
| 30X-2, 78-80                    | 269.68          | 48.0                | 92.5     | 1.50                         | 0.78 | 2.64  | 70.5            | 2.39          |
| 30X-3, 32-34                    | 270.72          | 42.4                | 73.5     | 1.58                         | 0.91 | 2.61  | 65.2            | 1.87          |
| 30X-4, 92-94                    | 272.82          | 41.3                | 70.4     | 1.60                         | 0.94 | 2.64  | 64.5            | 1.82          |
| 31X-1, 70-72                    | 277.70          | 44.5                | 80.1     | 1.56                         | 0.87 | 2.68  | 67.7            | 2.10          |
| 31X-2, 53-55                    | 279.03          | 41.7                | 71.5     | 1.60                         | 0.93 | 2.68  | 65.1            | 1.87          |
| 31X-3, 70-72                    | 280.70          | 41.7                | 71.5     | 1.60                         | 0.93 | 2.65  | 65.0            | 1.85          |
| 31X-4, 73-75                    | 282.23          | 54.8                | 121.3    | 1.41                         | 0.64 | 2.57  | 75.3            | 3.05          |
| 31X-5, 20-22                    | 283.20          | 43.4                | 76.7     | 1.58                         | 0.90 | 2.73  | 67.1            | 2.04          |
| 31X-6, 28-30                    | 284.28          | 52.0                | 108.2    | 1.45                         | 0.70 | 2.63  | 73.5            | 2.78          |
| 32X-1, 70-72                    | 287.30          | 45.4                | 83.3     | 1.55                         | 0.85 | 2.73  | 69.0            | 2.22          |
| 32X-2, 70-72                    | 288.80          | 45.2                | 82.6     | 1.55                         | 0.85 | 2.70  | 68.5            | 2.18          |
| 32X-3, 69-71                    | 290.29          | 43.4                | 76.7     | 1.59                         | 0.90 | 2.76  | 67.4            | 2.07          |
| 32X-4, 73-75                    | 291.83          | 42.4                | 73.6     | 1.60                         | 0.92 | 2.75  | 66.4            | 1.98          |
| 32X-5, 67-69                    | 293.27          | 43.3                | 76.3     | 1.57                         | 0.89 | 2.67  | 66.5            | 1.99          |
| 32X-6, 52-54                    | 294.62          | 41.8                | 71.8     | 1.60                         | 0.93 | 2.70  | 65.4            | 1.89          |
| 32X-6, 85-87                    | 294.95          | 38.5                | 62.7     | 1.65                         | 1.02 | 2.69  | 62.2            | 1.65          |
| 33X-1, 70-72                    | 296.60          | 38.6                | 63.0     | 1.66                         | 1.02 | 2.72  | 62.5            | 1.67          |
| 33X-2, 70-72                    | 298.10          | 40.5                | 68.1     | 1.63                         | 0.97 | 2.74  | 64.5            | 1.82          |
| 33X-3, 70-72                    | 299.60          | 40.2                | 67.2     | 1.62                         | 0.97 | 2.68  | 63.7            | 1.76          |
| 33X-4, 77-79                    | 301.17          | 39.2                | 64.4     | 1.66                         | 1.01 | 2.75  | 63.3            | 1.73          |
| 33X-5, 66-68                    | 302.56          | 40.6                | 68.4     | 1.63                         | 0.97 | 2.73  | 64.5            | 1.82          |
| 34X-1, 13-15                    | 305.73          | 39.2                | 64.5     | 1.65                         | 1.00 | 2.70  | 63.0            | 1.70          |
| 34X-2, 27-29                    | 307.37          | 36.2                | 56.6     | 1.72                         | 1.10 | 2.79  | 60.7            | 1.54          |
| 34X-3, 17-19                    | 308.77          | 36.8                | 58.1     | 1.71                         | 1.08 | 2.80  | 61.4            | 1.59          |

Table T9 (continued).

| Core, section,<br>interval (cm) | Depth<br>(mbsf) | Water content (wt%) |          | Density (g/cm <sup>3</sup> ) |      |       | Porosity<br>(%) | Void<br>ratio |
|---------------------------------|-----------------|---------------------|----------|------------------------------|------|-------|-----------------|---------------|
|                                 |                 | Bulk mass           | Dry mass | Bulk                         | Dry  | Grain |                 |               |
| 34X-4, 77-79                    | 310.87          | 40.6                | 68.3     | 1.64                         | 0.97 | 2.76  | 64.8            | 1.84          |
| 34X-5, 57-59                    | 312.17          | 46.4                | 86.6     | 1.54                         | 0.83 | 2.76  | 70.0            | 2.33          |
| 34X-6, 64-66                    | 313.74          | 43.3                | 76.5     | 1.60                         | 0.91 | 2.80  | 67.7            | 2.09          |
| 35X-1, 31-33                    | 315.61          | 32.8                | 48.7     | 1.80                         | 1.21 | 2.84  | 57.5            | 1.35          |
| 35X-2, 33-35                    | 317.13          | 34.2                | 52.1     | 1.76                         | 1.16 | 2.82  | 58.9            | 1.43          |
| 35X-3, 47-49                    | 318.77          | 29.9                | 42.6     | 1.82                         | 1.28 | 2.73  | 53.2            | 1.14          |
| 37X-1, 70-72                    | 335.20          | 35.9                | 56.0     | 1.70                         | 1.09 | 2.70  | 59.6            | 1.48          |
| 37X-2, 70-72                    | 336.70          | 35.1                | 54.1     | 1.72                         | 1.12 | 2.73  | 59.1            | 1.44          |
| 37X-3, 70-72                    | 338.20          | 30.4                | 43.8     | 1.80                         | 1.26 | 2.71  | 53.7            | 1.16          |
| 37X-4, 70-72                    | 339.70          | 34.8                | 53.4     | 1.72                         | 1.12 | 2.71  | 58.6            | 1.42          |
| 38X-1, 70-72                    | 344.80          | 32.1                | 47.2     | 1.78                         | 1.21 | 2.73  | 55.7            | 1.26          |
| 38X-2, 70-72                    | 346.30          | 34.0                | 51.5     | 1.74                         | 1.15 | 2.73  | 57.9            | 1.37          |
| 38X-3, 70-72                    | 347.80          | 31.2                | 45.3     | 1.78                         | 1.23 | 2.68  | 54.2            | 1.18          |
| 38X-4, 70-72                    | 349.30          | 32.0                | 47.0     | 1.78                         | 1.21 | 2.71  | 55.4            | 1.24          |
| 38X-5, 70-72                    | 350.80          | 34.1                | 51.7     | 1.75                         | 1.15 | 2.76  | 58.2            | 1.39          |
| 38X-6, 67-69                    | 352.27          | 32.3                | 47.8     | 1.76                         | 1.19 | 2.70  | 55.7            | 1.26          |
| 39X-1, 67-69                    | 354.47          | 29.8                | 42.5     | 1.81                         | 1.27 | 2.70  | 52.8            | 1.12          |
| 39X-2, 70-72                    | 356.00          | 32.8                | 48.9     | 1.76                         | 1.18 | 2.70  | 56.3            | 1.29          |
| 39X-3, 70-72                    | 357.50          | 34.5                | 52.8     | 1.74                         | 1.14 | 2.74  | 58.5            | 1.41          |
| 39X-4, 70-72                    | 359.00          | 34.1                | 51.7     | 1.74                         | 1.15 | 2.74  | 58.0            | 1.38          |
| 39X-5, 66-68                    | 360.46          | 32.0                | 47.0     | 1.78                         | 1.21 | 2.72  | 55.5            | 1.25          |
| 40X-1, 70-72                    | 364.10          | 38.4                | 62.3     | 1.68                         | 1.04 | 2.80  | 63.0            | 1.70          |
| 40X-2, 70-72                    | 365.60          | 32.7                | 48.7     | 1.77                         | 1.19 | 2.74  | 56.5            | 1.30          |
| 40X-3, 70-72                    | 367.10          | 36.0                | 56.2     | 1.71                         | 1.10 | 2.75  | 60.1            | 1.51          |
| 40X-4, 70-72                    | 368.60          | 32.9                | 49.0     | 1.76                         | 1.18 | 2.72  | 56.6            | 1.30          |
| 40X-5, 70-72                    | 370.10          | 27.8                | 38.5     | 1.86                         | 1.34 | 2.72  | 50.5            | 1.02          |
| 41X-1, 64-66                    | 373.74          | 26.7                | 36.4     | 1.89                         | 1.38 | 2.72  | 49.2            | 0.97          |
| 41X-2, 70-72                    | 375.30          | 23.4                | 30.5     | 1.96                         | 1.50 | 2.71  | 44.7            | 0.81          |

**Table T10.** Discrete measurements of *P*-wave velocity, Site 1208. (Continued on next page.)

| Core, section,<br>interval (cm) | Depth<br>(mbsf) | Velocity<br>(m/s) | Core, section,<br>interval (cm) | Depth<br>(mbsf) | Velocity<br>(m/s) | Core, section,<br>interval (cm) | Depth<br>(mbsf) | Velocity<br>(m/s) |
|---------------------------------|-----------------|-------------------|---------------------------------|-----------------|-------------------|---------------------------------|-----------------|-------------------|
| 198-1208A-                      |                 |                   | 10H-6, 19                       | 88.39           | 1521.1            | 20H-7, 18                       | 184.88          | 1535.8            |
| 1H-1, 63                        | 0.63            | 1510.8            | 11H-1, 21                       | 90.41           | 1520.3            | 21X-1, 24                       | 185.44          | 1547.6            |
| 1H-2, 64                        | 2.14            | 1511.1            | 11H-2, 66                       | 92.36           | 1509.3            | 21X-2, 37                       | 187.07          | 1523.5            |
| 1H-3, 51                        | 3.51            | 1504.3            | 11H-3, 66                       | 93.86           | 1519.3            | 21X-3, 18                       | 188.38          | 1529.7            |
| 1H-4, 54                        | 4.34            | 1504.9            | 11H-4, 66                       | 95.36           | 1514.6            | 21X-4, 9                        | 189.79          | 1526.8            |
| 2H-1, 65                        | 5.35            | 1497.9            | 11H-5, 64                       | 96.84           | 1514.6            | 22X-1, 9                        | 190.49          | 1533.1            |
| 2H-2, 66                        | 6.86            | 1505.9            | 11H-6, 66                       | 98.36           | 1524.4            | 22X-2, 10                       | 191.99          | 1520.5            |
| 2H-3, 64                        | 8.34            | 1503.1            | 12H-1, 66                       | 100.36          | 1526.0            | 22X-3, 23                       | 193.63          | 1526.9            |
| 2H-4, 65                        | 9.85            | 1516.0            | 12H-2, 76                       | 101.96          | 1507.8            | 22X-4, 18                       | 195.08          | 1519.9            |
| 2H-5, 60                        | 11.30           | 1502.9            | 12H-3, 63                       | 103.33          | 1512.1            | 22X-5, 19                       | 196.59          | 1519.5            |
| 2H-6, 83                        | 13.03           | 1505.5            | 12H-4, 65                       | 104.85          | 1512.2            | 22X-6, 10                       | 197.99          | 1530.8            |
| 3H-1, 122                       | 15.42           | 1503.0            | 12H-5, 65                       | 106.35          | 1516.5            | 22X-7, 10                       | 199.20          | 1525.9            |
| 3H-2, 64                        | 16.34           | 1522.1            | 12H-6, 66                       | 107.86          | 1520.3            | 23X-1, 8                        | 200.18          | 1521.4            |
| 3H-3, 65                        | 17.85           | 1509.4            | 13H-1, 64                       | 109.84          | 1509.1            | 23X-2, 6                        | 201.66          | 1515.0            |
| 3H-4, 66                        | 19.36           | 1501.0            | 13H-2, 65                       | 111.35          | 1516.3            | 23X-3, 8                        | 203.18          | 1519.3            |
| 3H-5, 66                        | 20.86           | 1503.8            | 13H-3, 66                       | 112.86          | 1513.3            | 23X-4, 20                       | 204.79          | 1526.7            |
| 3H-6, 66                        | 22.35           | 1503.7            | 13H-4, 82                       | 114.52          | 1513.4            | 23X-5, 38                       | 206.48          | 1512.9            |
| 4H-1, 66                        | 24.36           | 1505.7            | 13H-5, 66                       | 115.86          | 1547.4            | 23X-6, 4                        | 207.14          | 1548.9            |
| 4H-2, 65                        | 25.85           | 1500.3            | 13H-5, 106                      | 116.26          | 1524.0            | 24X-1, 20                       | 210.00          | 1517.7            |
| 4H-3, 64                        | 27.34           | 1502.0            | 13H-6, 66                       | 117.36          | 1522.0            | 24X-2, 9                        | 211.39          | 1533.3            |
| 4H-4, 66                        | 28.86           | 1505.1            | 14H-1, 66                       | 119.36          | 1523.5            | 24X-3, 15                       | 212.95          | 1535.7            |
| 4H-5, 66                        | 30.36           | 1511.4            | 14H-2, 75                       | 120.95          | 1519.7            | 24X-3, 101                      | 213.81          | 1530.4            |
| 4H-6, 65                        | 31.85           | 1506.3            | 14H-3, 75                       | 122.45          | 1516.0            | 24X-3, 110                      | 213.90          | 1512.6            |
| 4H-7, 32                        | 33.02           | 1503.9            | 14H-4, 66                       | 123.86          | 1520.9            | 24X-3, 121                      | 214.01          | 1519.2            |
| 5H-1, 36                        | 33.56           | 1509.4            | 14H-5, 75                       | 125.45          | 1522.6            | 24X-3, 133                      | 214.13          | 1531.1            |
| 5H-2, 55                        | 35.25           | 1516.8            | 14H-6, 75                       | 126.95          | 1518.9            | 24X-3, 141                      | 214.21          | 1546.9            |
| 5H-3, 18                        | 36.38           | 1516.9            | 14H-7, 8                        | 127.78          | 1518.1            | 24X-4, 9                        | 214.39          | 1521.1            |
| 5H-4, 17                        | 37.87           | 1510.5            | 15H-1, 10                       | 128.30          | 1521.9            | 24X-4, 24                       | 214.54          | 1534.6            |
| 5H-5, 19                        | 39.39           | 1523.9            | 15H-2, 10                       | 129.80          | 1519.3            | 24X-4, 32                       | 214.62          | 1531.6            |
| 5H-6, 6                         | 40.76           | 1515.2            | 15H-3, 5                        | 131.25          | 1524.6            | 24X-4, 42                       | 214.72          | 1538.5            |
| 5H-7, 21                        | 42.41           | 1518.3            | 15H-4, 10                       | 132.80          | 1521.5            | 24X-4, 55                       | 214.85          | 1538.9            |
| 6H-1, 18                        | 42.88           | 1508.3            | 15H-5, 11                       | 134.31          | 1519.2            | 24X-4, 68                       | 214.98          | 1542.5            |
| 6H-2, 19                        | 44.39           | 1500.4            | 15H-6, 11                       | 135.81          | 1512.6            | 24X-4, 77                       | 215.07          | 1526.9            |
| 6H-3, 18                        | 45.88           | 1516.9            | 15H-7, 8                        | 137.28          | 1519.2            | 24X-4, 87                       | 215.17          | 1525.4            |
| 6H-4, 19                        | 47.39           | 1505.2            | 16H-1, 10                       | 137.80          | 1516.1            | 24X-4, 115                      | 215.45          | 1541.6            |
| 6H-5, 19                        | 48.88           | 1497.7            | 16H-2, 10                       | 139.30          | 1515.8            | 24X-4, 124                      | 215.54          | 1534.1            |
| 6H-5, 39                        | 49.08           | 1507.4            | 16H-3, 10                       | 140.80          | 1520.5            | 24X-4, 147                      | 215.77          | 1537.8            |
| 6H-5, 66                        | 49.36           | 1507.7            | 16H-4, 9                        | 142.29          | 1522.4            | 24X-5, 10                       | 215.90          | 1537.2            |
| 6H-5, 88                        | 49.58           | 1498.5            | 16H-5, 9                        | 143.79          | 1536.6            | 24X-5, 19                       | 215.99          | 1526.1            |
| 6H-5, 111                       | 49.81           | 1496.2            | 16H-6, 12                       | 145.32          | 1520.9            | 24X-5, 63                       | 216.43          | 1523.4            |
| 6H-5, 136                       | 50.06           | 1500.6            | 16H-7, 12                       | 146.82          | 1533.6            | 24X-5, 88                       | 216.68          | 1510.4            |
| 6H-6, 10                        | 50.30           | 1502.0            | 17H-1, 16                       | 147.36          | 1511.2            | 24X-5, 106                      | 216.86          | 1536.7            |
| 6H-7, 9                         | 51.78           | 1509.2            | 17H-2, 19                       | 148.89          | 1521.4            | 24X-5, 124                      | 217.04          | 1531.0            |
| 7H-1, 22                        | 52.42           | 1508.3            | 17H-3, 19                       | 150.39          | 1515.5            | 24X-6, 56                       | 217.86          | 1527.9            |
| 7H-2, 19                        | 53.89           | 1507.2            | 17H-4, 18                       | 151.88          | 1533.9            | 25X-1, 24                       | 219.64          | 1534.2            |
| 7H-3, 10                        | 55.30           | 1527.1            | 17H-5, 19                       | 153.39          | 1529.2            | 25X-2, 48                       | 221.38          | 1523.3            |
| 7H-4, 10                        | 56.80           | 1509.0            | 17H-6, 19                       | 154.89          | 1519.0            | 25X-3, 52                       | 222.92          | 1516.0            |
| 7H-5, 9                         | 58.29           | 1518.1            | 17H-7, 18                       | 156.38          | 1521.5            | 25X-4, 44                       | 224.04          | 1514.7            |
| 7H-6, 6                         | 59.76           | 1524.8            | 18H-1, 19                       | 156.89          | 1508.0            | 26X-1, 24                       | 229.34          | 1524.9            |
| 7H-7, 10                        | 61.30           | 1538.5            | 18H-2, 20                       | 158.40          | 1524.7            | 26X-2, 65                       | 231.25          | 1552.9            |
| 8H-1, 9                         | 61.79           | 1523.4            | 18H-3, 21                       | 159.91          | 1521.1            | 26X-3, 47                       | 232.57          | 1535.1            |
| 8H-2, 10                        | 63.30           | 1528.2            | 18H-4, 19                       | 161.39          | 1521.2            | 26X-4, 42                       | 234.02          | 1548.6            |
| 8H-3, 10                        | 64.80           | 1534.1            | 18H-5, 20                       | 162.90          | 1531.0            | 26X-5, 34                       | 234.89          | 1535.2            |
| 8H-4, 10                        | 66.30           | 1530.2            | 18H-6, 30                       | 164.50          | 1514.0            | 27X-1, 83                       | 239.53          | 1520.2            |
| 8H-5, 10                        | 67.80           | 1524.0            | 18H-7, 22                       | 165.92          | 1514.9            | 27X-2, 64                       | 240.84          | 1532.1            |
| 8H-6, 12                        | 69.32           | 1559.8            | 19H-1, 17                       | 166.37          | 1525.9            | 27X-3, 83                       | 242.53          | 1542.0            |
| 8H-7, 9                         | 70.79           | 1521.7            | 19H-2, 19                       | 167.88          | 1524.0            | 27X-4, 94                       | 244.14          | 1555.7            |
| 9H-1, 9                         | 71.29           | 1523.4            | 19H-3, 18                       | 169.38          | 1538.6            | 27X-5, 66                       | 245.36          | 1545.0            |
| 9H-2, 9                         | 72.79           | 1519.1            | 19H-4, 18                       | 170.88          | 1521.9            | 28X-1, 70                       | 248.80          | 1560.0            |
| 9H-3, 17                        | 74.37           | 1517.5            | 19H-5, 18                       | 172.38          | 1521.3            | 28X-2, 61                       | 250.21          | 1522.1            |
| 9H-4, 21                        | 75.91           | 1504.7            | 19H-6, 20                       | 173.90          | 1516.2            | 28X-3, 52                       | 251.62          | 1549.2            |
| 9H-5, 18                        | 77.38           | 1519.7            | 19H-7, 18                       | 175.38          | 1522.9            | 28X-4, 63                       | 253.23          | 1576.8            |
| 9H-6, 17                        | 78.87           | 1504.6            | 20H-1, 22                       | 175.92          | 1514.2            | 28X-5, 62                       | 254.71          | 1556.1            |
| 10H-1, 18                       | 80.88           | 1514.1            | 20H-2, 19                       | 177.39          | 1526.7            | 28X-6, 16                       | 255.76          | 1570.4            |
| 10H-2, 17                       | 82.37           | 1523.7            | 20H-3, 19                       | 178.89          | 1516.2            | 29X-1, 89                       | 258.69          | 1534.0            |
| 10H-3, 18                       | 83.88           | 1520.9            | 20H-4, 20                       | 180.40          | 1518.7            | 29X-2, 80                       | 260.10          | 1565.8            |
| 10H-4, 21                       | 85.41           | 1517.4            | 20H-5, 19                       | 181.89          | 1535.2            | 29X-3, 63                       | 261.43          | 1579.3            |
| 10H-5, 21                       | 86.91           | 1520.8            | 20H-6, 19                       | 183.39          | 1536.4            | 29X-4, 63                       | 262.93          | 1528.1            |

**Table T10 (continued).**

| Core, section,<br>interval (cm) | Depth<br>(mbsf) | Velocity<br>(m/s) | Core, section,<br>interval (cm) | Depth<br>(mbsf) | Velocity<br>(m/s) |
|---------------------------------|-----------------|-------------------|---------------------------------|-----------------|-------------------|
| 29X-5, 83                       | 264.63          | 1511.0            | 34X-3, 91                       | 309.51          | 1566.4            |
| 29X-6, 14                       | 265.24          | 1551.7            | 34X-4, 56                       | 310.65          | 1583.4            |
| 30X-1, 66                       | 268.06          | 1556.6            | 34X-5, 75                       | 312.35          | 1570.7            |
| 30X-2, 77                       | 269.67          | 1567.0            | 34X-6, 71                       | 313.81          | 1574.9            |
| 30X-3, 33                       | 270.73          | 1554.7            | 35X-1, 21                       | 315.51          | 1593.9            |
| 30X-4, 94                       | 272.84          | 1541.6            | 35X-2, 14                       | 316.94          | 1602.7            |
| 31X-1, 78                       | 277.78          | 1522.6            | 35X-3, 34                       | 318.64          | 1607.4            |
| 31X-2, 59                       | 279.09          | 1513.8            | 35X-4, 33                       | 320.13          | 1647.5            |
| 31X-3, 78                       | 280.78          | 1542.0            | 35X-5, 18                       | 320.98          | 1650.1            |
| 31X-4, 79                       | 282.29          | 1547.5            | 36X-2, 32                       | 326.72          | 1625.6            |
| 31X-5, 15                       | 283.15          | 1547.1            | 37X-1, 63                       | 335.13          | 1542.1            |
| 31X-6, 23                       | 284.23          | 1541.7            | 37X-1, 131                      | 335.81          | 1539.9            |
| 32X-1, 77                       | 287.37          | 1562.0            | 37X-2, 61                       | 336.61          | 1560.8            |
| 32X-2, 66                       | 288.76          | 1570.8            | 37X-2, 105                      | 337.05          | 1555.3            |
| 32X-2, 139                      | 289.49          | 1542.2            | 37X-3, 31                       | 337.81          | 1559.8            |
| 32X-3, 19                       | 289.79          | 1531.2            | 37X-3, 64                       | 338.14          | 1555.2            |
| 32X-3, 60                       | 290.20          | 1552.5            | 37X-3, 120                      | 338.70          | 1539.3            |
| 32X-3, 118                      | 290.78          | 1554.2            | 37X-4, 9                        | 339.09          | 1558.8            |
| 32X-4, 37                       | 291.47          | 1553.1            | 37X-4, 64                       | 339.64          | 1548.5            |
| 32X-4, 84                       | 291.94          | 1555.5            | 37X-4, 125                      | 340.25          | 1559.4            |
| 32X-4, 139                      | 292.49          | 1543.2            | 38X-1, 63                       | 344.73          | 1553.5            |
| 32X-5, 39                       | 292.99          | 1563.8            | 38X-2, 10                       | 345.70          | 1555.6            |
| 32X-5, 62                       | 293.22          | 1541.7            | 38X-2, 85                       | 346.45          | 1536.3            |
| 32X-5, 113                      | 293.73          | 1540.9            | 38X-3, 64                       | 347.74          | 1537.2            |
| 32X-6, 30                       | 294.40          | 1546.2            | 38X-3, 101                      | 348.11          | 1541.0            |
| 32X-6, 66                       | 294.76          | 1547.1            | 38X-4, 74                       | 349.34          | 1546.9            |
| 32X-6, 92                       | 295.02          | 1521.9            | 38X-5, 76                       | 350.86          | 1543.6            |
| 33X-1, 58                       | 296.48          | 1525.6            | 38X-6, 31                       | 351.91          | 1569.9            |
| 33X-1, 117                      | 297.07          | 1526.0            | 39X-1, 59                       | 354.39          | 1564.8            |
| 33X-2, 28                       | 297.68          | 1522.1            | 39X-2, 62                       | 355.92          | 1583.4            |
| 33X-2, 85                       | 298.25          | 1516.5            | 39X-3, 63                       | 357.43          | 1556.1            |
| 33X-2, 133                      | 298.73          | 1530.0            | 39X-4, 65                       | 358.95          | 1549.5            |
| 33X-3, 26                       | 299.16          | 1524.9            | 39X-5, 59                       | 360.39          | 1568.8            |
| 33X-3, 86                       | 299.76          | 1559.0            | 40X-1, 78                       | 364.18          | 1530.8            |
| 33X-3, 118                      | 300.08          | 1525.0            | 40X-2, 77                       | 365.67          | 1548.3            |
| 33X-4, 18                       | 300.58          | 1525.9            | 40X-3, 80                       | 367.20          | 1549.3            |
| 33X-4, 97                       | 301.37          | 1548.6            | 40X-4, 76                       | 368.65          | 1542.3            |
| 33X-4, 121                      | 301.61          | 1540.4            | 40X-5, 65                       | 370.05          | 1554.4            |
| 33X-5, 39                       | 302.29          | 1568.2            | 41X-1, 56                       | 373.66          | 1581.5            |
| 34X-1, 24                       | 305.84          | 1548.6            | 41X-2, 66                       | 375.26          | 1638.5            |
| 34X-2, 91                       | 308.01          | 1574.5            | 41X-2, 103                      | 375.63          | 1605.0            |

**Table T11.** Discrete measurements of thermal conductivity, Site 1208.

| Core, section,<br>interval (cm) | Depth<br>(mbsf) | Thermal<br>conductivity<br>(W/[m-K]) | Core, section,<br>interval (cm) | Depth<br>(mbsf) | Thermal<br>conductivity<br>(W/[m-K]) |
|---------------------------------|-----------------|--------------------------------------|---------------------------------|-----------------|--------------------------------------|
| 198-1208A-                      |                 |                                      | 21X-1, 55                       | 185.75          | 0.70                                 |
| 1H-1, 55                        | 0.55            | 0.79                                 | 21X-3, 55                       | 188.75          | 0.82                                 |
| 1H-3, 55                        | 3.55            | 0.87                                 | 22X-1, 55                       | 190.95          | 0.67                                 |
| 2H-1, 55                        | 5.25            | 0.80                                 | 22X-3, 55                       | 193.95          | 0.96                                 |
| 2H-3, 55                        | 8.25            | 0.84                                 | 23X-1, 55                       | 200.65          | 0.90                                 |
| 3H-1, 55                        | 14.75           | 0.80                                 | 23X-3, 55                       | 203.65          | 0.83                                 |
| 3H-3, 55                        | 17.75           | 0.82                                 | 24X-1, 55                       | 210.35          | 0.95                                 |
| 4H-1, 55                        | 24.25           | 0.96                                 | 24X-3, 55                       | 213.35          | 0.82                                 |
| 4H-3, 55                        | 27.25           | 0.88                                 | 25X-1, 55                       | 219.95          | 0.89                                 |
| 5H-1, 55                        | 33.75           | 0.83                                 | 25X-3, 55                       | 222.95          | 1.05                                 |
| 5H-3, 48                        | 36.68           | 0.86                                 | 26X-1, 55                       | 229.65          | 0.94                                 |
| 6H-1, 48                        | 43.18           | 0.82                                 | 26X-3, 55                       | 232.65          | 0.88                                 |
| 6H-3, 48                        | 46.18           | 0.86                                 | 27X-1, 55                       | 239.25          | 0.95                                 |
| 7H-1, 55                        | 52.75           | 0.89                                 | 27X-3, 55                       | 242.25          | 0.82                                 |
| 7H-3, 55                        | 55.75           | 0.88                                 | 28X-1, 55                       | 248.65          | 0.85                                 |
| 8H-1, 55                        | 62.25           | 0.90                                 | 28X-3, 55                       | 251.65          | 0.84                                 |
| 8H-3, 55                        | 65.25           | 0.88                                 | 29X-1, 55                       | 258.35          | 0.84                                 |
| 9H-1, 55                        | 71.75           | 0.89                                 | 29X-3, 55                       | 261.35          | 1.07                                 |
| 9H-3, 55                        | 74.75           | 0.97                                 | 30X-1, 55                       | 267.95          | 0.86                                 |
| 10H-1, 55                       | 81.25           | 0.91                                 | 30X-3, 55                       | 270.95          | 0.95                                 |
| 10H-3, 55                       | 84.25           | 0.81                                 | 31X-1, 55                       | 277.55          | 0.82                                 |
| 11H-1, 55                       | 90.75           | 0.86                                 | 31X-3, 55                       | 280.55          | 1.02                                 |
| 11H-3, 55                       | 93.75           | 0.87                                 | 32X-1, 55                       | 287.15          | 0.70                                 |
| 12H-1, 55                       | 100.25          | 0.80                                 | 32X-3, 55                       | 290.15          | 0.94                                 |
| 12H-3, 55                       | 103.25          | 0.87                                 | 33X-1, 55                       | 296.45          | 0.92                                 |
| 13H-1, 55                       | 109.75          | 0.94                                 | 33X-3, 55                       | 299.45          | 0.95                                 |
| 13H-3, 55                       | 112.75          | 0.88                                 | 34X-1, 55                       | 306.15          | 0.97                                 |
| 14H-1, 55                       | 119.25          | 0.96                                 | 34X-3, 55                       | 309.15          | 1.01                                 |
| 14H-3, 55                       | 122.25          | 0.93                                 | 35X-1, 55                       | 315.85          | 0.99                                 |
| 15H-1, 55                       | 128.75          | 0.96                                 | 35X-3, 55                       | 318.85          | 1.21                                 |
| 15H-3, 55                       | 131.75          | 0.96                                 | 36X-1, 55                       | 325.45          | 0.97                                 |
| 16H-1, 55                       | 138.25          | 0.86                                 | 36X-3, 55                       | 326.95          | 0.99                                 |
| 16H-3, 55                       | 141.25          | 1.04                                 | 37X-1, 55                       | 335.05          | 1.17                                 |
| 17H-1, 55                       | 147.75          | 0.97                                 | 37X-3, 55                       | 338.05          | 1.21                                 |
| 17H-3, 55                       | 150.75          | 1.07                                 | 38X-1, 55                       | 344.65          | 1.12                                 |
| 18H-1, 55                       | 157.25          | 0.96                                 | 38X-3, 55                       | 347.65          | 1.28                                 |
| 18H-3, 55                       | 160.25          | 0.88                                 | 39X-1, 55                       | 354.35          | 1.18                                 |
| 19H-1, 55                       | 166.75          | 0.92                                 | 39X-3, 55                       | 357.35          | 1.24                                 |
| 19H-3, 55                       | 169.75          | 0.91                                 | 40X-1, 55                       | 363.95          | 1.06                                 |
| 20H-1, 55                       | 176.25          | 0.96                                 | 40X-3, 55                       | 366.95          | 1.24                                 |
| 20H-3, 55                       | 179.25          | 0.98                                 | 41X-1, 55                       | 373.65          | 1.28                                 |